DEVELOPMENT OF A 60 W PULSED FIBER LASER AMPLIFIER FOR MATERIALS PROCESSING

A THESIS SUBMITTED TO
THE GRADUATE SCHOOL OF NATURAL AND APPLIED SCIENCES
OF
MIDDLE EAST TECHNICAL UNIVERSITY

BY

YİĞİT OZAN AYDIN

IN PARTIAL FULFILLMENT OF THE REQUIREMENTS
FOR
THE DEGREE OF MASTER OF SCIENCE
IN
MICRO AND NANOTECHNOLOGY

JUNE 2014

Approval of the Thesis:

DEVELOPMENT OF A 60 W PULSED FIBER LASER AMPLIFIER FOR MATERIALS PROCESSING

Submitted by **YİĞİT OZAN AYDIN** in partial fulfillment of the requirements for the degree of **Master of Science in Micro and Nanotechnology Department, Middle East Technical University** by,

Prof. Dr. Canan Özgen
Dean, Graduate School of **Natural and Applied Sciences** _____

Prof. Dr. Tayfun Akın
Head of Department, **Micro and Nanotechnology** _____

Assist. Prof. Dr. Alpan Bek
Supervisor, **Physics Dept., METU** _____

Assoc. Prof. Dr. Asaf Behzat Şahin
Co-Supervisor, **Electronics and Communications Eng., YBU** _____

Examining Committee Members:

Prof. Dr. Raşit Turan
Physics Dept., METU _____

Assist. Prof. Dr. Alpan Bek
Physics Dept., METU _____

Assoc. Prof. Dr. F.Ömer İlday
Physics Dept., Bilkent Univ. _____

Assist. Prof. Dr. Halil Berberoğlu
Physics Dept., Gazi Univ. _____

Koray Eken, M. Sc.
FiberLAST Inc. _____

Date: *30.06.2014*

I hereby declare that all information in this document has been obtained and presented in accordance with academic rules and ethical conduct. I also declare that, as required by these rules and conduct, I have fully cited and referenced all material and results that are not original to this work.

Name, Last name : Yiğit Ozan Aydın

Signature :

ABSTRACT

DEVELOPMENT OF A 60 W PULSED FIBER LASER AMPLIFIER FOR MATERIALS PROCESSING

Aydın, Yiğit Ozan
M. Sc. Department of Micro and Nanotechnology
Supervisor: Assist. Prof. Dr. AlpanBek
Co-Supervisor: Assoc. Prof. Dr. Asaf Behzat Şahin

June 2014, 116 pages

Fiber lasers have the advantage of high beam quality, high efficiency, small size, air cooling and therefore much interest in the development of high power fiber laser systems have arisen recently in the world. Almost all commercially developed fiber lasers with nanosecond pulse duration, that are being used for material processing, are Q-switched systems. Vital parameters in the material processing such as repetition rate, pulse energy and pulse duration are correlated with each other and they cannot be adjusted independently in the Q-switch mechanism.

In this study, ytterbium doped all-fiber laser amplifier with 60 W average power and more than 20 kW peak power at 1 μm wavelength was developed, and its potential for processing of different material types is investigated. This master-oscillator power-amplifier (MOPA) architectured system is composed of pulses, produced by an electronically pumped diode, and amplified by a series of fiber amplifiers. In contrast with Q-switch lasers, MOPA architecture allows us to adjust pulse duration, repetition rate and power independently. Beam quality is nearly diffraction limited, and the typical M^2 value is1.5. The system is an all-fiber one where the maximum pulse energy achieved at 100 kHz repetition rate is 0.6 mJ and minimum pulse duration is ~30 ns at this energy level. Due to multi-stage architecture and special precautions, the system works without a high amplified spontaneous emission (ASE) level and shows an optical efficiency of 76%. After development of the laser amplifier, and certification of its materials processing capability, an industrial prototype was configured by taking the cost-efficiency into account . The laser components were placed into a compact case which has a simple design for thermal

cooling. The developed industrial laser amplifier prototype has several unique properties with respect to other equivalent MOPA design fiber lasers.

In material processing, high stability and high beam quality lead to high consistency. Reduced diameters of active and passive fiber cores and specially optimized fiber splices, which are used in the system architecture, result with higher beam quality thus the focusing is superior to many contemporary commercial lasers. As the intensity (areal power density) is the physical quantity that drives the nature of interaction of laser output with materials, the developed system offers long operation life-time due to its capability of operation at lower power levels than its contemporaries.

In order to demonstrate the efficiency and the ability of processing various different kinds of materials with the developed laser amplifier system, a multitude of processing applications such as micro drilling, solar cell edge isolation, deep engraving and color marking were tested on metal, semiconductor and insulator surfaces and the results are discussing in relationship with various system operation parameters.

Keywords : fiber laser, materials processing, pulsed lasers, ytterbium laser, MOPA lasers

ÖZ

MALZEME İŞLEME İÇİN 60 W DARBELİ FİBER LAZER YÜKSELTECİ GELİŞTİRİLMESİ

Aydın, Yiğit Ozan
Yüksek Lisans, Mikro ve Nanoteknoloji Bölümü
Tez Yöneticisi: Yard. Doç. Dr. Alpan Bek
Ortak Tez Yöneticisi: Doç. Dr. Asaf Behzat Şahin

Haziran 2014, 116 sayfa

Günümüzde fiber lazer teknolojisi, uygulamalı fiziğin en hızlı gelişen alanlarından bir tanesidir. Kompakt olarak tasarlanabilmesi, esnek ve taşınabilirliği, yüksek ışın kalitesi, hassas malzeme işleme kabiliyeti, yüksek verimlilikte çalışması, su ile soğutma gerektirmemesi, düşük bakım maliyetine sahip olması gibi önemli pratik avantajları bu gelişmedeki en önemli etkenler arasındadır. Endüstriyel olarak geliştirilen ve malzeme işlemek için kullanılan nanosaniye mertebesindeki darbelere sahip fiber lazer sistemlerinin neredeyse tamamına yakını Q-Switch konfigürasyonuna sahiptir. Malzeme işleme uygulamalarındaki tekrar frekansı, darbe enerjisi ve darbe süresi gibi önemli parametreler Q-Switch sistemlerde birbirinden bağımsız olarak ayarlanamamaktadır.

Bu çalışmada malzeme işleme uygulamalarında kullanılmak üzere, iterbiyum katkılı, tümleşik, 60 W ortalama güce ve 20 kW'dan fazla tepe gücüne sahip, 1 μm dalga boyunda çalışan bir lazer kaynağı geliştirilmiş, lazerin çeşitli malzemeler üzerindeki etkisi incelenmiştir. MOPA mimarisi ile tasarlanan sistemde elektronik olarak modüle edilen bir lazer diyod aracılığıyla üretilen darbeler, tasarlanan yükselteçlerle bir kaç mW güç seviyesinden 60 W ortalama güce çıkartılmıştır. Q-Switch tasarımdan farklı olarak MOPA mimarisi bizlere darbe süresinin tekrar frekansından ve ortalama güçten bağımsız olarak ayarlanabilmesi imkanını vermiştir. Sistemden elde edilen lazerin ışın kalitesi neredeyse kırınımla sınırlı olup $M^2 \sim 1,5$ seviyelerindedir. Sistem, fiberle tümleşik ve 100 kHz tekrar freakansında 0.6 mJ darbe enerjisine sahip olup, minimum 30 ns'ye kadar darbe süresine

sahip lazer ışını üretebilmektedir. Çok kademeli tasarım sayesinde kendiliğinden yükseltilmiş ışıma (amplified spontaneous emission) baskılanmış ve son yükselteçte %76 optik verimlilik elde edilmiştir. Lazer yükselticinin geliştirilme aşamasının ardından, uygun maliyetlilik göz önüne alınarak sistemin endüstriyelleşmesi sağlanmıştır. Lazerin yükseltecinin oluşturulması sırasında kullanılan komponentler termal etkileri azaltabilecek şekilde dizayn edilen kompakt bir yapı içerisinde muhafaza edilerek son ürün haline getirilmiştir. Geliştirilen fiber lazer yükselteci, muadillerine göre birçok özgün özellik barındırmaktadır.

Lazerle malzeme işleme uygulamalarında, yüksek kararlılık ve ışın kalitesi verimli işleme sonuçlarını kullanıcıyı sağlamaktadır. Düşük çekirdek yarıçaplı aktif ve pasif fiberler ve optimizasyonu yapılan fiber kaynakları ile elde edilen yüksek ışın kalitesi ile iyi bir odaklama imkanı sağlanmıştır. Malzeme ve lazer etkileşiminde, gücün etki ettiği alan (yoğunluk) işlemin sonucunu belirleyen yegane unsurlardan birisi olup, yüksek ışın kalitesi ile küçük bir alana etki malze işleme kalitesini arttırmaktadır.

Sistemin farklı malzemeler üzerindeki işleme verimliliğini ve yeteneğini anlamak için mikrodelme, güneş hücresi kenar izolasyonu, derin kazıma ve renkli markalama gibi uygulamalar gerçekleştirilip lazer parametrelerinin bu uygulamalar üzerindeki etkisi tartışılmıştır.

Anahtar kelimeler : fiber lazer, malzeme işleme, darbeli lazerler, iterbiyum fiber lazer, MOPA lazer

to all my family…

ACKNOWLEDGEMENTS

First and foremost, I would like to thank my supervisor Assist. Prof. Dr. Alpan Bek, who have provided me guidance, enlightened and motivated me with his immense knowledge and enthusiasm.

I am very grateful to FiberLAST Inc., especially company manager Koray Eken who provided me a great laboratory and support throughout the production of my thesis. Very special thanks to my colleagues Emre Yağcı , Sarper Salman, Mesut Tasalı, Seydi Yavaş for assisting and helping me in the development of fiber laser part of this study.

I would like to thank F.Ömer İlday who guided me with his precious suggestions for maturing my ideas and opinions.

Very special thanks to Fırat Es, Mona Zolfaghari Borra, Yusuf Kasap which assisted and helped me in the materials processing applications part of this study.

I am greatly indebted to my family; in particular to my mother Alev Aydın, my father Hasan Aydın, my brother Ahmet Can Aydın, my aunt Ayfer Gündoğan, my uncle Atila Cindemir for their unconditional love and limitless patience. Also I would like to thank Tolga Tezcan, Onur Kara, Hasan Mert Bozacı, Levent Öztürk, Murat Çalık and Berçin Pınar for their friendship, special effort and interest during this thesis period.

TABLE OF CONTENTS

LIST OF TABLES

TABLES

LIST OF FIGURES

FIGURES

CHAPTER 1

INTRODUCTION

1.1 Brief History and Evolution of Fiber Lasers and Amplifiers

The idea of generating fiber lasers and amplifiers began with the development of fiber optical communication technology. The first fibers which were based on total internal reflection principle [1], were uncladded and so, guiding of light was a problem. After development of the silica cladded fibers in 1950s [2; 3], progress of fiber laser technology accelerated because guiding of light was improved by clads. The cladded fibers enhanced fiber performance and changed the perspective of scientists to fiber optics technology. The first fiber laser cavity was built in 1961 by using a neodymium 3^+ doped fiber [4]. Then, the reduction in required pump power for a laser gain in lasers and amplifiers was first demonstrated in 1960s [5; 6] in which both signal and pump propagated in a small diameter fiber core. However, scientists used a lamp source to pump the laser medium in fibers so it took more than ten years for diode pumps to reach maturity. The development of first ytterbium fiber laser in 1962 [7] showed that ytterbium was less attractive than neodymium as an active ion and thus conversion efficiencies and high output powers became crucial. Fibers with losses less than 20 dB/km were developed and this made them convenient for telecom applications in 1970 [8]. The development of first room temperature operation Nd-doped fiber lasers also made a contribution to progress of fiber lasers and amplifiers in 1970s [9]. Despite progress on different doped type of fibers, laser systems were operating with low conversion efficiency. The progress of fiber clad technology went on by trying different dopants and dopant concentrations to reach high conversion efficiency. After the evolution of diode pumps and developing techniques for producing low insertion loss rare-earth metal doped fibers for 1550 nm wavelength in the late 1970s [10] and with the emergence of optical communications, first erbium doped fiber amplifier was demonstrated in 1987 [11]. In terms of average power, the basic problem was low conversion efficiency of erbium due to limitation of doping concentration of erbium fibers, so development of ytterbium and neodymium doped fibers became crucial for high

average power outputs. The first fiber laser amplifiers, where the pump and signal propagated in a small core, were hard to couple a high power signal and pump light into the core. In addition, single mode diodes which are power limited and expensive need to be used to achieve core pumping method. The cladding pumping technique was developed in order to solve this problem in 1988 [12], which was another significant step forward in the evolution of high average powers of fiber lasers. If the geometry of fiber clad and core are appropriate, doped core can absorb pump more effectively and high optical gain can be produced by active ions in the core. The absorption of pump light of a rare-earth metal double clad was improved by modelling different fiber designs such as D-shaped and rectangular core typed fibers.

The development of cladding pumping technique lead to increase in the average powers gradually since the mid-1990s. After recognition of the potential of ytterbium doped fiber lasers, the first watt-level ytterbium fiber laser was built in 1995 [13]. The deep understanding of thermo optical properties of doped fibers evoked 35 watts single mode ytterbium doped double clad configuration continuous (CW) fiber laser development in 1997 [14]. The first fiber laser above 100 watt average power was built in 1999 with 58% optical to optical conversion efficiency. [15]. Then, the first kW regime fiber laser was reported in 2002 [16] by developing 1 kW ytterbium doped fiber laser with 80% conversion efficiency at the 1.09 μm wavelength. 1.36 kW and nearly diffraction limited fiber laser system was constructed with 83% slope efficiency at 1.1 um wavelength regime in 2004 [17]. The first commercial 10 kW fiber laser, which was planned to weld metal parts, was reported in 2010 [18]. In addition, average power rate and peak power of pulsed fiber laser systems increased at a similar rate. Ultrashort pulsed fiber laser systems which have almost kW peak power can be built with today's technology [19], while the average power range used to be about 100 W in 2005 [20]. 2.2 mJ pulse energy has been achieved in 2011 with 3.8 GW peak power by a fiber chirped amplification system which has sub 500 fs pulses [21]. The rapid development was also seen in nanosecond pulsed fiber laser amplifiers. The kW peak power level nanosecond pulsed fiber laser system, which has 49% optical to optical efficiency, was developed in 2009 [22]. The high pulse energy generating techniques were also developed and 11 mJ fiber master oscillator amplifier was built in 2013 with 660 ns pulse duration [23]. The evolution of the average power of continuous and ultrashort pulsed fiber laser systems are shown in Figure 1.1.

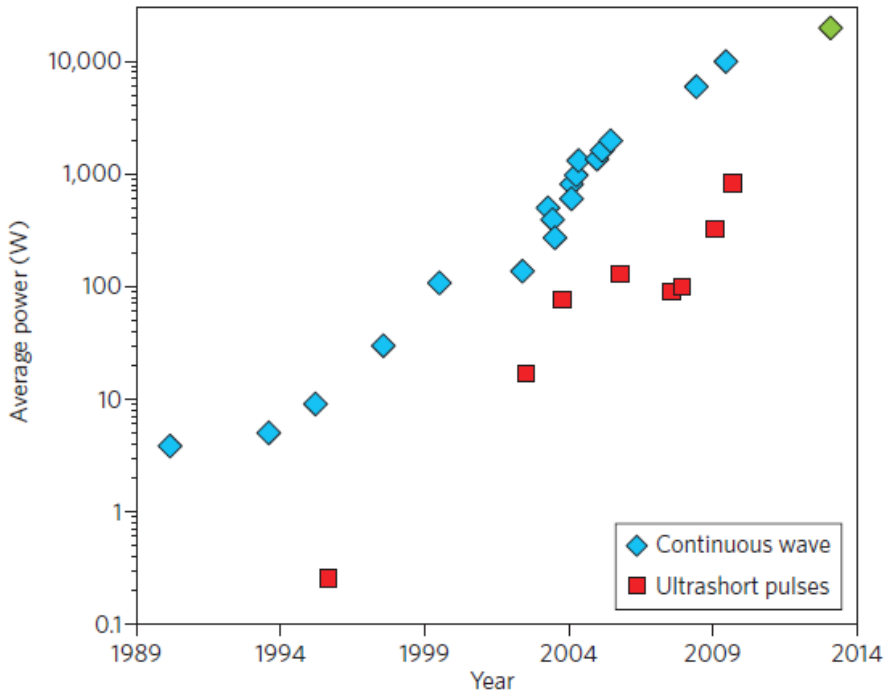

Figure 1.1. Power evolution of the diffraction limited fiber lasers (adopted from [24])

Laser science improves its basic specifications such as average power, peak power, pulse energy and wavelength characterization with improving fiber optic components day by day and fiber lasers represent the latest generation of laser technology. Today, the fundamental loss of fused silica fibers reached down to 0.15 dB/km for 1550 nm. Besides several types of fibers with different doping concentration and geometry and high power fiber coupled diodes, new beam combining techniques, as well as below 35 fs pulses, can be produced [25]. The improvements of fiber laser technology shifted fiber laser usage from being merely a laboratory tool to very welcomed industrial solutions thanks to its high efficiency, good beam quality, high brightness, high power, low noise, low cost, low maintenance requirement, long life time, high reliability and compact size properties. The fiber laser systems have found themselves a broad application range in daily technological practice due to their versatility. . On the one hand, the fiber laser technology can be used as a tool for cutting thick ship body or marking a rocket as a military application, on the other hand it can be used for an eye surgery or micro-machining on a solar cell. While all fiber optic component based developments proceed, new fiber laser based application fields are also discovered every passing day.

There are several techniques used to build a fiber laser amplifier depending on the application but the core technology mainly depends on master oscillator power amplifier design.

1.2 Laser Material Processing

The laser material interaction is one of the ever-growing field of science for years and its progress is parallel to emerging designs of new laser systems. Material processing with lasers has several advantages as compared to traditional methods. Material processing applications with lasers are used since 1960s [26] and demand grows day by day. After invention of new laser types and development in applied sciences and industry in the world, processing of materials with lasers became increasingly important.

Using a laser as a material processor have several advantages. One of the main advantages is the ability to control laser beam and laser energy on the material with high precision. The second main advantage is that the processing techniques with laser are very cost effective since laser processing is non-contact and eliminates tool wearing. Third, it is a chemical free application, that is, it is a clean technique for processing applications. Fourth, it is possible to remove material by adjusting the wavelength or intensity, selective material removal is possible without damaging the under layer. The evolution of the laser material processing accelerated with increasing laser output power levels. The first studies for laser processing applications was made by ruby laser after realizing that it can be used as a good pulsed laser drilling tool. The first attempts to use lasers for material processing took place in mid-1960s. The first pulsed ruby laser for welding applications was demonstrated by Platte and Smith in 1963 to weld a stainless steel foil. Then the first scientific test drilling applications were used for Gillette company to drill razor blades [27]. The first ruby laser was used as an industrial tool by Western Electric to drill wire drawing die in 1965 [28]. After discovering the ability of CO_2 lasers as a cutting tool, 1 mm thick steel was cut by the first oxygen assisted 300 W CO_2 laser. Later, CO_2 lasers were commercially used for scribing ceramics by Western Electric in 1967 [27]. The lasers were considered as a material process tool rather than a simple light source in 1970s. The new techniques and new laser types were developed for industrial applications such as cutting, marking, drilling and welding as the first successful industrialized lasers were produced. The usage of lasers in heat treatment, alloying, glazing and as a thin film

deposition tool started in the early 1980s and accelerated in early 1990s. The studies on high precision material processing has accelerated with development of the high power fiber lasers as an industrial product in the early 1990s. By the invention of fiber lasers, fast, efficient and precise material processing period started.

The material processing with laser is a unique way for a wide range of materials such as metals, ceramics, alloys, polymers, composites and glasses and the laser radiation can be generated as pulsed or continuous wave at various wavelengths, at power levels ranging miliwatts to kilowatts. Processing matter in macroscopic and microscopic scales is also possible by using different properties of laser. There are several types of lasers to perform material processing tasks, which can be listed as marking, cutting, surface treatment, coding, engraving, welding, drilling, rapid prototyping and others. The typical lasers for materials processing are Nd-YAG, CO_2, fiber lasers, excimer lasers, atomic gas lasers, ion lasers, and molecular gas lasers.

CHAPTER 2

THE OPERATION PRINCIPLES OF FIBER LASER COMPONENTS

2.1 Theory of Fiber Lasers and Amplifiers

In this section, theory of the fiber lasers and amplifiers will be discussed in relationship with the components constituting the fiber laser amplifiers.

2.1.1 Optical Fibers

There are several types of fibers available for many different applications. The simplest fiber design can be shown in Figure 2.1. The fiber design which is represented in Figure 2.1 is a step index fiber. The fiber is formed as a fused silica glass core and a clad with different refractive indexes n_1 and n_2 and a coating with refractive index n_3. The refractive index of core is always slightly higher than refractive index of the clad and it is controlled during the manufacturing process by changing amount of dopants in the preform. For instance, while adding zinc sulfide increases the refractive index, adding magnesium fluoride lowers it.

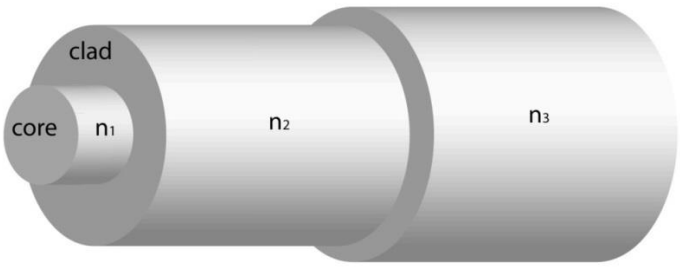

Figure 2.1. The structure of a step index fiber

The guiding of the light occurs inside the fiber by the help of the clad and the guiding is based on the total internal reflection principle (Figure 2.2). The light propagate inside the core and some part of it penetrates into the cladding of the fiber. The protective coating (primary buffer) of the fiber is used to protect glass surface of clad from the external damage and strip away unwanted light inside the fiber and it reduces the internal reflection at the cladding.

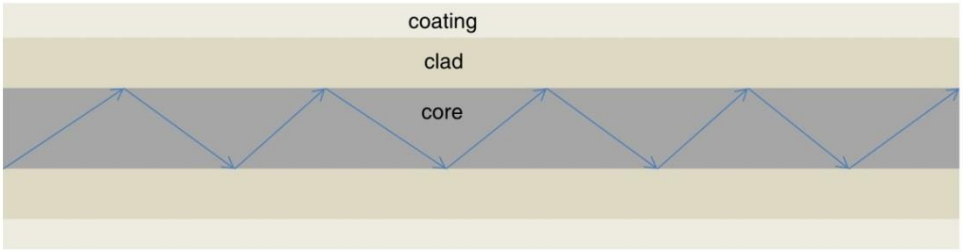

Figure 2.2. The propagation of light inside the fiber

The total internal reflection principle works by the help of index differences of the core and clad of the fiber. The index differences of the core and clad determine the numerical aperture (NA) of the fiber which is a parameter defining how much light can be collected by the fiber (Figure 2.3).

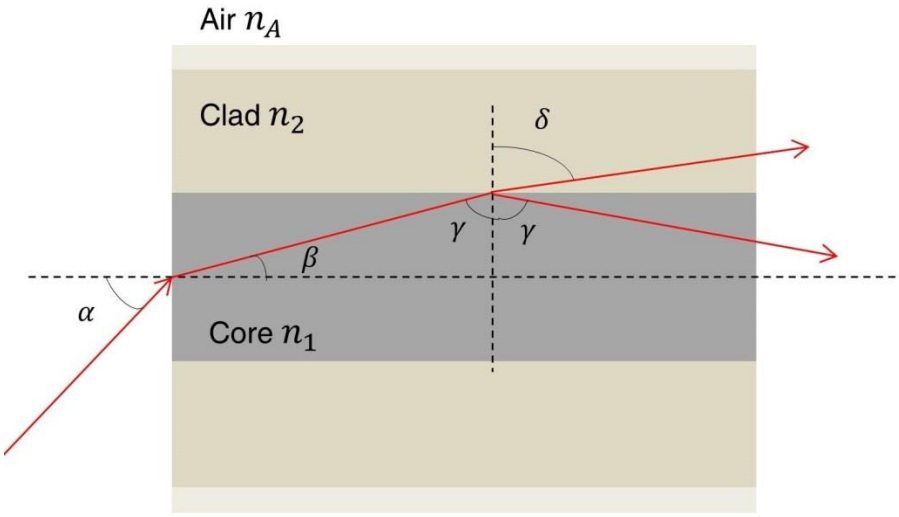

Figure 2.3. Light Propagation for calculating total internal reflection

In fiber end face, critical angle can be calculated by using Snell's law;

$$\mathbf{n_A \sin \alpha = n_1 \sin \beta} \quad (2.1)$$

$$\mathbf{n_2 \sin \gamma = n_2 \sin \delta} \quad (2.2)$$

If the fiber axis is assumed to be perpendicular to the front face and by using the relation $\beta + \gamma = {}^{\pi}/_{2}$ and $\sin\beta = \cos\gamma$;

$$\mathbf{\sin \beta = \sqrt{1 - \sin^2 \gamma}}. \quad (2.3)$$

The maximum acceptance angle for total internal reflection principle is defined by;

$$\mathbf{\sin \delta_{max} = 1 \rightarrow \sin \gamma_{max} = n_2/n_1} \quad (2.4)$$

Inserting Eq. 2.4 in 2.3 and that in 2.1, we can obtain equation as

$$\mathbf{n_A \sin \alpha_{max} = n_1 \sqrt{1 - \frac{n_1^2}{n_2^2}} = \sqrt{n_2^2 - n_1^2}} \quad (2.5)$$

After assuming $n_A = 1$ for air, α_{max} can be defined as

$$\mathbf{\alpha_{max} = \sin^{-1} \sqrt{n_2^2 - n_1^2}} \quad (2.6)$$

The $\sqrt{n_1^2 - n_2^2}$ part of equation is defined as the numerical aperture (*NA*). The maximum acceptance angle for rays propagate from fiber face is given by $\sin \alpha_{max} = NA$.

The number of the guided modes of the fiber is determined by V number which is also called as normalized frequency. In addition, it determines the fraction of the power of the mode in the core of the fiber. The operating wavelength, the core radius and NA of the fiber determine the V number.

$$\mathrm{V} = \frac{\mathbf{2\pi}}{\boldsymbol{\lambda}} \boldsymbol{a}\, \mathrm{NA} \quad (2.7)$$

a is radius of the fiber core and λ is wavelength of the light. If the V number is smaller than 2.405, a single mode propagation is obtained in fiber. The single mode fiber allows to transmit only fundamental mode of light. A multi-mode propagation is seen, if the V number is higher than 2.405. For multi-mode fibers, loss of propagation in the core is higher than single-mode fibers due the high numerical aperture. They allow guiding of different wavelengths of light. Multi-mode fibers have much higher V numbers and the number of supported modes for a multi-mode step index fiber can be approximated as;

$$M \approx \frac{4}{\pi} V^2 \tag{2.8}$$

2.1.2 Ytterbium Doped Silica Fibers

Ytterbium is a rare-earth metal and has a number of interesting properties for the fiber laser amplifiers especially for high power applications. Using a rare-earth metal doped fiber in a fiber laser amplifier provides low noise, high power output, broad gain bandwidth, high beam quality, tunability, narrow linewidth and low cost design.

Absorption and emission cross section of ytterbium are very broad and absorption spectra allows wide range of wavelength to pump. It has a very simple electronic structure with a ground state manifold ${}^2F_{7/2}$ with three Stark sub-levels and an excited manifold ${}^2F_{5/2}$ with four Stark sub-levels. The energy gap between the ground and the exited state is large (Figure 2.4) and this situation prevents nonradiative decay by way of multiphoton emission from exited manifold even in a small sized high energy silica material, hence the fibers doped with ytterbium element allows very high power efficiencies of fiber laser amplifiers. They also have lower thermal effects than other laser gain medias due to small quantum defect of ytterbium element, so the heating effect of such media is three times smaller than Nd-YAG [13]. Moreover, the ytterbium doped gain media has a longer relaxation time than other types of media, thus lower threshold pump power may be adequate for signal gain.

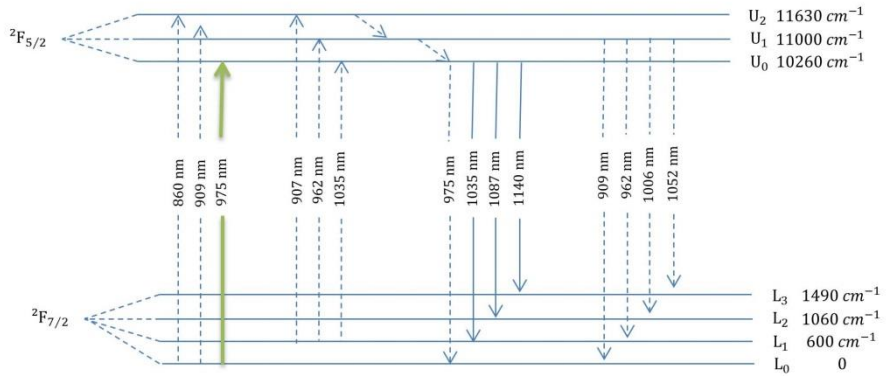

Figure 2.4. Energy level structure of ytterbium ion.

The emission spectra of ytterbium doped fibers depends on composition of host glass [27]. The emission and absorption cross-sections of ytterbium doped germanosilicate glass are shown in the Figure 2.5 and cross-sections can vary depending on the content of host glass composition. The local maxima of cross-sections of ytterbium is at 975 nm and 910 nm. The first absorption peak of the ytterbium ion is 975 nm which represents zero-line transition between the lowest levels of higher state and lower state. The laser dynamics at 975 nm wavelength is three level since the emission is based upon a transition to the lowest Stark level. The other peak at 910 nm has broad cross-section where high power pumping is required to get high gain since the absorption is three times lower than 975 nm cross-section. Hence, while pumping at 910 nm, longer fiber should be used to achieve same output power as in the case of 975 nm.

While the lifetime of the Yb^{+3} in excited state for a pure silicate glass is 1.5 ms, it is 0.8 ms for a germanosilicate glass since higher germanium content in the core tends shorten lifetimes. The situation affects the performance of a master oscillator power amplifier (MOPA) system which typically operates at kHz levels since lower repetition rate means higher spontaneous emission.

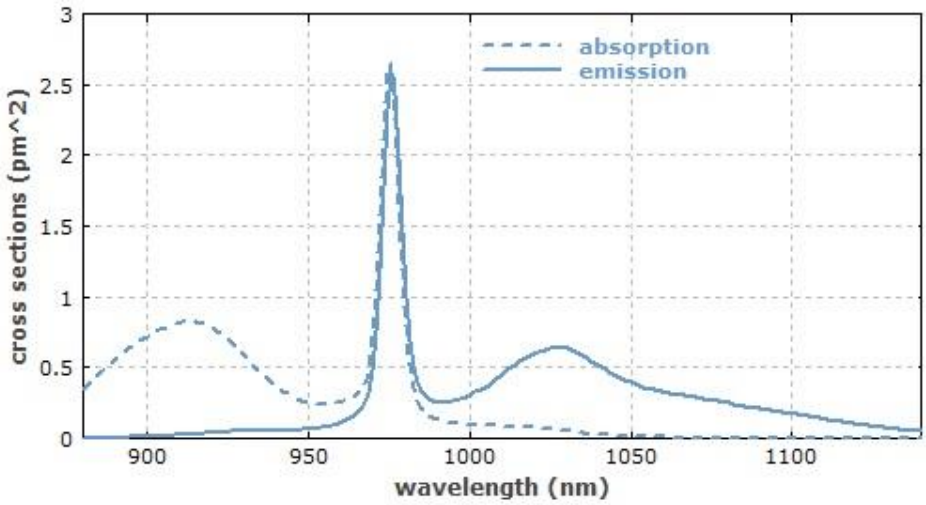

Figure 2.5. Emission and absorption cross-sections of ytterbium doped germanosilicate glass as used in the cores of ytterbium doped fiber.

2.1.3 Double-Clad Fibers

After the development of the double-clad fibers, achieving high power output by a fiber laser amplifier became possible since pumping a single clad fiber with high pump levels is extremely difficult. The powers for pumping a single mode fiber are limited below 1 W. The development of the fiber coupled multimode diodes lead to reach more than 100 W pump power by a single emitter. The cladding pumping technique with double clad fibers became essential to transfer high pump power into the small core of the fiber. The design of a double clad fiber can be seen in Figure 2.6 where the outer cladding with lower refractive index than inner cladding and core. The low numerical aperture of core leads to a single mode propagation inside the core and the high numerical aperture and greater than hundred micrometers of inner clad supports in a large number of modes. To increase the pump absorption in a double clad fiber, different fiber geometries such as offset-core, octagonal, D-shaped and square can be used.

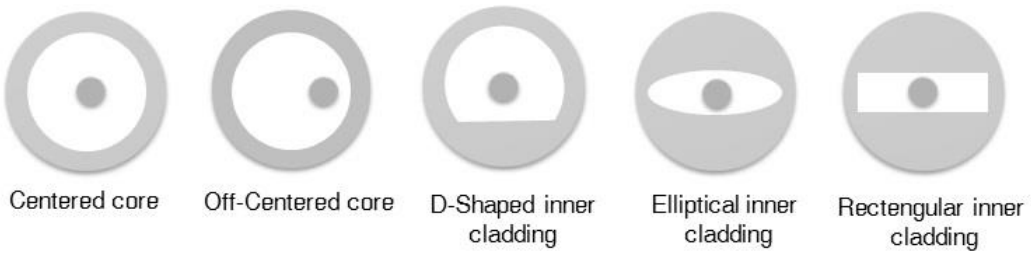

Figure 2.6. Cross sections of different type of double clad fibers.

While outer cladding is designed in various kinds of shapes, the inner cladding is designed so that non-circular profile can be used to increase the absorption of pump light in the core by light reflections. In this study, centered core fibers were used in the amplifier design of the fiber laser system since splicing with centered core to centered core is easier and more reliable than splicing of two different geometries.

2.1.4 Large Mode Area Fibers

The maximum output power of a fiber laser system is determined by the number of supported modes of the fiber and the bending loss. To increase the energy in a fiber and reduce the nonlinear effects in a single-mode fiber, it is essential to increase the mode area of the fiber. When core diameter of a fiber increases, the number of modes in amplifier also increases. The single mode fibers can maintain low maximal pump powers and thus are limited in reaching high output powers. Therefore, large mode area (LMA) fibers are used to achieve high power with diffraction limited beam output. The LMA fibers are produced in a range of 15 μm to 40 μm core size with NAs around 0.07. The fibers are designed with low core NA to decrease the refractive index difference between the core and the cladding of the fiber. To achieve single mode operation, high powers and low nonlinear effects, LMA fibers should be preferred in a fiber laser systems.

2.1.5 Gain and Laser Amplification

There are several rare earth elements used in developing optical gain in a fiber laser but ytterbium makes difference because of availability of low cost industrial pump

sources and emission spectrum. The gain dynamics of the rare earth element doped fibers is similar although they have different emission and absorption spectra and applications. The gain dynamics can be categorized into three groups, such as two level, three level and four level systems. The two level laser medium cannot be used for light amplification since probability of pumping the ions into higher energy state is equal the probability of stimulating them back down. The three and four level system are illustrated in Figure 2.7.

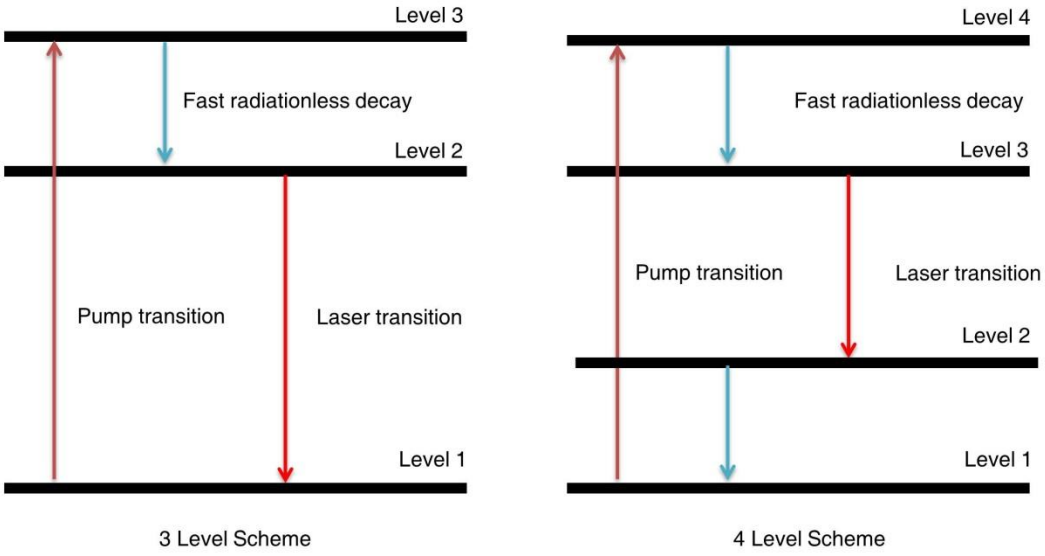

Figure 2.7. Illustration of three and four level lasing

In both three and four level lasing, rare earth ions are excited to higher energy levels via the absorption of high energy pump photons. This process is known as "pumping". The higher state is a short-lived state, so ions rapidly decay to lower energy state which is also called a metastable state, without radiation just after the pumping process. The energy which is achieved in higher energy levels is used to amplify signal by stimulated emission. The amplification achieved via transfer from pump to signal. The difference between three and four level system is in type of the final energy state of ions after the stimulated emission process. The process ends up in the ground state for a three-level system, while it ends up at an excited state in a four-level system. Higher population density in the upper energy level is required for both of the systems, accordingly so high pump power is a necessity.

In this study, ytterbium doped gain media is used to amplify signals where ytterbium has a three level lasing scheme. Rate equations are very important to understand the amplification behavior of this type of systems. Ytterbium based fiber laser amplifier theory was first discussed for rare-earth metal doped fiber lasers for a shorter emission wavelength in 1994 [28]. In this thesis, a ytterbium doped media will be discussed and it can be modeled by pump excitation and de-excitation rates and seed absorption and emission rates. A two-level laser scheme can be used to model 976 nm ytterbium fiber laser pumping. The Figure 2.8 shows an energy diagram of a two level system where excitation and de-excitation rates of pump are indicated as R_{12} and R_{21} respectively, signal absorption and emission rates are W_{12} and W_{21}respectively. A_{21} is the spontaneous emission rate.

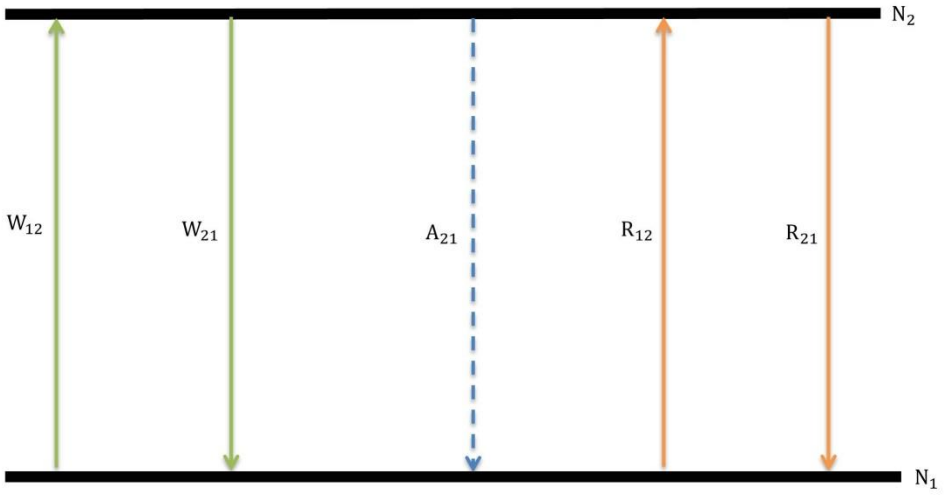

Figure 2.8. Energy levels for a two level system.

The rate equations can be written by indicating population densities as N_1, N_2 for lower and upper state respectively.

$$\frac{\boldsymbol{dN_2}}{\boldsymbol{dt}} = (\mathbf{W_{12}} + \mathbf{R_{12}})\mathbf{N_1} - (\mathbf{W_{21}} + \mathbf{R_{21}})\mathbf{N_2} - \mathbf{A_{21}}\mathbf{N_2} \qquad (2.9)$$

$$\frac{dN_1}{dt} = -(W_{12} + R_{12})N_1 + (W_{21} + R_{21})N_2 + A_{21}N_2 \qquad (2.10)$$

Where $N_1 + N_2 = 1$ by the energy conservation law and $dN_i/dt = 0$ for steady state conditions so;

$$N_1 = \frac{W_{21} + R_{21} + A_{21}}{W_{21} + W_{12} + R_{21} + R_{12} + A_{21}} \tag{2.11}$$

$$N_2 = \frac{W_{12} + R_{12}}{W_{21} + W_{12} + R_{21} + R_{12} + A_{21}} \tag{2.12}$$

where the spontaneous emission rate is depend on the life time of the Yb ions (τ) in upper level and can be shown;

$$A_{21} = \frac{1}{\tau} \tag{2.13}$$

The absorption and emission cross section of Yb ion in the fiber core determine the signal and pump transition rates of system and can be defined as;

$$W_{12} = \frac{\sigma_{as} I_s}{h v_s}, \qquad W_{21} = \frac{\sigma_{es} I_s}{h v_s}, \tag{2.14}$$

$$R_{12} = \frac{\sigma_{ap} I_p}{h v_p}, \qquad R_{21} = \frac{\sigma_{ep} I_p}{h v_p}, \tag{2.15}$$

where I_s and I_p are corresponding intensities for signal and pump respectively with transition frequencies of signal v_s and transition frequency of pump hv_p. σ_{as} and σ_{ap} are the absorption of signal and pump cross sections respectively. σ_{es} and σ_{ep} are the emission of signal and pump cross sections respectively. The pump and signal power variations can be expressed for a two level system. The propagation equation of the pump and signal along the fiber is defined in equations Eq. 2.16 and Eq. 2.17 respectively;

$$\frac{dP_p}{dz} = I_p N_t(\sigma_{ep} N_2 - \sigma_{ap} N_1) P_p(z) \tag{2.16}$$

$$\frac{dP_s}{dz} = I_s N_t(\sigma_{es} N_2 - \sigma_{as} N_1) P_s(z) \tag{2.17}$$

In the equations above, N_t is the ion density and $\lceil_p$ and $\lceil_s$ are pump overlap factor and the signal overlap factor respectively. $\lceil_p$ can be defined as equation

$$\frac{S_{pc}}{S_d} \tag{2.18}$$

where S_{pc} is area of the pumping core and S_d is doped area of the gain and $\lceil_s$ is the overlap of mode field with doped media. The small gain coefficient $g(z)$ can be defined by using propagation of seed equation as;

$$g(z) = I_s N_t(\sigma_{es} N_2 - \sigma_{as} N_1) \tag{2.19}$$

2.1.6 Limitations of the amplifier

To develop a reliable and durable fiber laser amplifier, many physical limitations should be eliminated and experimental outputs should be monitored accurately. Since the light propagates in a very small mode size and long nonlinear medium, encountering nonlinear effects is inevitable in a fiber laser amplifier. Moreover, damage thresholds of the components and thermal limitations, splice losses and photodarkening are the other main factors which affect the performance of the amplifier. In this section, the limitations which affects reaching high pulse energy and power in a nanosecond pulsed fiber laser amplifier will be explained.

The power density of electromagnetic field is very high in an optical fiber since the laser signal propagates in the order of micron size. Moreover, the cavity length of a laser system can be very long, thus the fibers exhibit a variety of nonlinear effects. The

nonlinear effects such as stimulated Raman scattering, stimulated Brilluion scattering and the Kerr effect play an important role in the performance of a high power fiber laser system, especially during high power and high pulse energy operation.

The interaction of light with acoustic phonons, which results in a frequency shift, lead to stimulated Brillouin scattering (SBS) in narrow linewidth fiber laser amplifiers. SBS can be observed even in very low power levels [29]. The scattered photons propagate in the opposite direction of the pump photons by the reason of conservation of momentum principle. If a narrow pulse is used in an fiber optical system and annihilation of signal is neglected, the threshold of SBS can be expressed as,

$$P_{CR} = 21\frac{A_{eff}}{g_B L_{eff}} \tag{2.20}$$

where g_B is the Brillouin factor and it is equal to 5×10^{-11} m/W for a typical doped silica fiber [30], P_{CR} is the critical power where Brillouin scattering occurs, A_{eff} is the effective mode area of the fiber, L_{eff} is the effective fiber length. The effective fiber length depends on attenuation coefficient of the fiber α_p and can be expressed as

$$L_{eff} = \frac{1}{\alpha_p}[1 - e^{-(\alpha_p L)}]. \tag{2.21}$$

Stimulated Raman scattering (SRS) is an inelastic scattering and it is observed due to scattering of photons by optical phonons. In SRS process, forward and backward scattering can be observed and it limits the average power of pulsed fiber laser systems. It is observed in fiber laser amplifiers while pumping a gain to amplify signal. The peak of the Raman gain is 1×10^{-13} m/W for 1 μm wavelength. The same approach with equation 2.20 can be used to calculate threshold power for SRS,

$$P_{CR} = 16\frac{A_{eff}}{g_R L_{eff}} \tag{2.22}$$

where $g_R$is the Raman factor and equal to 3.2×10^{-13} m/W for silica [29].

Four-wave mixing (FWM) is another nonlinear effect which occurs when at least two different wavelengths propagate in an optical fiber. In a fiber laser amplifier, FWM can be defined as noise generation by energy transfer of pump to signal. FWM increases the noise of the amplifier and affects the performance of fiber laser amplifiers. If we assume that at least two incident different wavelength v_1 and v_2 where $v_2 > v_1$ propagate in an optical fiber, they interact with each other and create two new wavelengths v_3 and v_4 at different frequency by the following equations.

$$v_3 = v_1 - (v_2 - v_1), \tag{2.23}$$

$$v_4 = v_2 + (v_2 - v_1). \tag{2.24}$$

The refractive index in a non-linear optical medium, depends on the optical intensity and, can change at higher intensities. The change in refractive index of a material is referred as Kerr effect. Self-phase modulation (SPM) and cross-phase modulation are refractive index changes due to nonlinear effects. SPM occurs at high optical intensities and can be described by

$$n' = n + n_2 I, \tag{2.25}$$

where n_2 is the nonlinear index coefficient and I is the intensity inside the fiber. In this equation, $n' - n$ is nonlinear change in the refractive index. In SPM, when the refractive index of the medium increases, a phase shift in the pulse is observed. Cross-phase modulation (XPM) effect is also an optical phase shift in a light beam as SPM, however it is induced by changing a phase of a wavelength by another wavelength. SMP and XPM can be suppressed in a fiber laser amplifier by increasing the mode field diameter of the fiber.

Photodarkening is a transmission loss effect in the gain medium of amplifier in fiber lasers and it affects the long term reliability of system. In a doped media, the reversible absorption centers can be created in time via irradiation of light at a certain

wavelengths, hence transmission losses of the doped medium may increase. The higher doping concentration causes more reversible absorption centers, so choosing low doping concentration fibers is a solution to eliminate photodarkening affect.

Efficient light confinement in the core of a double clad fiber is another important factor in high power fiber lasers in constructing a good fiber amplifier, hence a good cladding strip operation is necessary to protect coating of the fiber. If residual pump light propagates in a double clad fiber, it can damage coating of the fiber or laser components even at low powers in time. The cladding pump can be eliminated from the fiber by using cladding pump strippers. The thermal effects on the fiber coating should be managed in order to maintain a long term high power output from the amplifier.

2.1.7 Amplified Spontaneous Emission

The physical and quantitative understandings of noise (or parasitic background) in an optically amplified system play an important role to optimize the fiber devices. Amplified spontaneous emission (ASE) is a type of noise that is caused by spontaneous de-excitation in an active media. After population inversion process, the excited ions without any coherence property can be generated while they turn back to the ground state without stimulation. The generated spontaneous emission gets amplified in forward and backward direction while it travels through the gain medium. All optical energy is consumed into ASE while pumping a system, if there is no input signal. ASE can reach high power level and saturate the gain of laser. There are several parameters that effect the ASE rate in a fiber amplifier system, such as doping concentration of gain media and length, signal and pump power, pump wavelength and repetition rate. ASE is one of the most dominant noise in a tens of kHz repetition rate MOPA design fiber laser amplifier that affects the performance of the system because ytterbium ion has 0.8-1 ms lifetime in its excited state.

ASE can be modeled by using equation of the number of the randomly polarized photons $dn(v)$ between the ν and ν+δν frequencies as [31];

$$dn(v) = A_{21} g(v) \delta(v) \frac{\Delta\Omega}{4\pi} dV \int_s N_2(r,\theta)\, \psi_s(r,\theta) r\, dr\, d\theta \qquad (2.26)$$

where A_{21} is the spontaneous decay rate which is equal to $1/\tau$. The lineshape function is defined as $g(v)$, $\frac{\Delta\Omega}{4\pi}$ is the spontaneous emission ration in the fiber and the volume element $dV = \pi w_s dz$. The overlap between the density distribution of excited ions and guided mode expressed in the integral where N_2 is the excited state populations, $\psi_s(r,\theta)$ is the mode envelope and (r,θ) represents cylindrical transverse coordinates.

The spontaneous emission power per unit frequency can be found by $dP_{SE} = hvdn(v)$ and creation rate of the spontaneous emission power in bandwidth δv is;

$$\frac{dP_{SE}}{dz} = 2P_0 \sigma_e(v) \int_s N_2(r,\theta)\, \psi_s(r,\theta) r\, dr\, d\theta \qquad (2.27)$$

where the power of one spontaneous photon in a bandwidth of δv is P_0.

2.1.8 Master Oscillator Power Amplifier (MOPA) Configuration

The master oscillator power amplifier is a type of fiber laser configuration where the power amplifier is designed via fiber based components. In this design, there is a low power laser seed which is increased to high power levels by rare-earth metal doped fibers and high power pump diodes. MOPA configuration provides higher output power levels, higher beam quality and higher efficiency than other type of bulk lasers. In a pulsed MOPA system, pulse width of the seed is modulated externally and the doping gain is pumped by a CW or pulsed pump source for achieving high power levels. The main advantages of MOPA based fiber laser systems are independent and flexible control of pulse width and repetition rate via external modulation. Moreover the systems can be designed as pulse shape tunable and upgradable to higher output powers. Simple schematic of a fiber MOPA system can be seen in Figure 2.9.

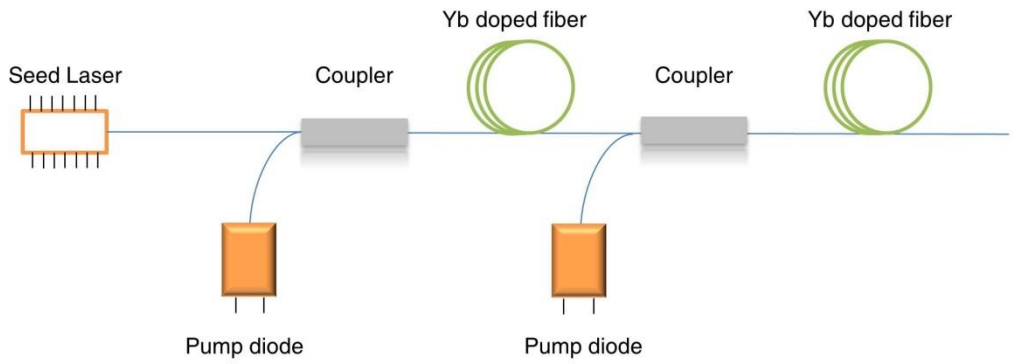

Figure 2.9. Schematic of a fiber MOPA system

The fiber MOPA system configuration can be as Figure 2.9 where fiber laser diode is used as a master oscillator. Then an amplifier, which is pumped by a pump diode, is constructed after oscillator stage to amplify seed laser. The seed signal and pump are combined via a fiber coupler then ytterbium doped fiber is used to create a gain. The amplification of the system can be raised by using another amplifier with ytterbium doped fiber and pump diode, hence the MOPA system can be formed by using several amplifier stages.

Despite the advantages of MOPA systems, their construction is more complicated than Q-switched lasers which are the other most type of pulsed fiber lasers. However, Q-switched fiber lasers are not flexible in their design. Moreover, changing of pulse duration and repetition rate is not possible independent of each other in a Q-switched fiber laser.

CHAPTER 3

PHYSICAL MECHANISM BEHIND LASER MATERIAL PROCESSING

The effect of laser radiation effects on matter can be studied in several aspects such as, electromagnetic, thermodynamic and optical interactions. After illuminating a material with laser beam, the energy of the beam is transformed into electronic excitation energy. After transforming process, by collisions between the lattice of material and that of electrons, energy is transferred to the lattice. The energy of laser affects the material in several ways such as ionization, temperature rise, vaporization and gasifying. The interaction of laser and material can be described in a simple way by using heat flow model which is represented in Figure 3.10. Here heat flow can be assumed to happen in z axis and radius of the spot is larger than the penetration depth. The diameter of the collimated beam is represented as D, focal length of the lens after focusing on a material is f, the spot size is $2w_0$.

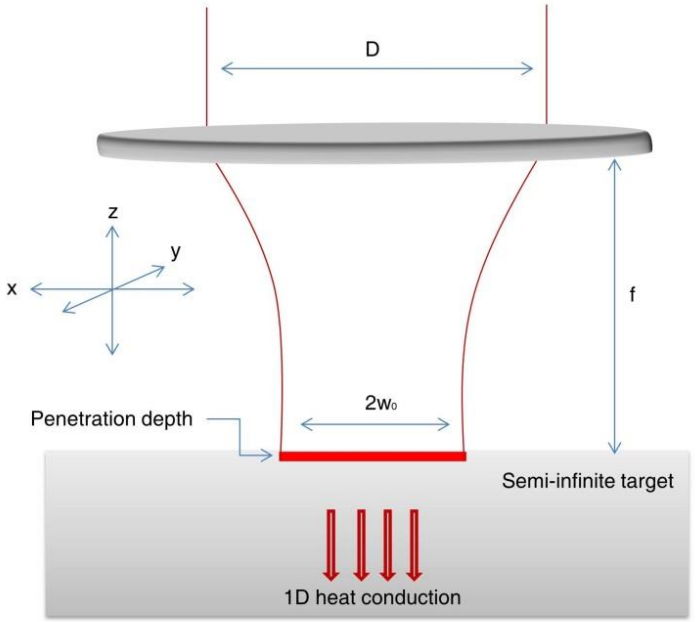

Figure 3.10. A simple laser – material interaction model

There are several parameters which affect the processing of the material with lasers. First, the material characteristic is important with specific property such as thermal diffusivity, thermal conductivity, temperature and heat of vaporization. The reflectivity of the material has a dependency on frequency of the laser radiation and temperature of the material. While many metals such as Ag, Au, Cu, Al have reflectivity higher than 0.8 in processing with Yb doped fiber laser at 1 μm wavelength, it decreases with increasing temperature. Thermal diffusivity and conductivity also affect the processing of the material. For instance, while processing a poor conductor with a 1 μm laser, local temperature becomes higher than high thermal conductor material like steel especially in high power laser applications. Moreover, removing materials from the laser application surface depends on the heat and temperature of vaporization. The higher material vaporization temperature and heat is, the better the material removal.

The other parameters for material processing with laser are depth of focus, intensity profiles, beam quality and beam diameter (beam spot size). The intensity profile of a laser beam can be divided into two groups as spatial and temporal profile intensity. Spatial distribution of power density can be defined as the intensity difference as a function of distance from the center of the beam, in a plane perpendicular to its direction of propagation. Temporal profile can change from CW operation to ultrashort pulses with very high repetition rate. Beam quality, beam diameter and depth of focus affect the process of material and they can be shown mathematically by using beam equation. For instance, if a collimated laser beam is focused to a material by a lens with a focal length f and diameter D, the beam radius w_z at a z distance from the focal plane in agreement with ;

$$w_z = w_0 \sqrt{1 + [\frac{M^2 \lambda_z}{\pi w_0}]^2} \tag{3.1}$$

where w_0 radius of waist, λ is the wavelength of laser beam and M^2 is the beam quality of the laser beam. The spot size of the laser for the equation 3.1 is $2w_0$ and shown as ;

$$2w_0 = \frac{4f\lambda}{\pi D} \tag{3.2}$$

The depth of focus (DOF), which is the distance where diameter of the beam continues smaller than $\sqrt{2}$ times the laser spot size, is represented as;

$$\frac{8\lambda f^2}{\pi D^2} \tag{3.3}$$

3.1 Physical Processes

The laser material interaction subject requires good background knowledge from different disciplines. The interaction processes of laser beam with material are absorption, reflection, transmission and scattering (Figure 3.1)

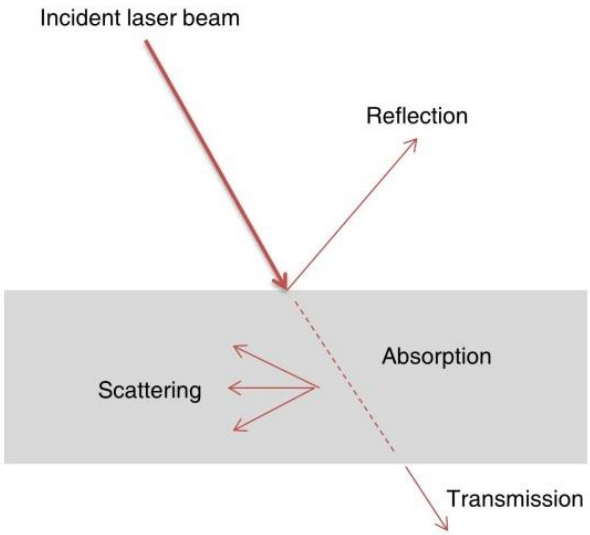

Figure 3.1 Laser light interactions with materials

The first interaction process of light with a metallic material is the reflection. After reflection process, much of laser energy is transferred to the material as a result of absorption. The absorption can be explained as an interaction of free or bound electrons of material with electromagnetic wave. The electromagnetic radiation and material interaction are mostly due

to the electrons of the material since nuclei are heavy to peruse high frequency of the laser radiation. The penetration depth of the metal for 1064 nm wavelength laser is typically about 10 nm. There are various effects occurring in material due to absorption. The basic effects for high power material processing are heating, vaporization, plasma formation and melting. When electromagnetic radiation passes by the electrons of the material, it induces a force to set electrons into motion by electric field. The exerted Lorentz force can be expressed as [32];

$$F = e\mathrm{E} + e(\frac{v}{c} \times \mathrm{H}) \tag{3.4}$$

where v is the velocity of electron, c is the speed of light. If we consider that electric field and magnetic field have same energy, the addition of magnetic field to the exerted force is less than that of electron field due to the factor of the order of v/c according to equation 3.4, thus the term eE is an important term for the equation above. The radiation absorbed by the material results in an extra energy of the charged particles. The extra energy can be kinetic energy of the free electrons or excitation energy of the bound electrons. Then, the heat generation occurs due to the degradation of the localized and ordered excitation energy. The absorption process for laser-material interaction can be expressed as equation;

$$I(z) = I_0 \mathrm{e}^{-\mu z} \tag{3.5}$$

where the expression known as Beer-Lambert law and $I(z)$ shows intensity of radiation at depth z, I_0 is the incedence intensity, μ is the absorption coefficient. As shown in the equation 3.5, intensity of the radiation of the laser attenuated through the material. The most of the attenuation of laser radiation appeared in a critical length as known as attenuation length L and it can be expressed as$L = 1/\mu$. The absorption coefficient for a high absorptive material is about 10^5 cm^{-1} and attenuation length is about 10^{-5} cm^{-1} [33].

The absorptivity and reflectivity are another important factors which effect laser material processing. The absorptivity of the material is an absorbed incident radiation at normal incidence. Absorptivity (A) and reflectivity are complimentary and they are related for opaque materials as in;

$$A = 1 - R \tag{3.6}$$

Absorptivity and reflectivity calculations can be done by using the complex refractive index (n_c) which depends on extinction coefficient and refractive index of the material and can be expressed as $n - ik$. The extinction and refractive index of the materials depend on the laser radiation wavelength and temperature of the material so reflectivity of the material is influenced by these two parameters and it can be expressed as;

$$R = \frac{(n-1)^2 + k^2}{(n+1)^2 + k^2} \tag{3.7}$$

The variation of absorption with the wavelength of common metallic materials can be shown in Figure 3.2. As shown in the figure, the absorption of the material generally decreases with increasing wavelength. The situation is opposite for the reflectivity. Hence, materials are less reflective at shorter wavelength lasers. The materials which are irradiated by a fiber laser are absorbed strongly than CO_2 laser but dependence of wavelength for absorption can be used only as a guidelines since there are several factors effecting absorptivity. For instance, the reflectivity generally decreases while temperature increase, thus a material can become high absorber for high temperature while it is a high reflective at low temperature. This important situation shows that the increasing temperature of the surface of the material occurs in while processing the materials with lasers.

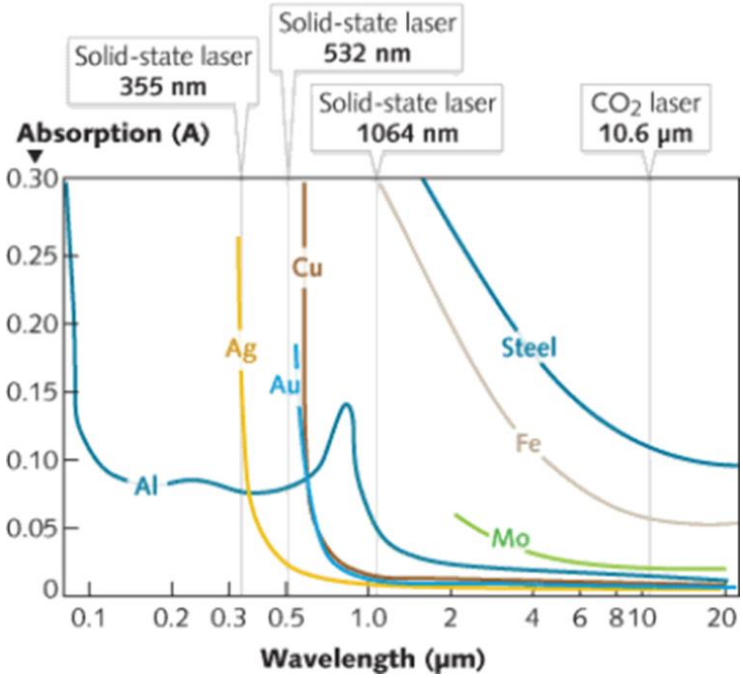

Figure 3.2 The absorption of laser output at different wavelengths varies according to the materials involved (adopted from [34])

The material which interacts with laser absorbs energy of the laser beam and then, absorbed energy is transformed into heat by reduction of primary localized and ordered excitation energy levels. The relaxation times of excitation energy levels are about 10^{-13} s for metals. After the conversion of the laser energy into the heat, the conduction process and temperature sharing occur. During the material process, the degree of the temperature and ionization of the vapor create physical effects in the material such as heating, vaporization, melting, plasma formation and ablation. (Figure 3.3)

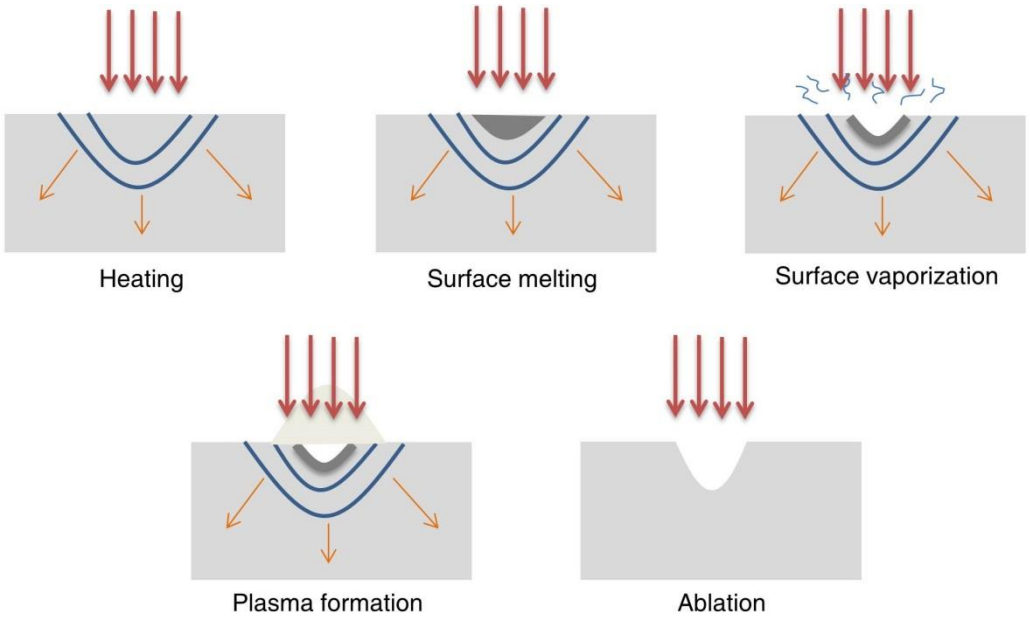

Figure 3.3 Effects after interaction of lasers with material. Orange arrows indicate heat conduction.

The physical effects can be categorized into three groups as thermal effects, plasma effects and ablation.

3.1.1 Heating

Heating process can be discussed by evaluating temperature distribution. The analysis of the thermal behavior of the material can be solved via using one-dimensional heat conduction equation which is indicated by Jager and Carslaw in 1959 [35]. In thermal analysis, material is assumed as homogeneous, the temperature of the material is constant at the beginning, heat is uniform during the radiation-material interaction and losses due to radiation and convection are negligible. If we assume that a temperature T is applied to location z, the heat transfer equation after time t can be shown as;

$$\frac{\partial T\ (z,t)}{\partial t} = \alpha \frac{\partial^2 T(z,t)}{\partial z^2} \tag{3.8}$$

where α is thermal diffusivity.

The laser irradiation scheme for initial, heating and cooling times can be seen in Figure 3.4.

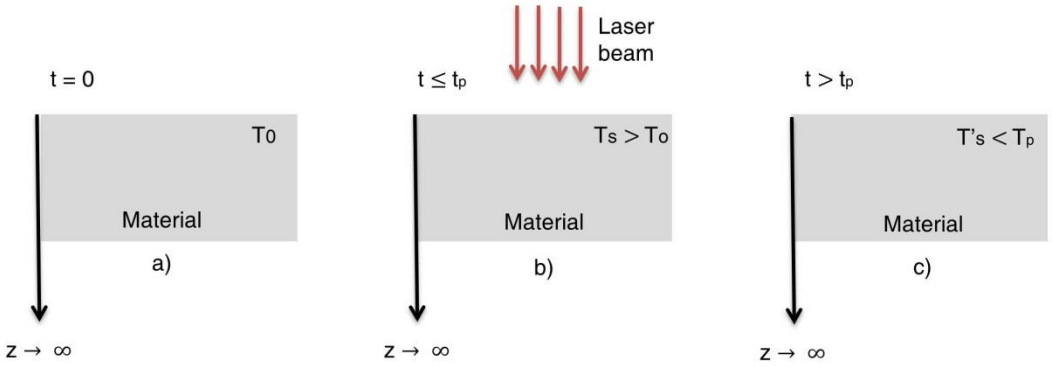

Figure 3.4 Laser interaction with matter at different times: a) Initial condition where temperature is uniform, T_0, b) Laser heating process where surface temperature T_s is higher than initial temperature T_0, c) Cooling of the material after laser off.

The initial condition of the temperature at $t = 0$ can be written as;

$$T(z,0) - T_0 \text{ where } z \geq 0 \tag{3.10}$$

If we assume that, energy of the laser beam which is absorbed by the material surface is equal to conducted energy, boundary condition at the surface can be written as;

$$\delta E_{abs} = -k \frac{\partial T(0,t)}{\partial z} \tag{3.11}$$

where E_{abs} absorbed energy by the material, k is the thermal conductivity. The equations during the heating and cooling can be obtained. If the laser is on, the irradiation time $t_p \geq t$ and if there is no any laser-material interaction, $t > t_p$. While laser is on, $\Delta T(z,t)_{t<t_p}$ can be defined as;

$$\frac{E_{abs}}{k} (4\alpha t)^{\frac{1}{2}} \text{ ierfc} \left(\frac{z}{(4\alpha t)^{\frac{1}{2}}} \right) \tag{3.12}$$

$$\frac{2E_{abs}\alpha^{\frac{1}{2}}}{k}\left[t^{\frac{1}{2}}\,\text{ierfc}\left(\frac{z}{(4\alpha t)^{\frac{1}{2}}}\right)-\left(t-t_p\right)^{\frac{1}{2}}i\text{erfc}\left(\frac{z}{\left(4\alpha\left(t-t_p\right)\right)^{\frac{1}{2}}}\right)\right] \tag{3.9}$$

In Eq. 3.12, $i$erfc(x) is the where ierfc is the integral of the complementary error function and it can be written as ;

$$\text{ierfc (x)} = \frac{1}{\sqrt{\pi}}\left\{\exp(-x^2) - x\left(1-\frac{2}{\sqrt{\pi}}\int_0^x e^{-\xi^2}d\xi\right)\right. \tag{3.13}$$

At $z = 0$, for the equations 3.12 and 3.13, temperature of the surface while cooling and heating of the material can be obtained;

$$\Delta T(0,t)_{t<t_p} = \frac{E_{abs}}{k}\left(\frac{4\alpha t}{\pi}\right)^{1/2} \tag{3.14}$$

$$\Delta T(0,t)_{t<t_p}\,\frac{E_{abs}}{k}\left[\left(\frac{4\alpha t}{\pi}\right)^{1/2} - \left(\frac{4\alpha(t-t_p)}{\pi}\right)^{1/2}\right] \tag{3.15}$$

3.1.2 Melting

Depending upon the material, the surface temperature of the material which interact with laser may reach the melting or boiling point at high or low power densities. The melting and boiling thresholds are very critical while processing a material with high power laser. After reaching melting temperature, the material stops raising its temperature, then it gains an energy to melt a volume V_{melt} and energy equation can be described as;

$$E_{melt} = H_f \rho V_{melt} \tag{3.16}$$

where H_f is the heat of fusion and ρ is density of the material. Hence, at an initial temperature T_i, energy for melting a volume of material V is;

$$E = E_{melt} + (T_m - T_i)C_p\ \rho V \tag{3.17}$$

where C_p is the specific heat and T_m is the melting temperature of the material. The maximum depth for a melting applications with constant pulsed lasers increases while laser power density increases (Figure 3. 5a). If the pulse time of the laser increase at constant laser power density, the depth of melting increases (Figure 3. 5b)

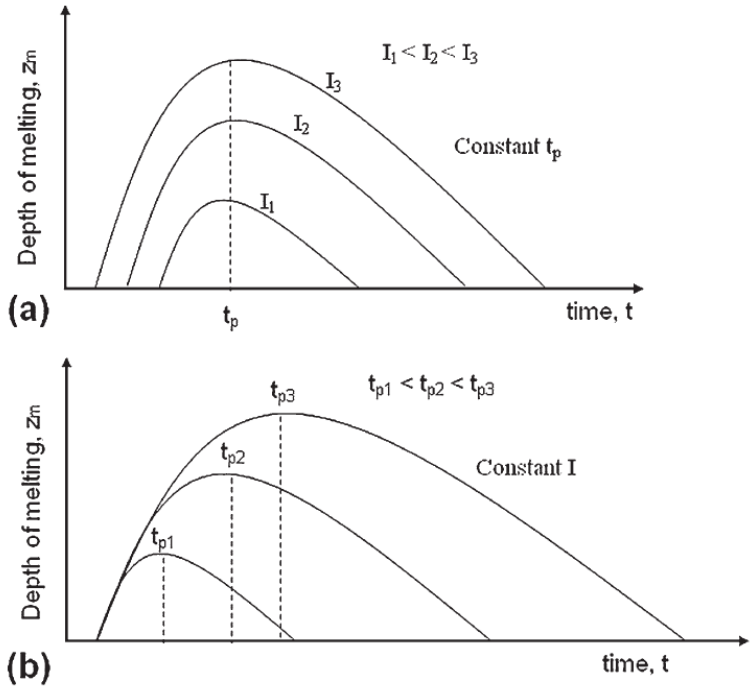

Figure 3. 5 The melting depths for pulsed laser applications. a) At constant pulse widths b) At constant power density (adopted from [36])

3.1.3 Vaporization

The depth of melting of the material is limited by the maximum surface temperature of the material so it is not possible to increase it to an infinitely large value

with high laser density. The maximum value of depth of melting Z_{max} is occured while temperature of the material reaches the boiling point. Z_{max} can be calculated while temperature at melting point T_m by;

$$T_m = \frac{E_{abs}}{k}(4\alpha t)^{\frac{1}{2}}\,\text{ierfc}\left(\frac{Z_{max}}{(4\alpha t)^{\frac{1}{2}}}\right) \tag{3.18}$$

If the temperature reaches boiling point of the surface of the material, T_b can be calculated by;

$$T_b = \frac{E_{abs}}{k}\left(\frac{4\alpha t}{\pi}\right)^{1/2} \tag{3.19}$$

The laser beam cause a liquid-vapor interface in order to move inside the material, after vaporization is achieved at the surface. Then, material removing from the surface above the interface of liquid-vapor is seen. The depth of the material, while vaporization process occurs, can be derived by using velocity of the liquid-vapor interface V_s.

$$V_s = \frac{E_{abs}}{\rho(cT_b + L_v)} \tag{3.20}$$

where L_v is the latent heat vaporization. The mass of the removed material per unit time (m) is equal to $V_s\rho$ and depth of vaporization (d) is equal to $V_s t_p$, thus;

$$d = \frac{E_{abs}t_p}{\rho(cT_b + L_v)} \tag{3.21}$$

3.1.4 Plasma Formation

After vaporization is initiated by irradiation of the material with high laser intensity, evaporation of the surface occurs. After vaporization process, the vapor and the laser beam on the material are important to understand and resolve comprehensive effects of the laser material interaction. The vapor can be ionized and this effect is an important

interaction. In a gas environment, the Saha equation [37] can be used to define degree of ionization by

$$\frac{\xi}{1-\xi} = \frac{2g_i}{g_a N_g}\left(\frac{2\pi m k_B T}{h^2}\right)^{3/2} e^{\left(\frac{-E_i}{k_B T}\right)} \tag{3.22}$$

where E_i is the energy of ionization and g_i is the degeneracy of states for ions and g_a is the degeneracy of states for the atoms or molecules. The total number densities of atoms or molecules and electrons are defined as N_g. The ratio of densities of electrons and total number densities of electrons give N_g.

The ionization can be partial or complete and it can be classified into two group which are cascade (avalanche) ionization and multiphoton absorption. If the laser beam energy is absorbed by seed electrons by bremsstrahlung absorption and energy of the free electrons exceeds ionization energy of the molecules, the ionization process of the molecules begins with collision (Figure 3.6a). The new electrons are achieved by the ionization and photon energy is absorbed by these electrons. Hence, the breakdown process (avalanche breakdown) starts. The plasma formation can be seen without any seed electrons, interaction of particle and collision, thus collision of each electron is ionized independently. This mechanism is named as multiphoton absorption (Figure 3.6b).

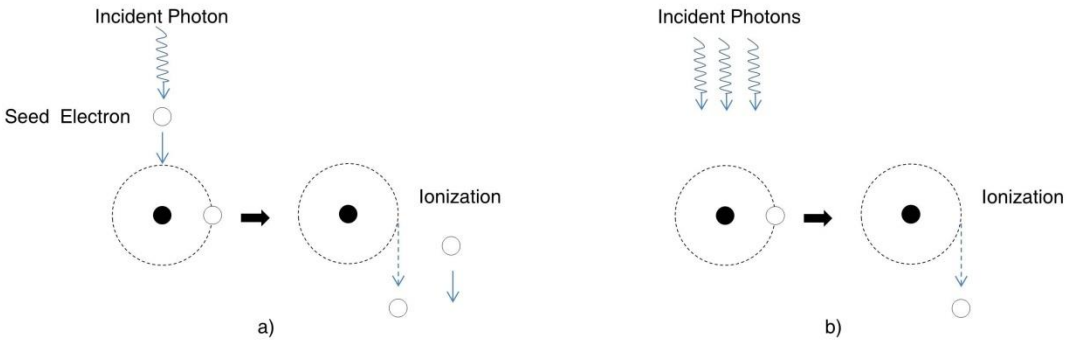

Figure 3.6 The laser induced breakdown mechanisms: ionization by a) avalanche breakdown b) multiphoton absorption

3.1.5 Ablation

The removal of the material from the surface by photochemical and photo thermal interactions can be defined as ablation. The laser energy absorbed by the material is converted into thermal energy. If the energy of the laser beam is very high and the temperature of the interacted part of the surface exceeds the boiling point, vaporization and thermal stresses occur. The vaporization and thermal stresses cause the removal of the material and this process is known as thermal ablation.

In organic materials, ablation process can occur by breaking of molecular bonds. The molecular order of the organic materials can be broken, if the incident photon energy is suitable for ablation of the material. This process is known as photo-chemical ablation. The ablation process occur not only by bond-dissociation energy but also lower bond-dissociation energy of material by the multi-photon absorption [36]. In this case, longer wavelength incident photons with smaller photon energies are absorbed simultaneously by two or higher number of photons, then they can break the bonds, although the energy of the each photon is lower than bond-dissociation energy.

To understand ablation process in laser-material interaction applications, photo-thermal and photo-chemical processes should be discussed together. The relaxation time of thermal process (τ), which is related with dissipation of heat, is important to determine long-short pulse relation. It can be defined by [38] ;

$$\tau = \frac{d^2}{4\alpha} \tag{3.23}$$

Where d and α show the depth of absorption and the thermal diffusivity, respectively. The thermal relaxation time determines choosing pulse duration of the laser for a well ablation with lasers so pulse duration is one of the key parameter for ablation process. If the pulse time of the laser is longer than τ, the laser energy is dissipated in the material. The material is damaged by thermal process; if pulse duration of the laser is higher than of the thermal relaxation time, short pulse durations result in the least dissipation.

One of the other parameters which affect the ablation of the material is pulse repetition rate of the laser. The repetition of the laser keeps material in ablation zone if the duration between the pulses is very short. Hence, high repetition rate is appreciated for an

efficient ablation process. The beam quality is another parameter which affects the efficiency of material ablation with lasers. The laser beam energy should be delivered to the ablation area efficiently by a controlled beam size in order to apply an effective ablation.

In industrial material processing and medical applications, laser ablation is used for marking, cutting, drilling, micro-machining, patterning and tissue ablation.

3.2 Temperature Effects in Pulsed Lasers

The defining thermal models for continuous wave lasers at constant intensity are the easiest models among the laser operation types. The thermal analysis for pulsed operation lasers is complex and depends on temporal shape of pulse and pulse width of the laser beam.

A laser system with multipulse operation causes temperature increase on material while each pulse interacts with the material. The generated pulses may be different shapes such as rectangular, smooth, triangular or random (Figure 3.7). The temperature of the material is affected by shape of the pulse. For instance, the higher temperature is reached by rectangular pulses than other pulse types [37].

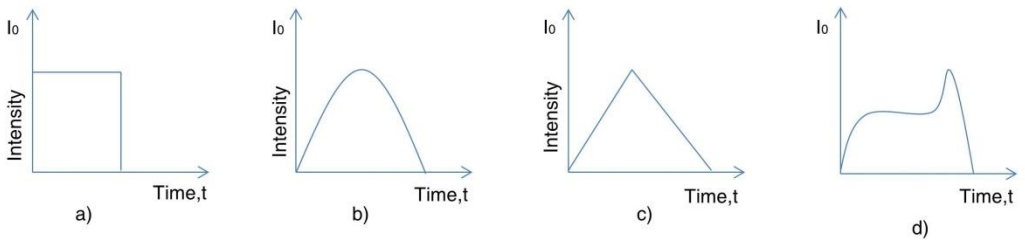

Figure 3.7 Different laser pulse shapes; a) rectangular, b) smooth, c) triangular, d) random shapes.

After each interaction of the pulse with material, a cooling time takes place till interaction of the next pulse. The cooling may not be enough for long pulse operation due to duration between the pulses. The temperature of the material while subsequent pulses interact with the material is higher than heating via prior pulses. Hence, the heating of the material for pulsed laser-matter interactions depends on the heating and cooling time which is

determined by pulse duration and time between the pulses. The relation can be seen in Figure 3. 8.

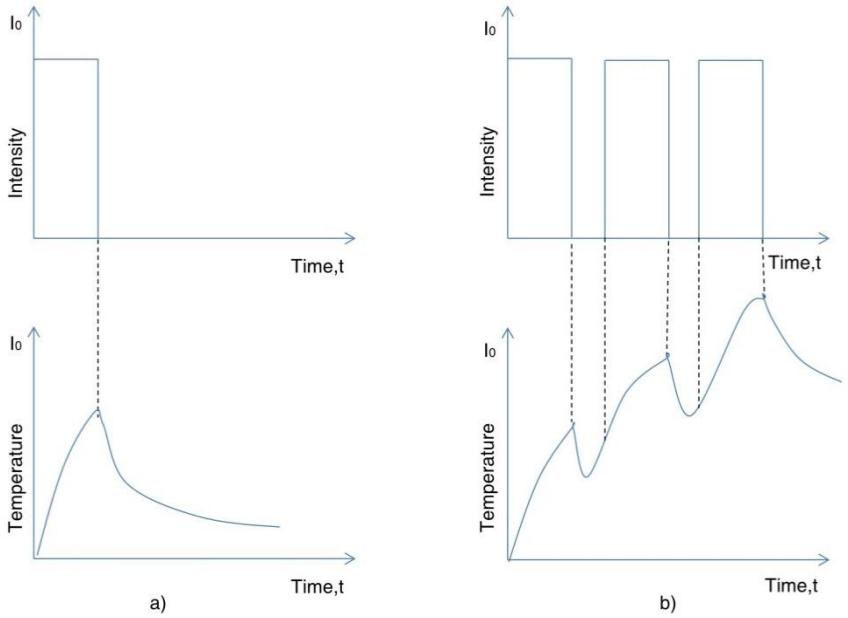

Figure 3. 8 Scheme of temperature difference on material surface during pulsed operation a) single pulse, b) multipulse laser operation on material.

3.3 Special Instrumentation for Laser Material Processing

The outcome quality of the laser material processing applications depends not only on the laser parameters but also on the careful instrumentation of the whole laser system. While constructing a system, it is very important to choose appropriate instruments such as galvanometric scanners and f-thetha objectives. The scan speed limits of the galvanometric scanner specify the overlap of the pulses at different repetition rate. The objectives which are used to focus laser beam, affect the depth of field and hence strongly influence of laser beam on the processed material.

3.3.1 Galvanometric Scanners for Material Processing

The galvanometric scanner systems help the material processing applications to achieve high speed and precise position on the material. They involve rotary motors which

direct focused laser beams onto target material. They are widely used in industrial applications especially in marking, engraving, sintering, melting, drilling, scribing process. Galvanometric scanners offer a number of advantages such as contact free and precision processing, high speed, flexibility without retooling, elimination of the mechanical tool wear. In today's world, they are equipped with a closed loop position control to achieve high scan speeds and precise laser process. The scanner consist pair of mirrors which are rotated by servo amplifiers. The simple schematic of a laser processing by galvanometric scanners is shown in the following figure.

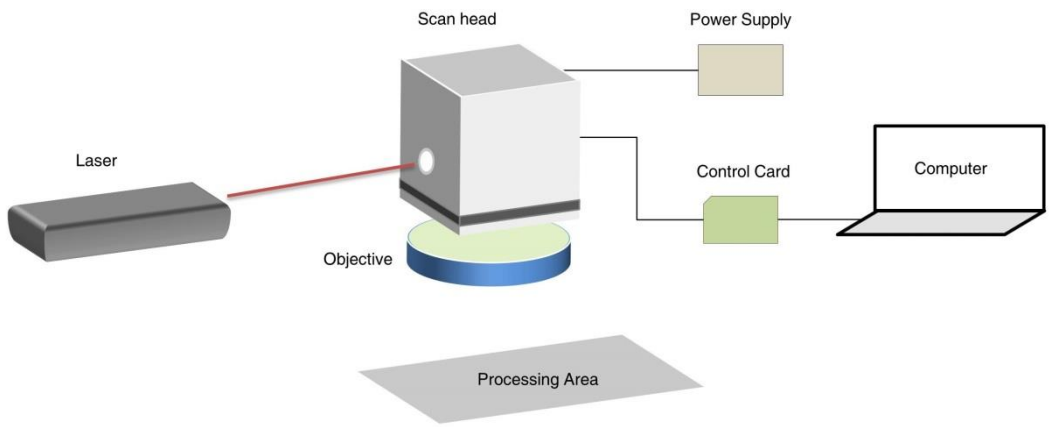

Figure 3.9 The basic configuration of material processing with scan head

A commanded position data is created in computer and a digital interface included in a control card is used to transfer data to scanner. There is a position detector inside the scan head, it provides closed loop feedback to the control card. The control card compares the data with actual position of the mirrors and adjusts current through the scan head to correct for any variances. After output of the scan head, an F-theta lens is used to focus laser beam to the material. The spot size and depth of focus is determined by the objective according to equation 3.3.

3.4 Main Parameters

While processing materials with a pulsed laser generating nanosecond pulses, several parameters such as pulse energy, pulse duration, peak power, power intensity are important for

the efficiency and quality of the processing. First, while pulse energy (E_p) of the laser increases, the depth of the processing area increase. It depends on the average power (P_{avg}) and repetition rate of the laser pulses (f_r) and is calculated by P_{avg}/f_r. Second, the pulse duration (t_p) is another factor which impacts the laser – material interaction duration. Third, the peak power of the laser beam which depends on the average power, repetition rate and pulse duration, is essential to overcome material processing thresholds. The pulse peak power of the laser is calculated by $\frac{E_p}{t_p}$. Fourth, power intensity of the laser depends on the average power of the laser effective focal spot area (cm^2). The calculation of the intensity of the power density is :

$$\frac{P_{avg}\ (W)}{Effective\ focal\ spot\ area\ (cm^2)}. \tag{3.24}$$

Also, fluence is used to calculate intensity of the laser beam by dividing the pulse energy by the radiated area as;

$$\frac{E_p\ (J)}{Effective\ focal\ spot\ area\ (cm^2)}. \tag{3.25}$$

Since intensity of the laser beam does not only depend on the first three parameters but depends also on the optical configuration of the system (such as focal length of the laser, beam quality, etc.), the optical configuration determines the response of the material to the laser beam more dominantly than other basic parameters.

CHAPTER 4

DESIGN AND IMPLEMENTATION OF A 60 W PULSED FIBER LASER AMPLIFIER

In this chapter, development of the nanosecond pulsed ytterbium doped fiber laser amplifier will be explained by discussing design and implementation parameters. First, modulation of the pulses of the seed signal will be discussed, then amplification of the seed will be explained by dividing each amplification stages. The fiber laser amplifier, which was constructed for this study, is based on MOPA configuration so, several pre-amplifiers were used to amplify power. The amplifier stage was divided into three stages as pre-amplifier, middle amplifier and main amplifier. Pre-amplifier stage can be defined as a seed of middle amplifier and it has two amplifier stages. In this chapter, all amplification processes are explained from seed to free space laser output in detail. The whole system was characterized by monitoring the spectrum and pulse shapes of the all stages. The nonlinear effects and ASE at the output of the system will be characterized to achieve a spectrum without ASE and SRS. Moreover, the components of the system were reduced, special electronic configurations and mechanical case were developed for industrialization of the system. Hence, the system was industrialized at the end of the experimental works.

4.1 Modulation and characterization of the seed signal

The fiber laser amplifiers with MOPA design is based on that a fiber laser architecture is divided into a seed laser and an amplification stage. The electronic modulation is an effective way to achieve controlled pulses from the seed of the laser. The modulation allows to generate optical pulses by the modulation of the current generator. The pulses of the system are created by modulation of the current of the laser diode.

In the industrialized of the system, an electronic controller with independently adjustable pulse duration and repetition rate property for modulation of the diode were developed. For the experimental setup, the modulation of the diode was performed at constant repetition rate and pulse duration 100 kHz and 203 ns respectively. In experiments, seed of the fiber laser amplifier is achieved by a 1064.15 nm broad bandwidth fiber coupled diode and pulse duration of the laser is generated via modulation of diode. The gratings inside the polarization maintaining fiber of the diode allow user short pulse modulation and keep peak lasing constant. While operating current of the diode is 0.75A, operating pulse peak current is 2A. The diode package is hermetically sealed 14-pin butterfly and the connection pins of the diode have peltier cooler pins to control temperature of the diode especially in pulsed applications. Moreover, it is capable of generating nanosecond pulses from 5 ns to 500 ns and repetition rate up to 500 kHz. The signal diode was modulated as seen in the following figure.

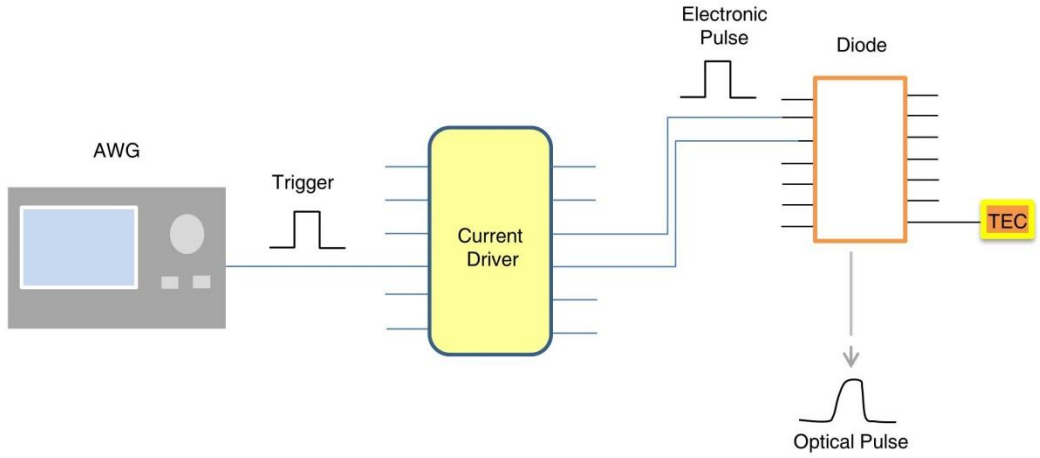

Figure 4.1 The configuration of the diode modulation system.

The pulse train was generated by arbitrary waveform generator (AWG) and sent to current driver, then an electronic pulse was generated for SM pump diode. The pulse was sent to diode for modulation. For this study, 100 kHz repetition rate with 203 ns pulse duration was generated. The duty cycle of the pulses is very short hence optical output of the diode become very low. For instance, diode output power is 294 mW when it is driven in CW

regime at operating current 0.75A, while output of the seed laser is 0.48 mW at the same current at 20 kHz repetition rate and 100 ns pulse duration. To overcome low output problem, the diode was driven at 1.77A which is near the maximum pulsed peak current by a current driver thus a sufficient seed signal was generated from the diode for preamplifier. The seed signal power from the diode is very important for reliability of the system. The temperature controlling of the diode is another important work, if the diodes are operated at high current. To control temperature of the diode, thermo-electric cooler (TEC), which controls the peltier inside the diode module, was used. The temperature data set in microcontroller and TEC is operated with microcontroller by receiving temperature data from it and stays temperature of the diode. The temperature controlling of the diode is important for efficiency of the signal seed since the optical power of the diode decreases at same current while temperature of the diode increases.

The modulation of the diode was characterized in different pulse duration steps by adjusting duty cycle. Four different pulse durations which start from 203 ns to 407 ns with about ~50 ns incrimination. While aiming to achieve high pulse energy and peak power at the output of the amplifier, SRS power should be minimized. To minimize nonlinear effects at the output of the system, there shouldn't be spikes at pulse formation of the seed signal. In this thesis, all characterization from preamplifier to output of the whole system was characterized for 203 ns and the shape of electrical pulse generated from current driver can be seen in Figure 4.2.

The optical pulse generated by using electrical pulse was measured and its shape can be seen with the pulse train which measured at 100 kHz repetition rate in Figure 4.3. As shown in figures, the shape of the optical pulse correspond to electrical pulse shape.

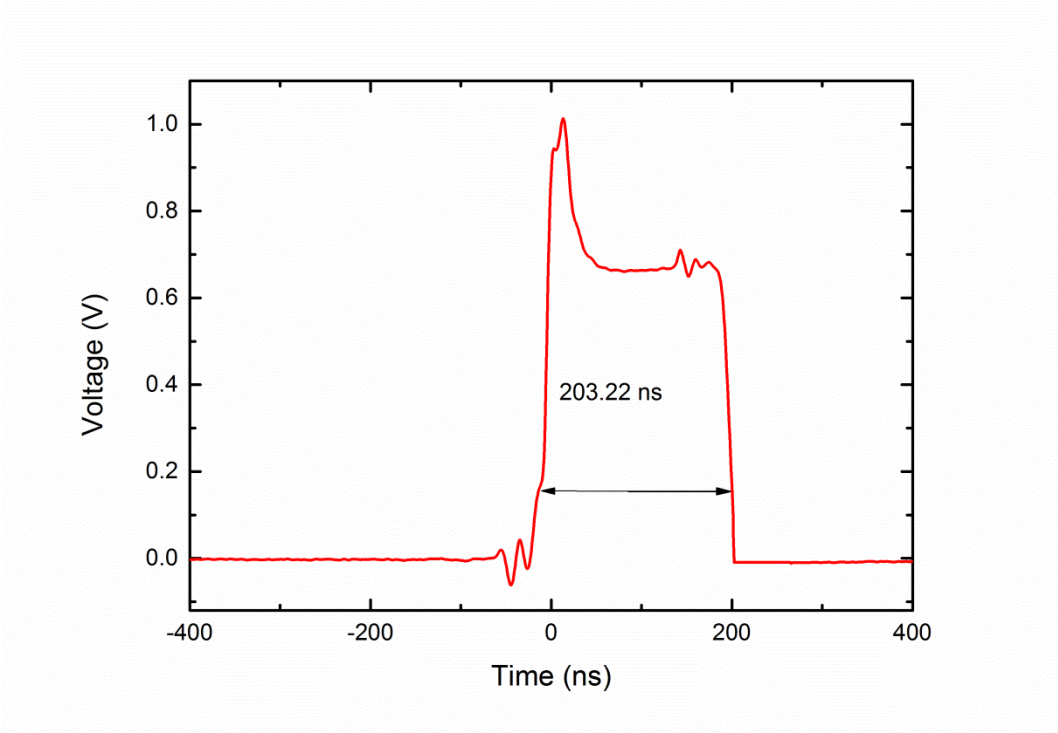

Figure 4.2 Pulse shape of the modulated seed signal

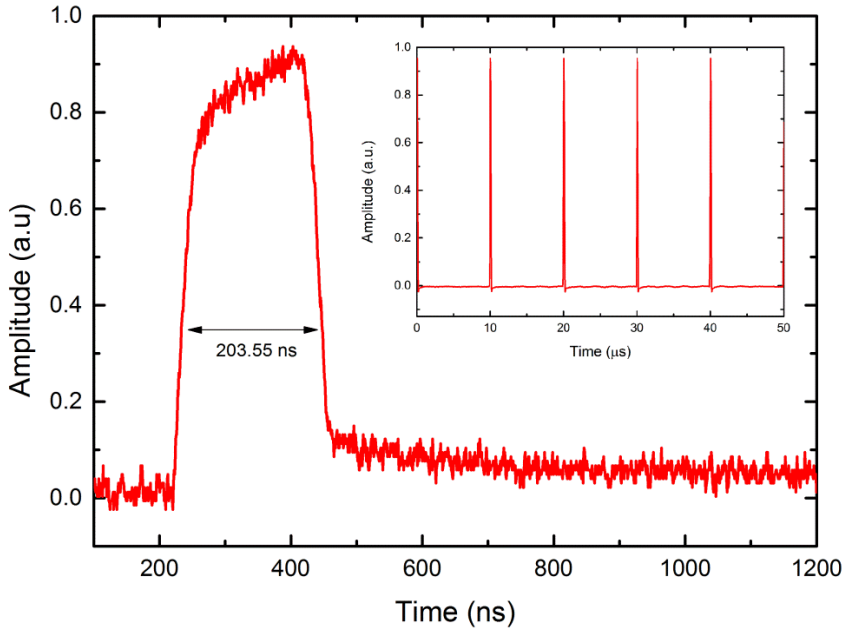

Figure 4.3 Optical pulse shape generated by electrical pulse (inset: pulse train for 100 kHz repetition rate)

In this thesis, the duty cycle configured 200:1, which means it is ~200 ns pulse duration at a repetition rate 100 kHz. The output power of the seed signal was characterized with different repetition rates and pulse durations. The change of the output power from the seed diode has shown while changing the repetition rate and pulse width respectively in Table 4.1 The results show that increasing average power corresponds to increasing repetition rate and pulse duration.

Table 4. 1 Output power of the seed diode with respect to different pulse durations and repetition rates.

	Power (mW)				
Repetition Rate (kHz)	203 ns	254 ns	304ns	359 ns	407 ns
100	4.9	6	7.3	9	10.6
150	7.2	8.6	10.6	13.8	15.1
200	9.6	11.3	14	17.1	19.2
250	11.9	14.2	17.9	20.8	23.5
300	14.1	18.2	21.3	24.7	27.8

4.2 Preamplifier Design

The preamplifier of the system can be defined as a seed of the laser for middle amplifier. To achieve a sufficient seed power for middle amplifier, two amplifier stages were set in preamplifier. Theoretically watt level output instead of miliwatt can be achieved in preamplifier stage by using only one amplification process from the seed laser. The reason that construction preamplifier stage in two amplification process is that high gain amplification from a low signal causes very high reflected ASE especially at low repetition rates. Hence, it is possible to damage seed laser diode. Moreover, the preamplifier was constructed by SM operation fiber in order to keep nearly diffraction limited beam shape at the output of the fiber laser and this type of fibers can be damaged at high level outputs. In addition, industrial fiber coupled SM components which are used

in preamplifier of the system are not capable of maintaining high peak power operation. For instance, SM fiber coupled band pass filters can be operated as reliable at maximum 500 mW CW signal power, while single mode polarization insensitive isolators are at 300 mW. These values are lower for pulsed laser signals.

The pulses generated by modulation with the approximate duration of 203 ns or longer are amplified to more than 200 mW power by a core pumped preamplifier stage. The simple schematic of the first stage of the preamplifier is shown in Figure 4.4.

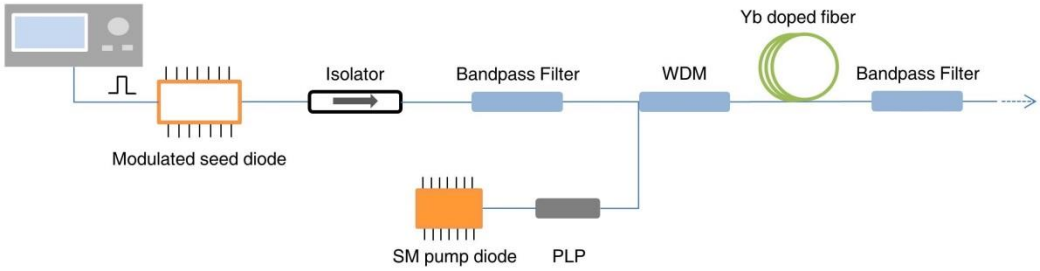

Figure 4.4 The first amplification part of the preamplifier stage. WDM: wavelength division multiplexer, PLP: pump laser protector

In the first stage of the preamplifier, 4.9 mW output power is achieved from the seed laser diode, which was made from a PM fiber of 5.5 µm core and 125 µm cladding, at 100 kHz repetition rate. The wavelength of the diode can be seen in Figure 4.5, where 0.988 nm FWHM was seen in spectrum.

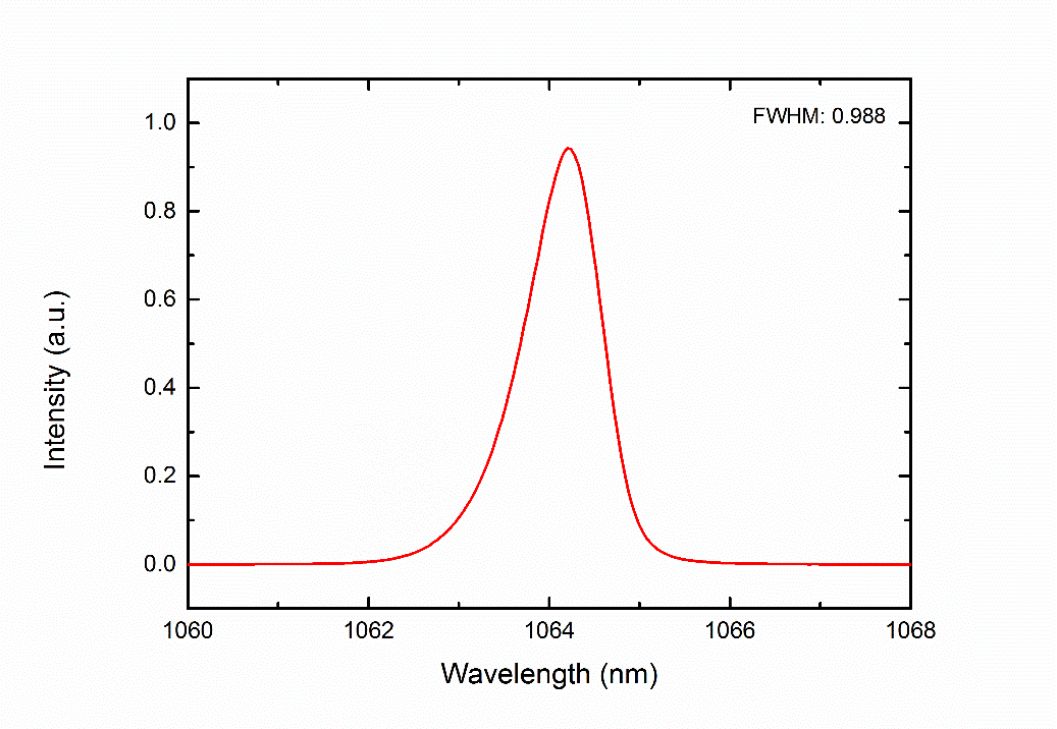

Figure 4.5 Spectrum of the seed diode

The laser diode is protected from the back reflection and amplification which potentially damages the seed laser diode, by a fiber coupled polarization insensitive isolator. Moreover, backward amplification is a factor for reducing efficiency of the whole system. The fiber coupled isolator has an operating wavelength $\pm$5 nm at 1064 nm and its fiber is HI1060 (mode field diameter of 6.2 μm, 0.14 NA, 125 μm cladding) which is a non-PM fiber and has different core structures than diode fiber. In addition, insertion loss of the isolator is 1.5 dB, thus splicing of diode and isolator with very low splice loss is very important to achieve high transmission rate. To overcome splice loss from PM to non-PM fiber splicing, longer arc-time with respect to same type of fiber splicing operated to the non-PM fiber to increase its NA for coupling much seed signal from the diode fiber. An efficient splice was achieved by 3.30 mW output power at the isolator output, hence the most of transmission loss caused insertion loss of the isolator. After isolator component, a 1064 nm fiber coupled band pass filter was used to protect diode from back reflected ASE which is generated in amplification process. 3.21 mW power was measured at the output of the band pass filter, after an efficient core to core splicing with isolator. The seed

laser signal and pump signal was combined at the same fiber for amplification in the ytterbium doped fiber by a two port wavelength division multiplexer (WDM). 3.17 mW seed laser power was achieved at the output of the WDM fiber. The seed signal was pumped with a 976.22 nm operating wavelength diode and pump diode temperature was stabilized by a TEC in order to prevent peak wavelength shifting of the pump source and efficiency of the amplification process. Moreover, a pump laser protector (PLP) was used to protect pump diode from the back reflected light. The gain of the stage was pumped within different ranges of pump powers and different types of ytterbium were tried to achieve an optimum signal for second amplification stage of the preamplifier. A HI1060 which is matched with ytterbium doped fiber (mode field diameter of 4 ± 1 μm, 0.22 NA, ~300 dB/m at 976 nm absorption) was used for amplification process. In order to choose correct fiber length with different pump signals, a simulation which was coded by Bilkent UfoLab members, implemented in MatLAB software. The simulation was examined for 3 mW signal seed to check ASE level, length of the ytterbium doped fiber for adequate amplified signal level. The simulation was generated for two-level gain medium. The simulation results about absorption of the pump, amplification of the signal power and ASE power along the fiber is shown in Figure 4.6.

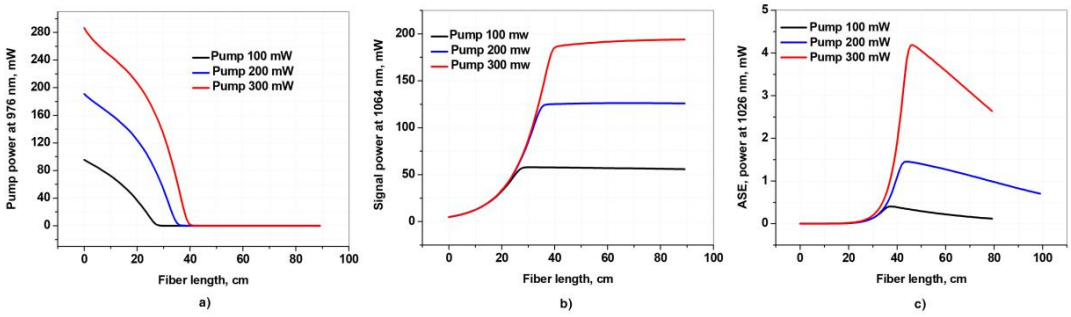

Figure 4.6 Numerical simulation results for a) pump power, b) signal power, c) ASE power as a function of fiber length for pump power of 100 mW, 200 mW and 300 mW.

The simulation results show that optimum fiber length for three different pump power is between 40 cm to 60 cm. As shown in Figure 4.6c. ASE power is increasing dramatically while pumping with more than 200 mW. When considering that higher ASE power than

simulation results in pulsed operation, maximum 100 mW pump source was applied to 60 cm Yb doped fiber for amplification process by forward and core pumping method. The output power of the Yb doped fiber with respect to the pump power is shown in following figure.

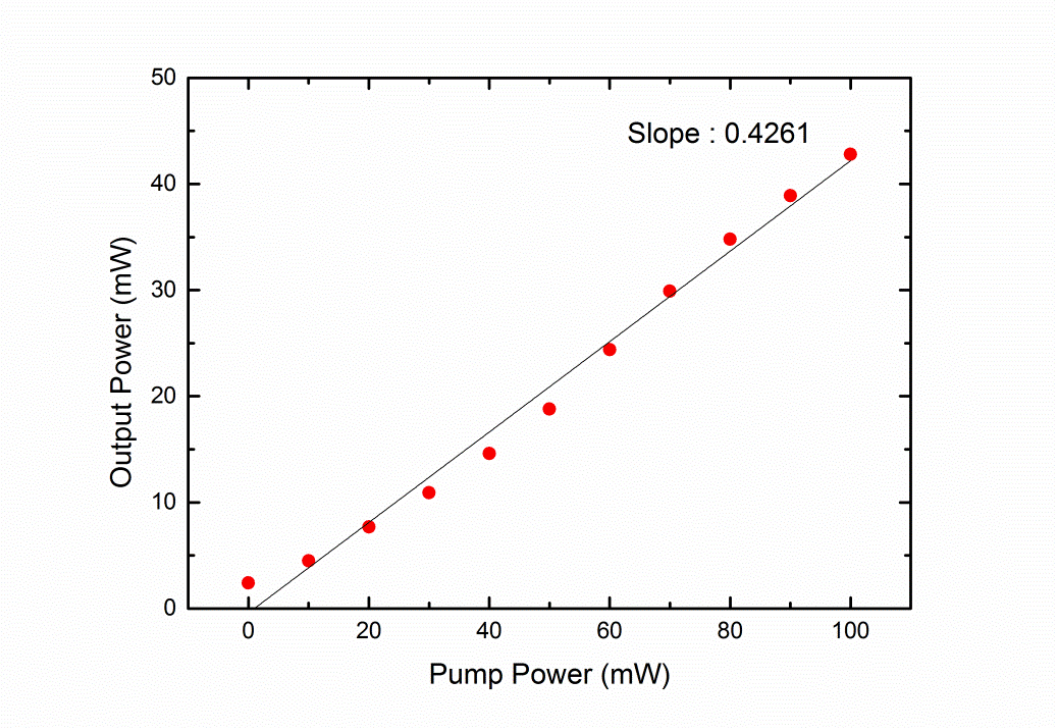

Figure 4.7 Pump power vs. output power from ytterbium doped fiber output.

The output power 42 mW was achieved from the Yb fiber output and a low level ASE was seen from the spectrum of the Yb fiber output. A fiber coupled band pass filter which works at nominal center wavelength 1064 nm, was used to eliminate ASE. After elimination of ASE and transmission loss from the band pass filter and splice loss, 39 mW output power was achieved at fiber output of the band pass filter. The spectrum of the signal at the ytterbium fiber and band pass filter output is shown in the following figure.

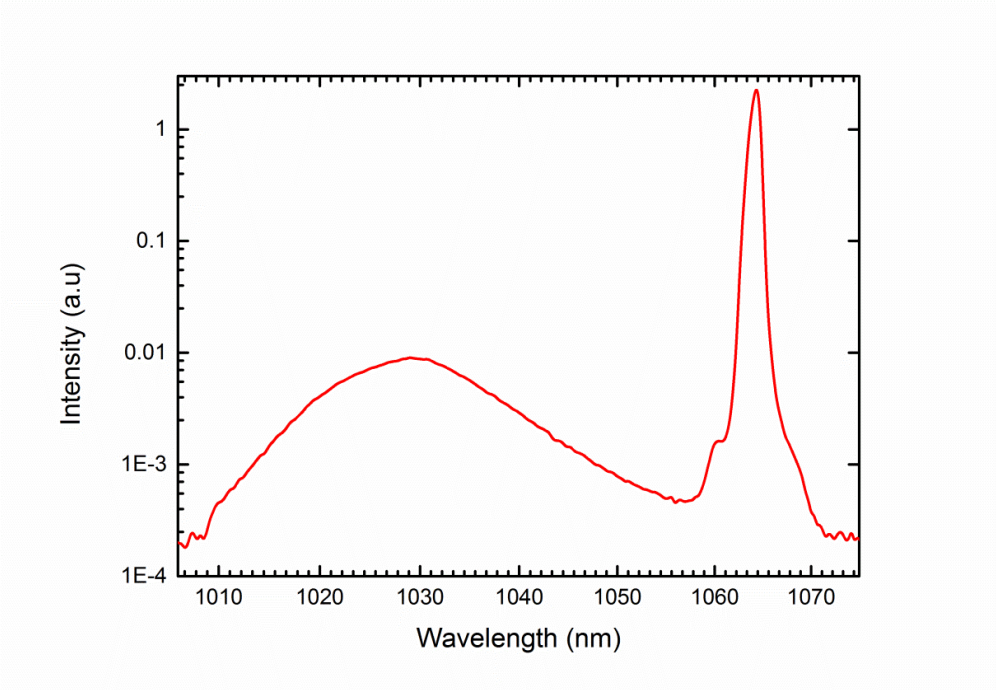

Figure 4.8 Spectrum of the a) ytterbium doped fiber output (logarithmic scale)

The signal from the band pass filter was used to amplify second stage of the preamplifier. Hence another amplification stage was used and its design can be shown with first amplifier in following figure.

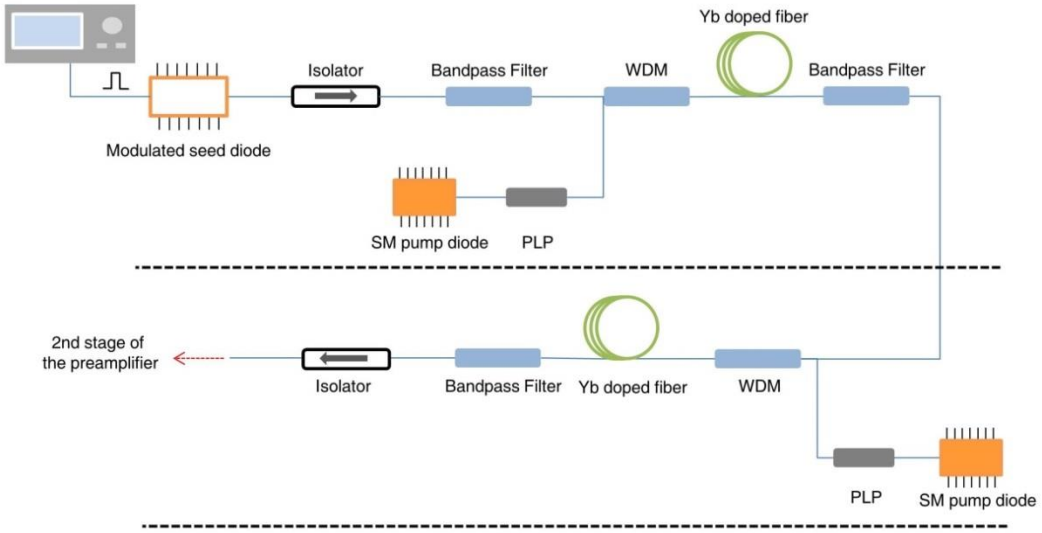

Figure 4.9 The preamplifier system

In the second stage of the preamplifier, Yb doped fiber was pumped by signal which propagate from band pass filter to WDM where 0.32 dB signal loss from band pass filter to WDM was seen due to splice loss and insertion loss of the WDM. Hence, 36, 3 mW signal was taken from the end of the WDM and it was pumped by 300 mW 976.09 nm SM pump diode for amplifying. A ytterbium doped (mode field diameter of 4.4 ± 1 μm, 0.22 NA, ~1200 db/m at 976 nm absorption) was used for amplification and length of the ytterbium doped fiber was determined by using numerical simulations. The numerical simulation results for second amplification stage of the preamplifier is shown in the following figure.

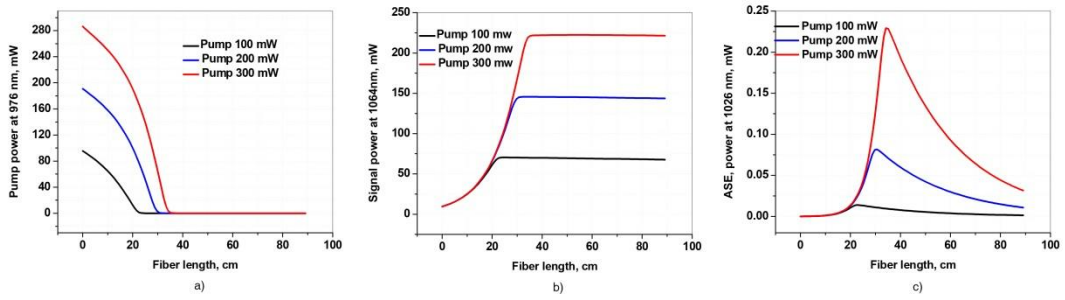

Figure 4.10 Numerical simulation results for a) pump power, b) signal power, c) ASE power as a function of fiber length for pump power of 100 mW, 200 mW and 300 mW for the 2nd stage of the preamplifier.

The maximum saturated laser power from preamplifier stage was limited to 200 mW to achieve an adequate signal in middle amplifier stage without ASE. In addition, components at the end of the preamplifier stage work reliable at this power range. The simulation results show that the maximum signal by pumping 300 mW pump power can be achieved with a fiber more than 50 cm. To achieve low ASE spectrum at the output of the ytterbium fiber 100 cm Yb doped fiber was used according to simulation results. After pumping gain with ~300 mW, 237 mW signal power with a low ASE achieved at the output of the ytterbium. The slope efficiency is 69.5% at this stage. The output power of the Yb doped fiber as a function of the pump power is shown in Figure 4.11. The spectrum of the ytterbium output can be seen in Figure 4.12.

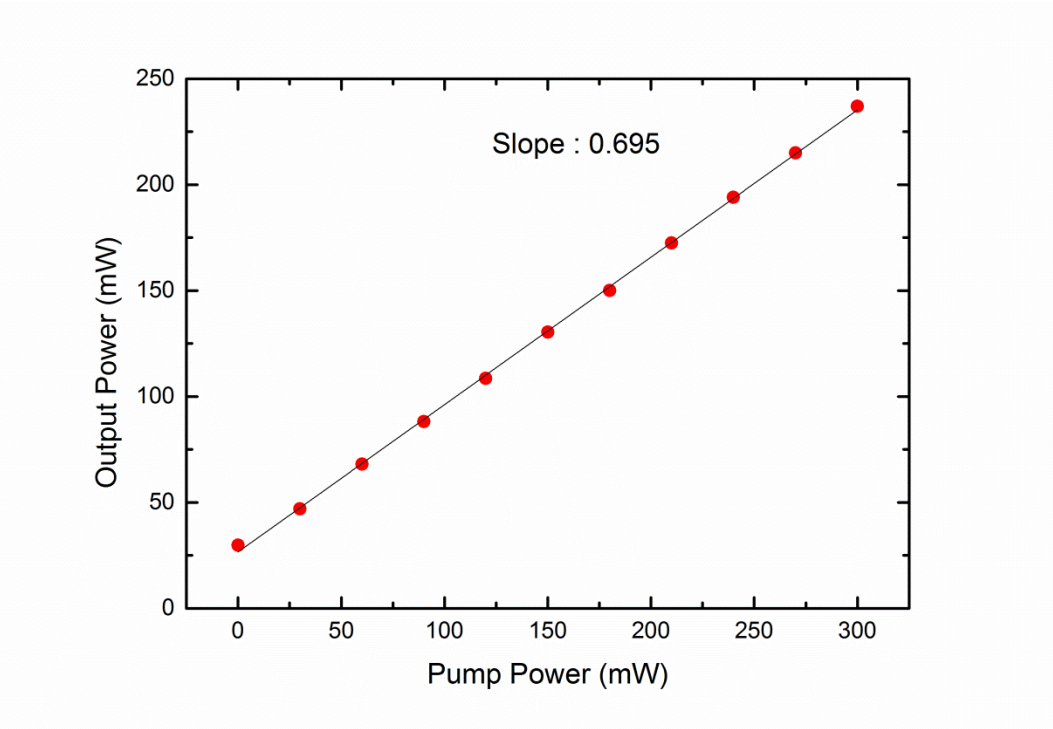

Figure 4.11 The output power of the Yb doped fiber as a function of the pump power

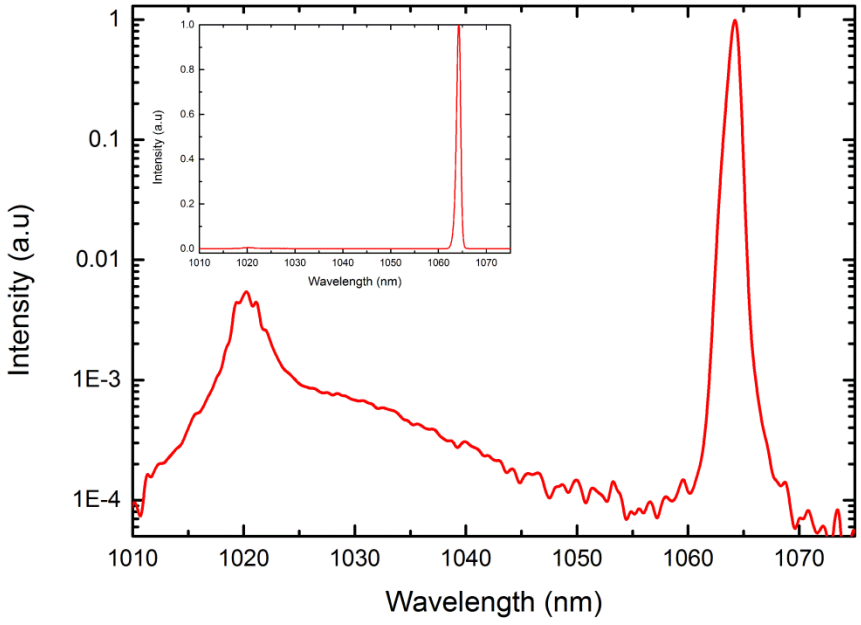

Figure 4.12 Spectrum of ytterbium output (logarithmic scale), inset : linear scale.

ASE of the last stage of the preamplifier was eliminated by using a 1030 band pass filter and after the elimination and splice loss, 227 mW signal was achieved at the band pass filter output. To protect preamplifier stage, a 1064 nm 2W polarization independent isolator was added to end of the preamplifier. The isolator has 0.41 dB insertion loss and has a matched SM fiber with band pass filter so core to core splice was performed. After isolator, 204 mW signal power was achieved. The spectrum of the preamplifier is shown in Figure 4.13.

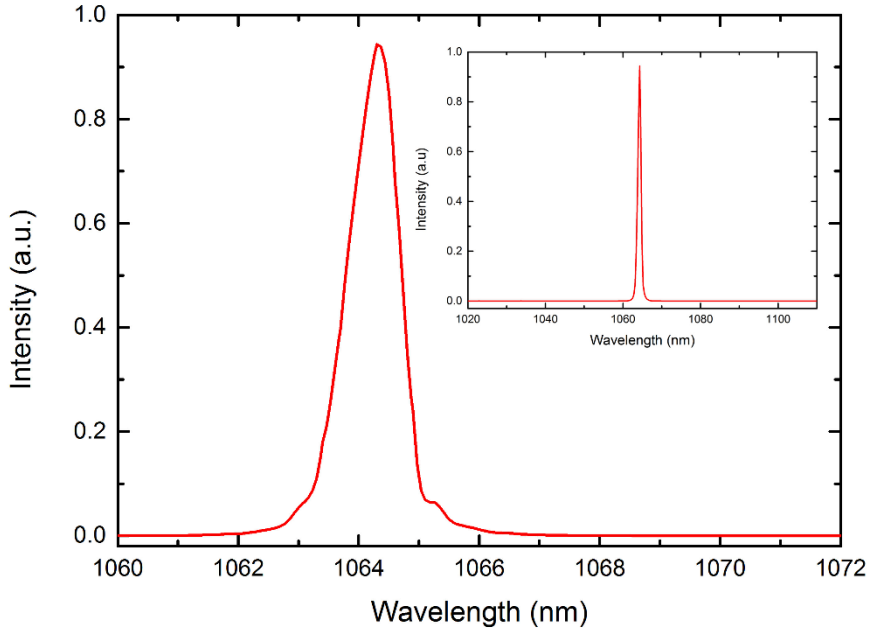

Figure 4.13 The spectrum of the preamplifier stage (logarithmic scale), inset: linear scale.

4.3 Middle Amplifier Design

The signal achieved from the preamplifier stage was used to amplify an adequate power for main amplifier stage. The multimode components was chosen to reduce nonlinear effects, pump power and ytterbium length was chosen with caution to suppress ASE. The simple schematic of the middle amplifier stage is shown in the following figure.

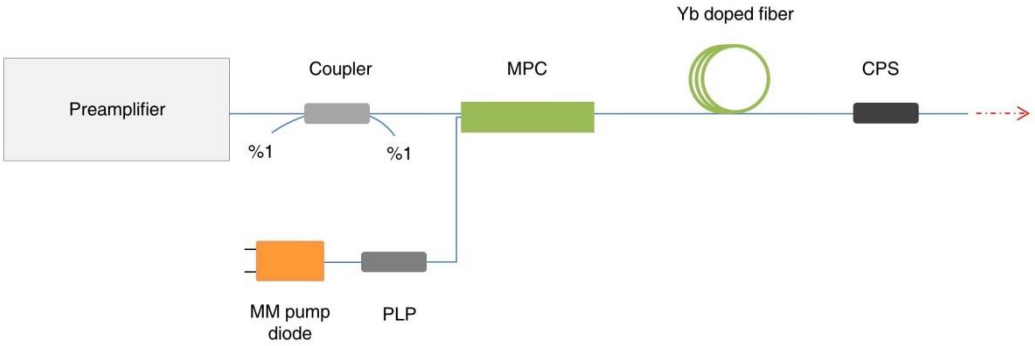

Figure 4.14 Simple schematic of the middle amplifier stage. CPS: Cladding pump stripper, MPC: multi pump combiner.

After preamplifier stage a 99:1 SM fiber coupled coupler was used to detect seed signal while laser is operating. The backward port of the coupler is used to detect back reflected signal. The signal was combined with pump by using a (1+1)x1 multi-pump combiner which has 10 µm core 125 µm double clad sized fiber. 164 mW output was achieved at the end of the MPC. 10W multi mode pump which has 976 ±4 nm wavelength was used to pump and it was protected by a MM PLP from the back reflection. A ytterbium fiber (core diameter of 10.1±1 μm, 0.07 NA, ~6.9 db/m at 976 nm absorption) was used as an amplification gain. The ytterbium was pumped up to 7.5 W and the length of the ytterbium for that pump power level was determined by simulations. First, simulation was performed for the pump wavelength 976 nm which is maximum absorption level of the ytterbium. The simulation result is shown in Figure 4.15.

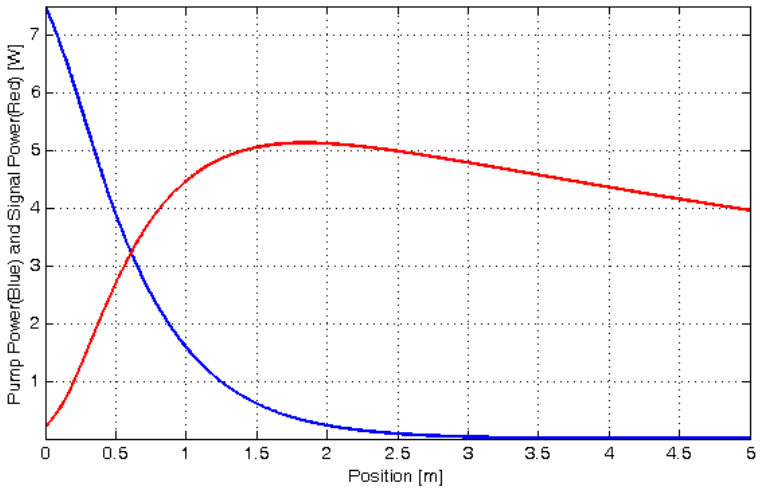

Figure 4.15 Simulation results for determining length of the fiber at 976 nm pump power

As shown in the Figure 4.15, pump signal at 976 nm is absorbed by using 4 m ytterbium doped fiber. The length of the ytterbium was chosen by the help of simulation results so 4 m ytterbium fiber was used for amplification process. 4.2 W power was achieved at ytterbium fiber output, however it involve a slightly pump power since some of the pump power cannot be absorbed by ytterbium fiber due to variable wavelength of the MM diodes at different temperatures or imperfect splice between preamplifier and middle amplifier stage. The multimode diodes which are used in that stage have 976 nm central wavelength, however it may change due to variation of temperature at different operating currents and environment. The changing wavelength means changing absorption of the pump. Thus, the simulation was performed for different wavelength 972 nm and 978 nm since MM diodes have 4 nm bandwidth and the peak wavelength which changes according to temperature of the environment and operating current of the diodes.

Hence, it is possible to detect a high level unabsorbed pump power for different wavelength. The results of simulations for 972 nm and 980 nm pump wavelength is shown in the following figure.

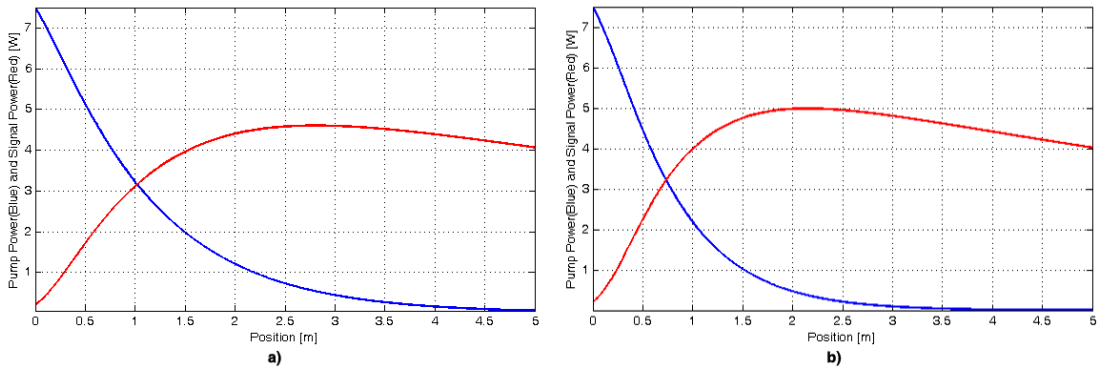

Figure 4.16 Simulation results for a)972 nm pump wavelength b) 980 nm pump wavelength.

Another reason which causes unabsorbed pump is imperfect mode matching while splicing fibers [41]. There are several splices which present in a whole fiber laser system, so the pump leakages from core to cladding may occur after a poor performance splice. Hence a long pass filter after ytterbium fiber was used to measure exact signal output from the ytterbium output. The signal with respect to pump graph is shown in the following figure.

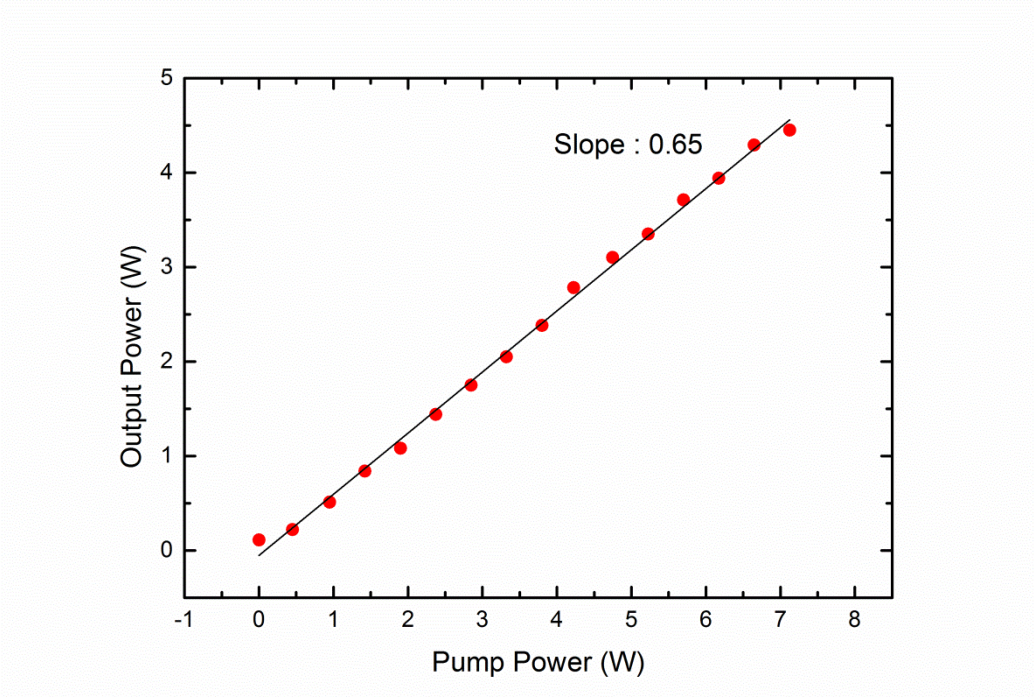

Figure 4.17 Measured signal power as a function of pump power.

After pumping ytterbium doped fiber by 7500 mW pump power, more than 200 mW unabsorbed pump eliminated by a long pass filter which only transmits photons higher than 1000 nm wavelength. In real system, elimination of unabsorbed pump power is very important since it may causes damage to fiber by localization of the heat at cladding. It is also important to reach a high beam quality laser output since laser output with residual pump reduce the quality of the beam. In addition, the reliability of the components are affected by the unabsorbed pump. There are several ways to eliminate unabsorbed pump from an all fiber laser amplifier. First, ytterbium doped fiber can be chosen longer than that of used in this stage. However, longer ytterbium causes nonlinear effects. The second way is using a temperature controller to keep diode at constant temperature but it's very difficult for a high power diode. This is because the MM industrial diodes have small case and it is very difficult to keep their cases at constant temperature especially at operating current. Third way is using a grating stabilized MM diode which have constant wavelength even in high temperatures, however they are new diode technology for high outputs and very expensive components. Fourth, using a cladding pump stripper (CPS) is a way to eliminate unabsorbed pump signal from the amplifier. In this design a CPS was developed for stripping unabsorbed pump. The schematic of the CPS is shown in the following figure.

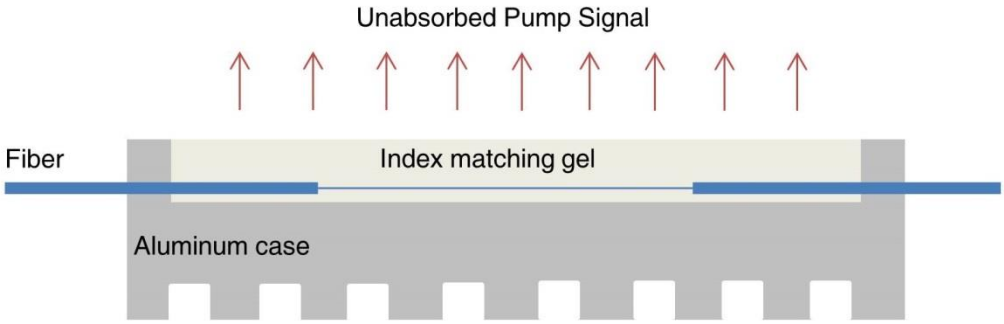

Figure 4.18 Design of the CPS

To develop CPS, a 10 um core μm core and 125 μm clad sized double clad fiber were used. The cladding of the fiber has a refractive index of 1.45, so the environment with

higher refractive index than clad can be developed for elimination of the unabsorbed pump. Hence the middle of the fiber coating and outer cladding was stripped and the unabsorbed pump which propagates at the cladding was eliminated by injecting an index matched gel to that region. The gel, which is colorless, clear and a kind of liquid photopolymer, has refraction index of 1.56. It is curable by UV light and it was used to recoat inner cladding of the fiber. The difference of the refractive index between the inner clad and recoated region assists to eliminate the residual pump power. After elimination process, 210 mW pump power was eliminated at middle amplifier stage of the fiber laser system. The spectrums of output of the ytterbium fiber and output of the CPS component at the operating current of the system is shown in the following figure.

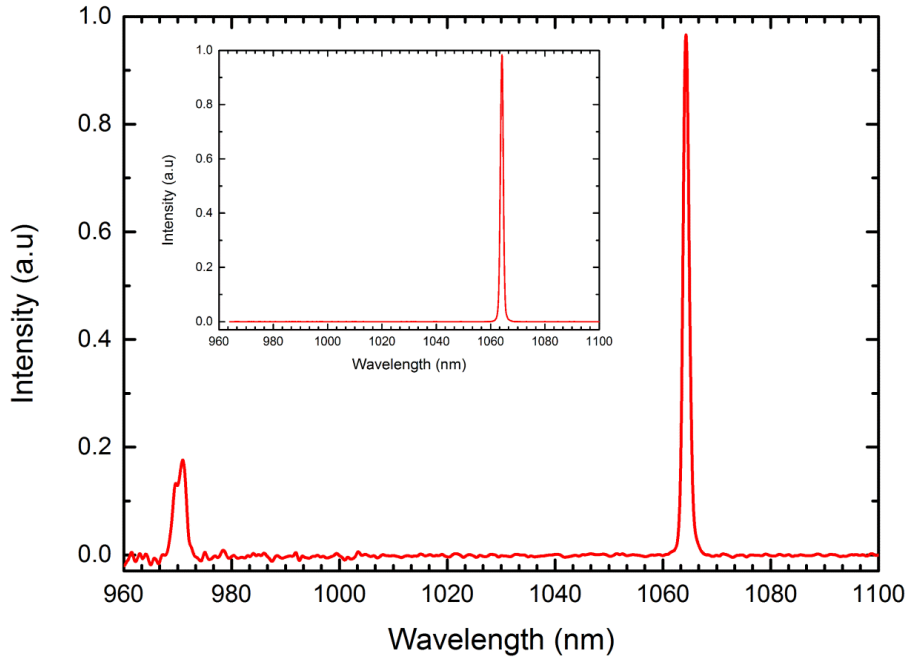

Figure 4.19 The spectrum of the ytterbium fiber output, inset: CPS output.

4.4 Main Amplifier Design

In the last stage of the fiber laser amplifier, the signal achieved from the middle amplifier stage was used for amplification process. After amplification process, more than

60W signal power and 0.6 mJ pulse energy were achieved with a high beam quality and good pulse-to-pulse stability. The output of the amplifier was characterized, long time tests were performed and stability of the laser parameters were observed. In this stage, it is possible to happen several challenges, such as splicing different cladding size fibers, reaching high beam quality, temperature stabilization of the MM diodes, elimination of the ASE and SRS, since reaching a high power laser output is a compelling way. Hence, several methods were created to solve challenges in different region of the main amplifier and they were explained in details. The simple configuration of the main amplifier is shown in the following figure.

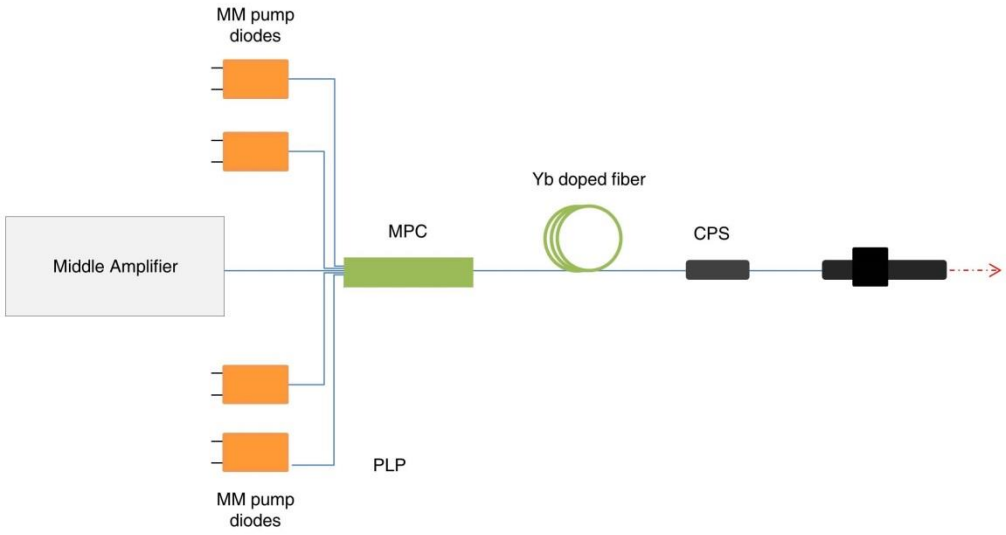

Figure 4.20 Simple schematic of the main amplifier of the system.

In this stage, a 25 µm core size and 250 µm cladding size double clad fiber input MPC was used to combine pump and signal power. Hence it is very important to achieve a low loss splice while splicing it with a 10 µm and 125 µm cladding size fiber which was used at the output of the middle amplifier. A commercial Fujikura FSM 100 splicer was employed to splice large and small diameter fibers. To achieve a low losses splice result with splicing different cladding sized two fibers, arc region was chosen on the 250 µm cladding size fiber instead of center of the two fibers. The reason is that large cladding

size fiber needs high arc power which is too much for a 10 µm fiber and it damages the fiber core and cladding structure while splicing. Hence, large diameter fiber were shifted 300 from the arc center and arc was applied to that region of the large diameter fiber. Moreover, NA of the large diameter fiber was increased in this way, hence coupling of the pump and signal was enhanced. The demonstration of the splicing process and image of the splice of different diameter fibers are shown in Figure 4.21b.

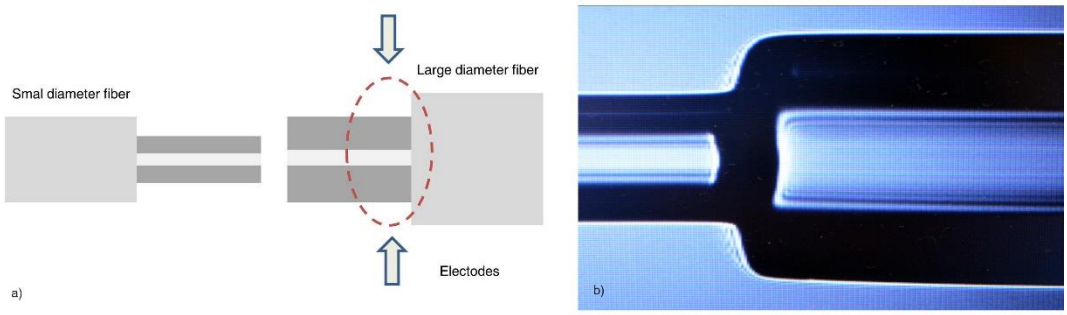

Figure 4.21 a) Simple schematic of the fiber splice, b) splice image of middle amplifier output fiber to MPC input fiber of the amplifier.

After splicing of middle amplifier with main amplifier stage, 4.08 W power was achieved at the output fiber of the MPC which has a same core/clad diameter with input. A high doping concentration ytterbium doped fiber (10.8 dB/m absorption at 976 nm) was chosen to amplify signal to keep fiber length short since the short fiber length provides to avoid nonlinear effects. The length of the ytterbium doped fiber, which has same core and cladding size with MPC output, was determined after characterization of the pump diodes. In this stage, four MM fiber coupled diodes whose maximum output power is 25W (975 $\pm$5 nm bandwidth, 0.15 core NA) were used to pump active medium by clad pumping. The diodes have protection filter inside so PLP components were not used. The pump diodes' central wavelengths depend on the operating current, wall plug efficiency, temperature of the environment and optical design. The temperature of the diodes increases with increasing applied current hence the central wavelengths shift. Driving

current dependency of the central wavelength of the diodes at room temperature is shown in the following figure.

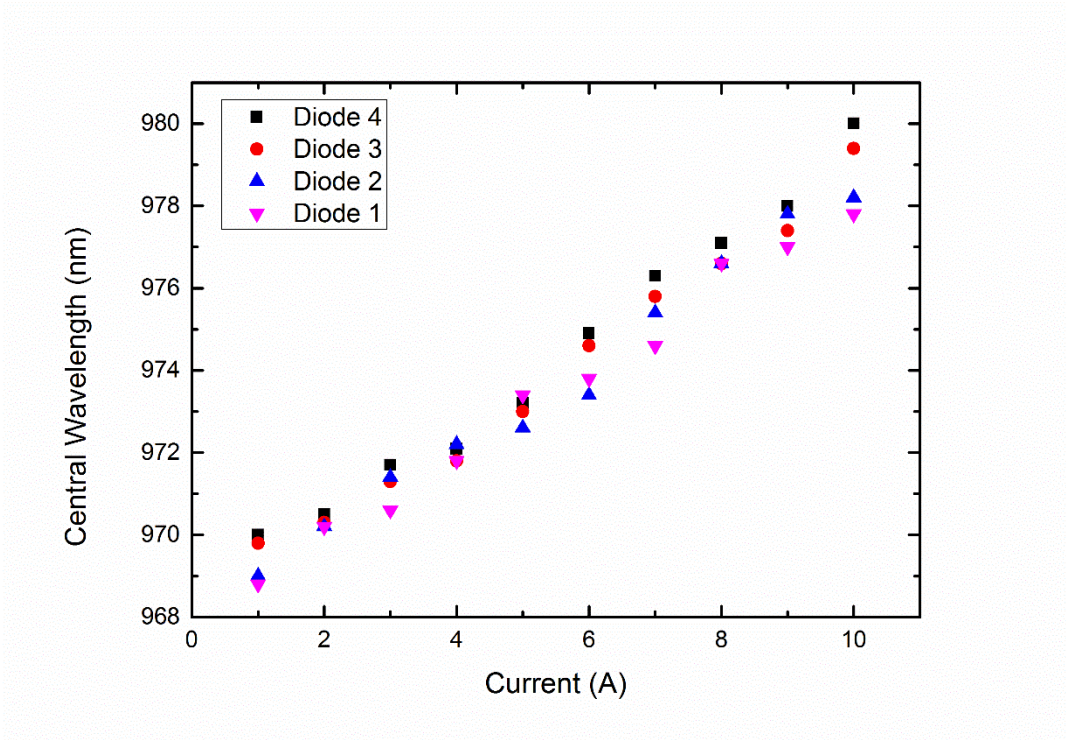

Figure 4.22 Measured maximum emission wavelengths of the diodes as a function of applied current at room temperature.

Hence, it is very important while choosing ytterbium doped fiber length, to perform a simulation for different pumping wavelengths. Fiber length should be analyzed for all different wavelengths and chosen optimal in regard to avoid from ASE and SRS. The simulation results of ytterbium doped fiber which is pumped with four different pump central wavelength diodes as a function of ytterbium doped fiber length are shown below.

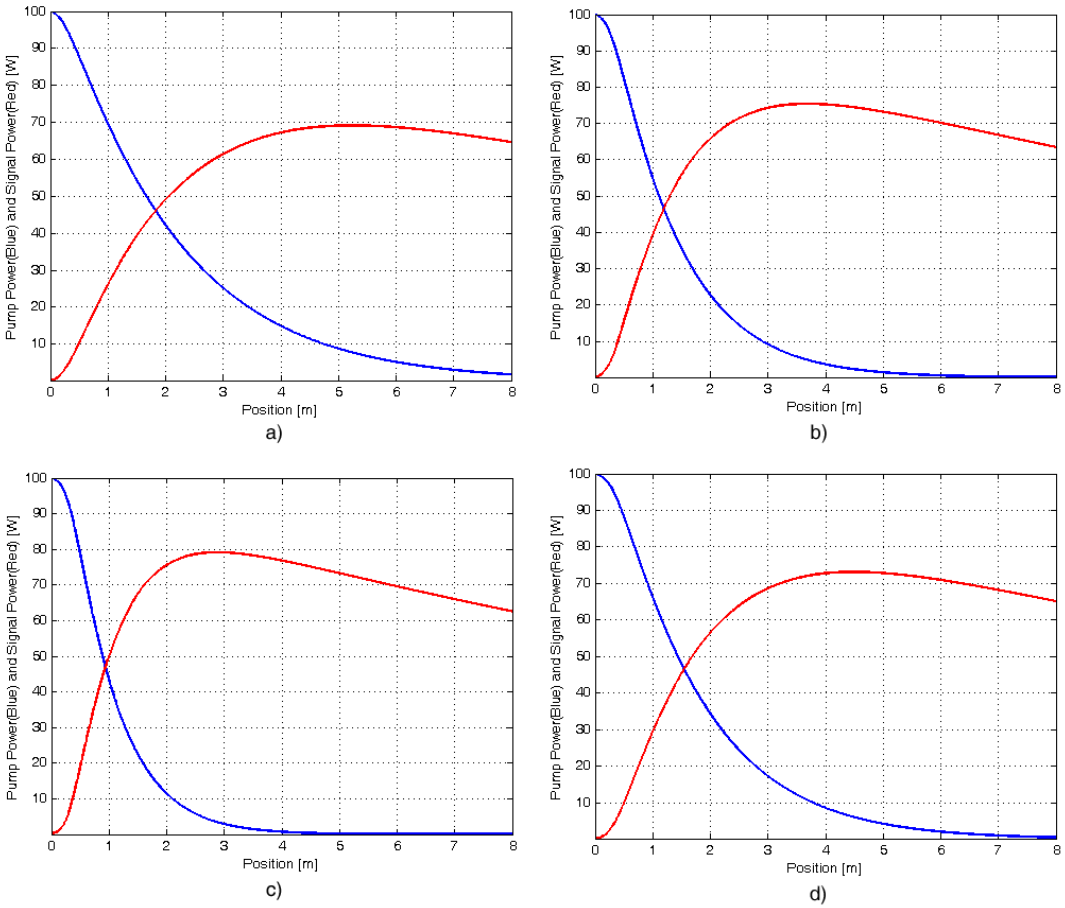

Figure 4.23 Simulation results for amplifier stage at different pump wavelengths at a) 970 nm b) 973 nm c) 976 nm d) 979 nm

The length of the ytterbium doped fiber was chosen as 7 meter via simulation results. It was thought that, elimination of unabsorbed pump power lower than 2 W is easy by the help of CPS and single clad fiber at the end of the system. After choosing the length of the ytterbium doped fiber, it is very important to achieve a low loss splice between ytterbium doped fiber and MPC. Ytterbium doped fiber was spliced to MPC by improving a special splice technique to achieve core to core splicing. In this stage, it's very important to achieve core to core alignment between ytterbium and passive fiber while splicing since leakage of the high intensity pump may damage the fiber coating or leakage of the signal from core to clad may amplify inside the cladding [42].

It's difficult to detect core of the ytterbium doped fiber by a splicer camera since its core geometry is octagonal. To overcome this problem, ytterbium doped fiber's coating was stripped and an arc power was applied to it in the splicer to change its geometry from

octagonal to round. After arc process, it was cleaved and prepared for core to core splicing and a low loss splice process was achieved. The image of splicing which was taken from the splicer after core to core splicing is shown in the following figure.

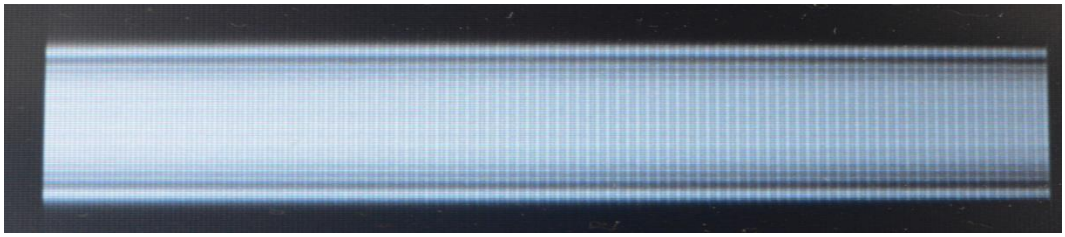

Figure 4.24 Splice image of MPC output fiber with ytterbium doped fiber.

Then, splice point was recoated with an UV curable flexible polymer gel whose refractive index is 1.33, to couple potential pump leakage and to protect this region from the external factors.

The diodes were spliced to (6+1)x1 MPC and operated 25 W of each by cooling on a heat sink. Ytterbium doped fiber was cleaved 8° to protect middle and preamplifier from back reflected light and output of the system was measured from that point at different pump levels. While pumping with different pump power levels, it's possible to encounter residual pump problem as encountered at middle amplifier stage. To develop a long time operational fiber laser system without a strict temperature control, elimination of the residual pump by a CPS was preferred. The residual pump at the end of the system was measured by using a long pass filter which only transmits 1000 nm and higher wavelength photons. To protect system from the residual pump, another CPS was developed as did at middle amplifier stage. A double clad 30 cm passive fiber was used. The fiber core and clad size, NA of the fiber core and clad preferred same as ytterbium doped fiber which was used in this stage. The fiber's jacket and outer cladding was stripped along 4 cm in the middle of it. The high refractive index (1.56), UV curable liquid photopolymer gel was injected and to that region and cured. After development of the CPS, it was spliced to ytterbium doped fiber by using same splice technique as splicing MPC to ytterbium. Output of the ytterbium doped fiber was measured 2.7 W, while middle

amplifier being operated. Then, active medium of main amplifier stage was pumped at different pump levels to detect residual pump levels. The elimination of the pump power for different pump levels by long pass filter and CPS respectively is shown in the following figure.

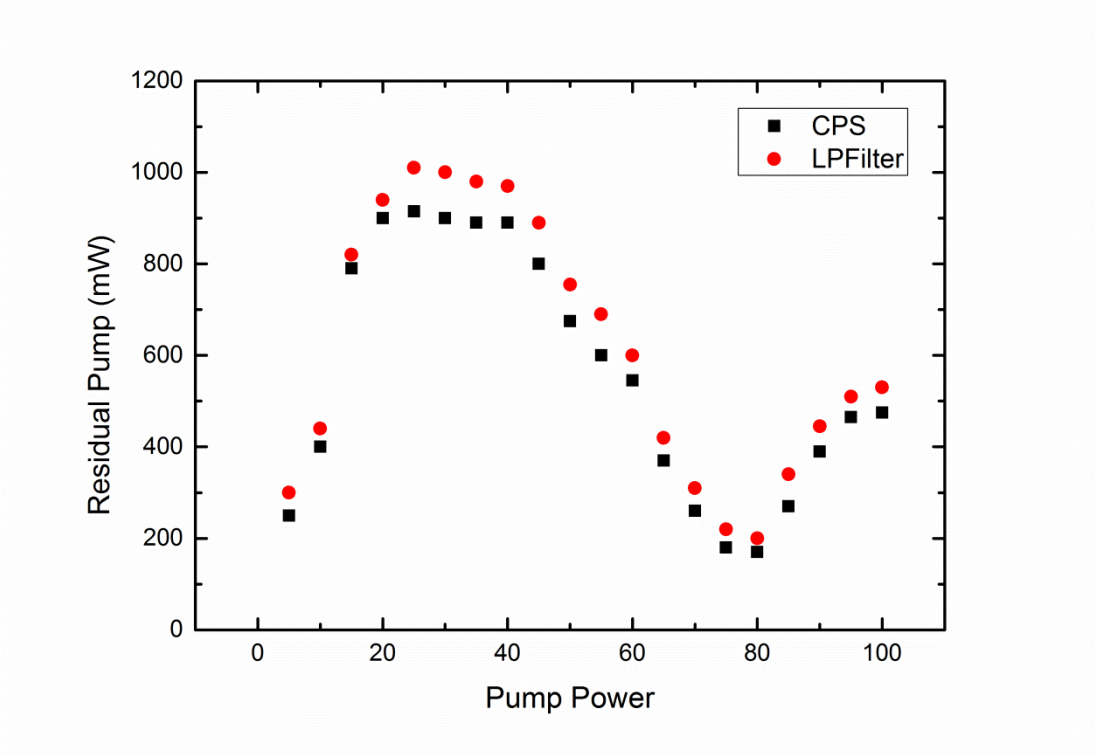

Figure 4.25 Residual pump at ytterbium fiber output as a function of pump power.

The active medium of the main amplifier was pumped by maximum 94.5 W pump power and output of the spectrum was characterized for different pump levels. The maximum output signal power from the CPS fiber was measured 69.1 W with a slope efficiency 76% at this pump level. Signal power at the output of the CPS fiber as a function of pump power is shown in the following figure.

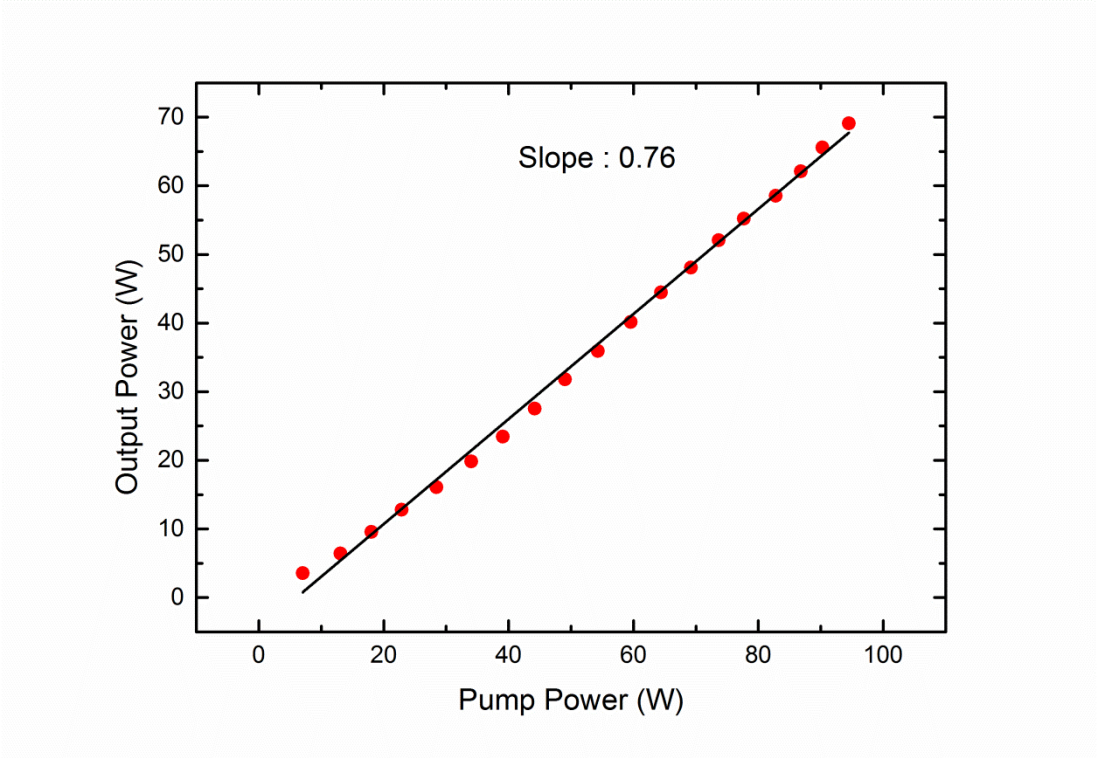

Figure 4.26 Measured signal power as a function of pump power at CPS fiber output.

For the protection of the whole system from back reflected signal while processing material, a 70 W collimated high power fiber coupled isolator was used. The nominal output beam diameter of isolator is 3.8 and it was enlarged by a beam expander to 8 mm. The eccentricity and ellipticity of isolator are 0.5 and 90 respectively. The fiber of the collimated isolator was chosen single clad (25 µm core and 250 µm cladding size, 0.07 NA) to eliminate possible residual pumps due to CPS-isolator splice. The transmission loss of isolator (0.3dB) and coiling of ytterbium fiber radius chosen 5 cm, hence transmission loss and coiling radius led a decrease in signal power to 60.4 W signal power at the output of the collimated isolator. The transmission loss of isolator (0.2dB) and loss at 5 cm coiling radius led a decrease in signal power to 60.4 W signal power at the output of the collimated isolator. The measured signal power as a function of pump power is shown in the following figure.

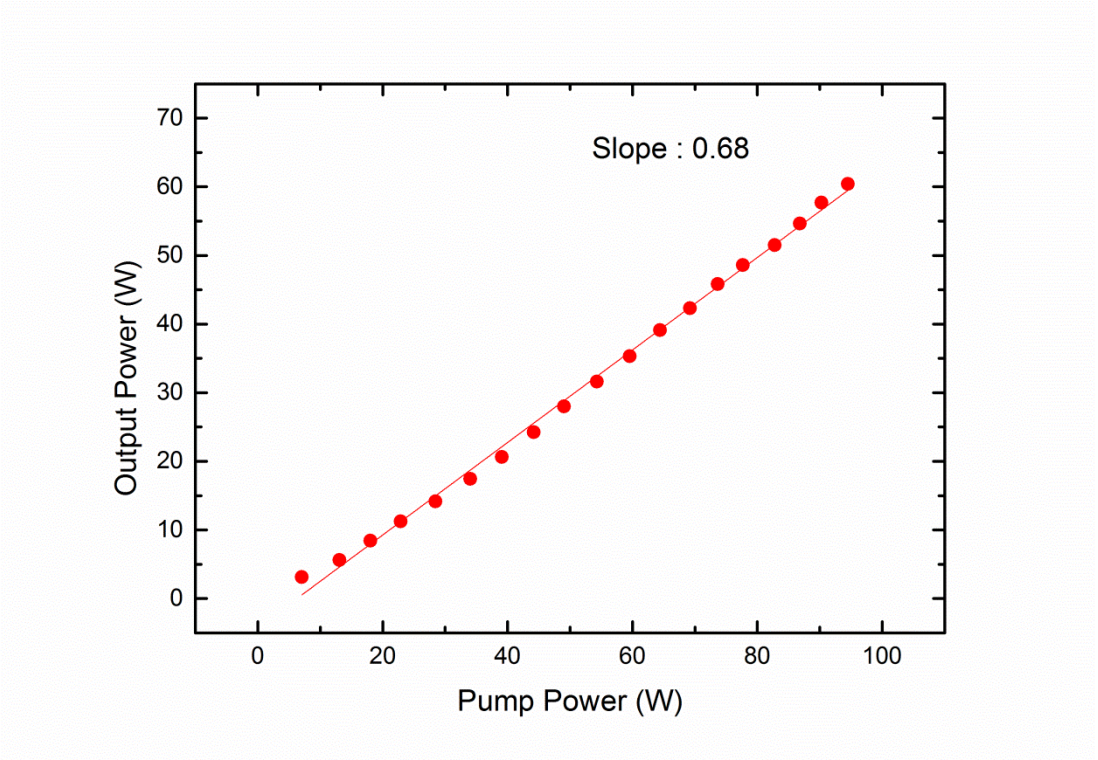

Figure 4.27 Measured power as a function of pump power at the output of the collimated isolator.

4.5 Characterization of the output signal

The whole amplifier and output signal of the system is characterized from various parameters such as beam quality, pulse duration, long term and pulse stability, spectrum of the signal for different parameters. In this section, all characterization process and characterization techniques will be discussed.

4.5.1 Pulse Duration

The pulse duration of the system was characterized as 204 ns square pulse at the beginning of the seed diode. While a square pulse is amplified in a high gain medium, the tail of the pulse amplify lower leading edge of the pulse [43]. Hence, a significant distortion of the pulse occurs at the output pulse. The distortion of the pulse causes pulse shaping with amplification gain at leading edge of the pulse lead high peak power. There is a relation between pulse energy $E(t)$ and effective mode area of the fiber A_{eff} as;

$$E(t) = \int_{t_0}^{t} A_{eff}\, I(t)dt = A_{eff} U(t) \tag{4.1}$$

where $I(t)$ is the signal intensity and $U(t)$ is the energy per unit area. If the input pulse is square the output pulse of the system can be calculated by

$$G(t) = 1 + (G_0 - 1)e^{-U_{out}/-U_{sat}} \tag{4.2}$$

where $G(t)$ is the time-varying gain at any instant time and output pulse can be calculated by;

$$I_{out} = I_{in}(t)G(t) \tag{4.3}$$

The pulse duration of the system was characterized for different power and different repetition rates. First, the pulse durations was measured at different output powers, while repetition rate is 100 kHz as shown in the Figure 4.28. Second, they are measured when repetition rate of the system changes in 20 kHz interval from 100 kHz to 300 kHz as shown in Figure 4.29. At highest peak power, 29 ns effective pulse duration (FWHM) was reached. The pulse width (FWHM) and shaping of the gain can be tailored to material processing application needs.

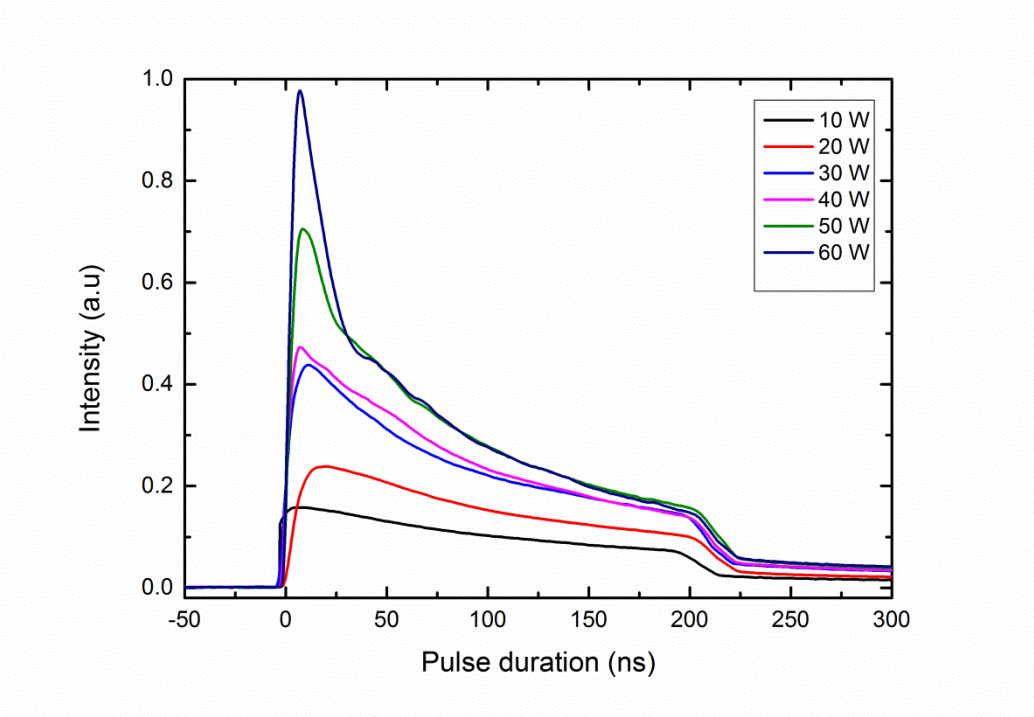

Figure 4.28 Pulse shapes at different output powers at 100 kHz repetition rate

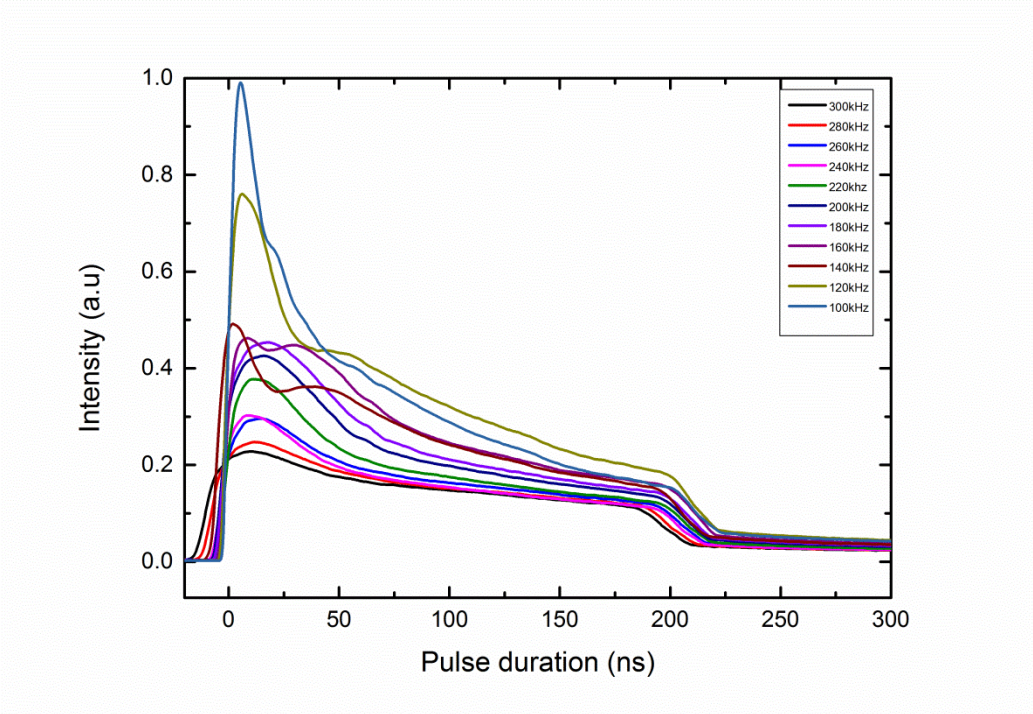

Figure 4.29 Pulse shapes and durations at different repetition rates at constant (60W) average power.

4.5.2 The spectra

The collimated isolator fiber was kept 2 m long and maximum peak power is 20 kW. The peak power, length and core size of the delivery fiber affect the SRS level (Eq. 2.22). Therefore, when the peak power increased, SRS was seen in the spectrum. While the peak power of the system is increased, it reaches SRS threshold and energy of the signal starts to transfer its energy to the nonlinear components. The spectrum of the system was measured at different pump levels by Anritsu MS9740 optical spectrum analyzer to analyze nonlinear and spontaneous emission behavior of the systems. After 14 kW peak power level, SRS starts and it became a large amount at 20 kW peak power since the spikes are formed at beginning of the pulse when the peak power is high and the pulse distortion become higher above the SRS threshold. For instance at 60 W average power level, peak of the pulse consists of higher SRS than other pulses. At maximum operating current, first order SRS which is 32 dB lower than peak was measured. The spectrum of the system for different signal powers at 100 kHz repetition rate is shown in the Figure 4.30. On the other hand, SRS decreases with increasing repetition rates since interaction peak power of the laser beam and distortion of the pulses decreases. In addition, SPM broadens the bandwidth of the spectrum as the peak power increases and a slight spectral enlargement at 1064 nm was observed. The ASE level of the amplifier is also very low. The spectra of the system at full power and different frequencies are shown in the Figure 4.31.

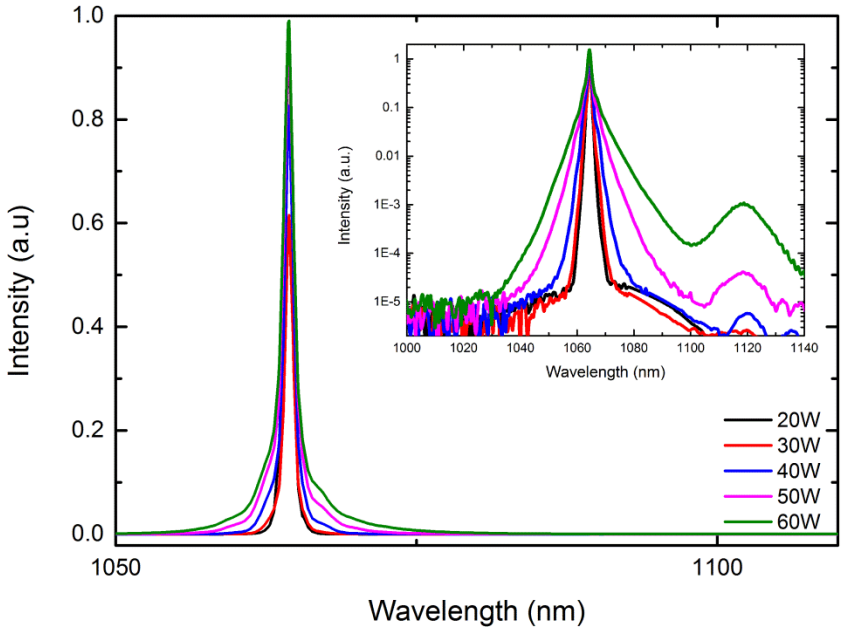

Figure 4.30 The optical spectra of the output signal for 20,30,40,50,60W powers. (inset: logarithmic scale).

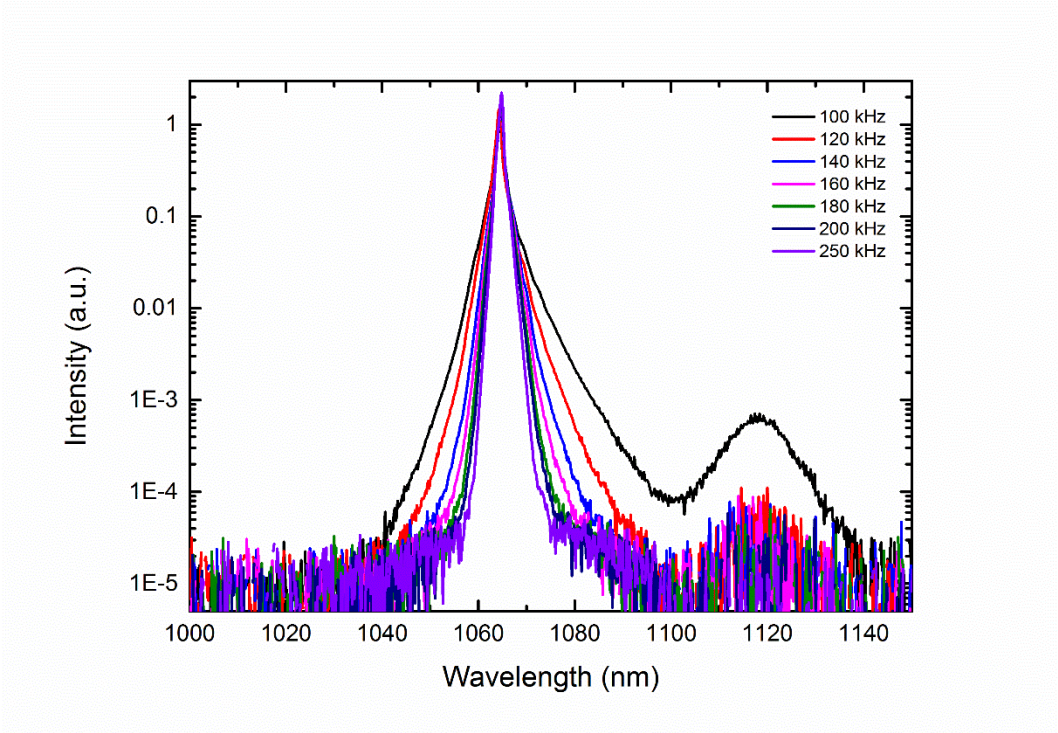

Figure 4.31 Spectrum of the signal at 60 W with different repetition rates. (logarithmic scale).

4.5.3 The beam quality

The brightness of the output signal of the system is determined not only output power but also beam quality. The non-linear effects can be diminished by using high core diameter; however this lowers the quality of the beam since transverse modes besides basic mode are guided inside the fiber core [44]. The beam quality (M^2) factor of the system was measured by using a CCD camera beam profiler (Thorlabs BC106N-VIS) for different signal powers according to 4 Sigma Diameter ISO11146 standard. [45]. The standard includes a fitting procedure to the measured beam radius along the propagation direction. In this thesis, a nearly diffraction limited M^2 was aimed. For this purpose, optimization of the minimizing thermal effects and coiling of the ytterbium doped fiber at the amplifier stage is very important. To achieve high beam quality, higher order modes were suppressed by coiling technique. The technique is not practicable for high NA and core diameter fiber. Our fiber type at the amplifier stage is applicable for using coiling technique. The characterization of M^2 was performed for different coiling radius of the ytterbium doped fiber and minimum 1.51 M^2 was achieved. While the middle and main amplifier gain medium of the system is cooled, the beam quality factor as a function of coiling radius of ytterbium doped fiber is shown in the Figure 4.32.

The maximum beam quality of the system while system is operated at maximum power and active mediums of middle and main amplifier were coiled 5 cm radius and cooled, is measured 1.52. The measured beam quality and 2D and 3D profile of the beam are shown in the Figure 4.33 and Figure 4.34 respectively.

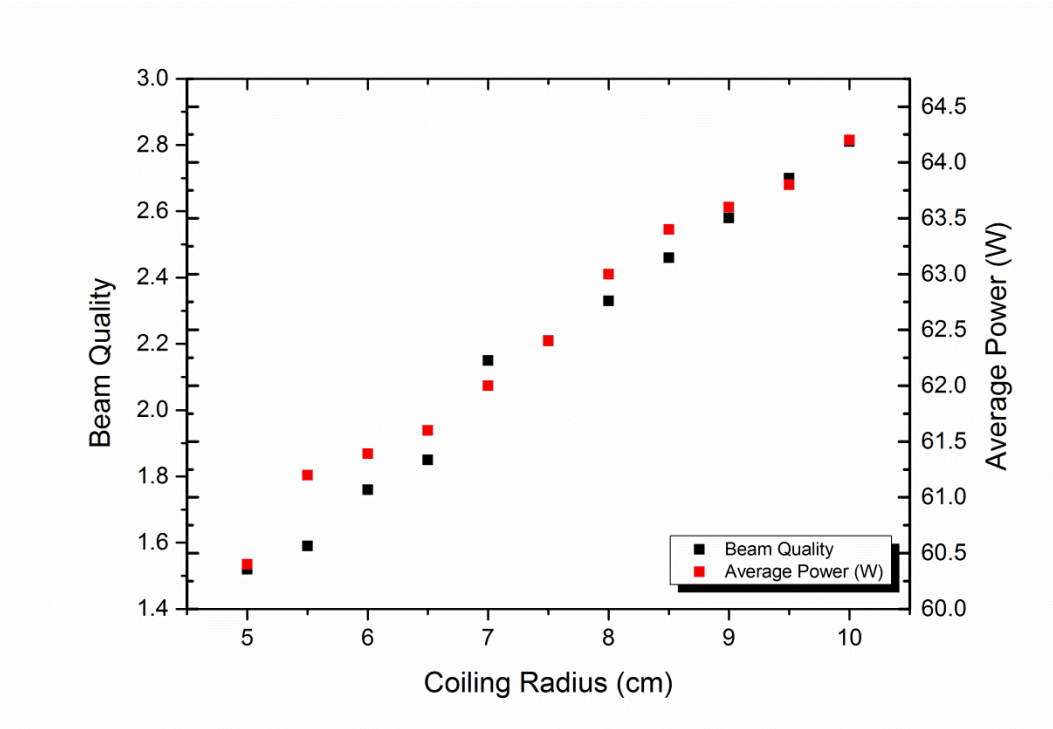

Figure 4.32 The beam quality factor as a function of coiling radius of ytterbium doped fiber.

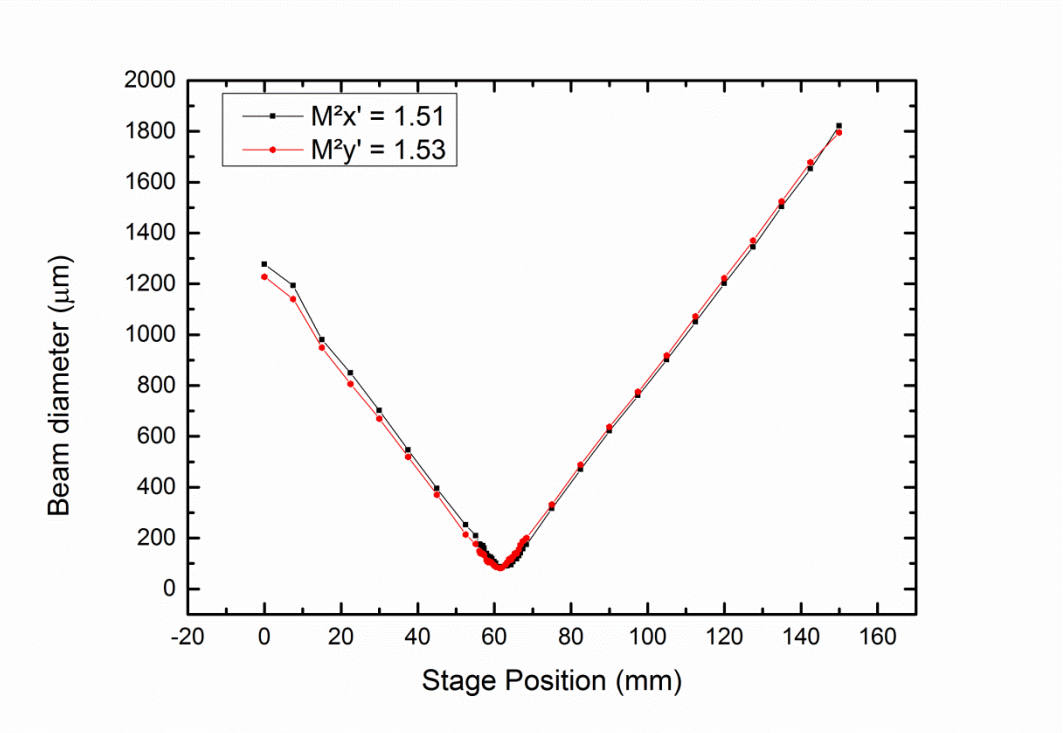

Figure 4.33 Beam quality factor measurement at maximum operating power.

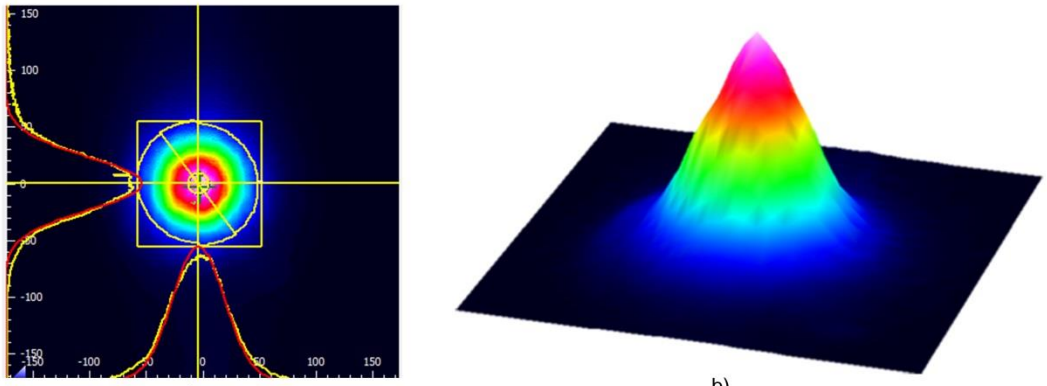

Figure 4.34 Beam profile of the laser output a) 2D profile, b) 3D profile

4.5.4 Long Term Power Stability

The long term power stability of the system at maximum average power was measured by operating system for 200 minutes. The output of the system was measured by a thermal sensor with Thorlabs PM320E power meter and output power data was recorded at 10 s interval up to 200 minutes. The laser output power was reached to 60.4 W average power after 10 minutes, then it decreased to 60.2 W after 80 minutes because temperature of the diodes led wavelength shifting of the pump signal. Hence, after system reaches its steady state value, change in output laser power became less. The change of the output power divided by output power is shown in the following figure.

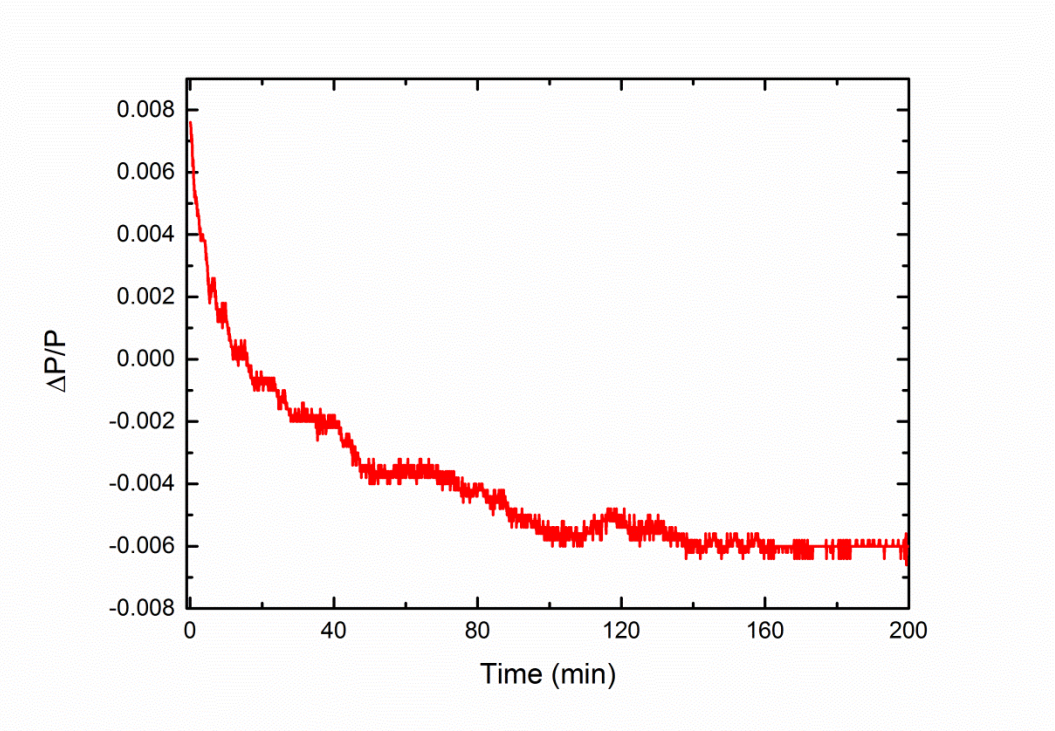

Figure 4.35 Output power fluctuations measured at 10 s intervals.

Table 4. 2 Summary of the fiber laser amplifier parameters.

Maximum Average Power	60 W
Repetition Rate	100 kHz
Pulse Duration at FWHM	29 ns to 203 ns
Pulse Energy	0.6 mJ
Peak Power	20.8 kW
Beam Quality	1.5
Beam Diameter	8.1 mm

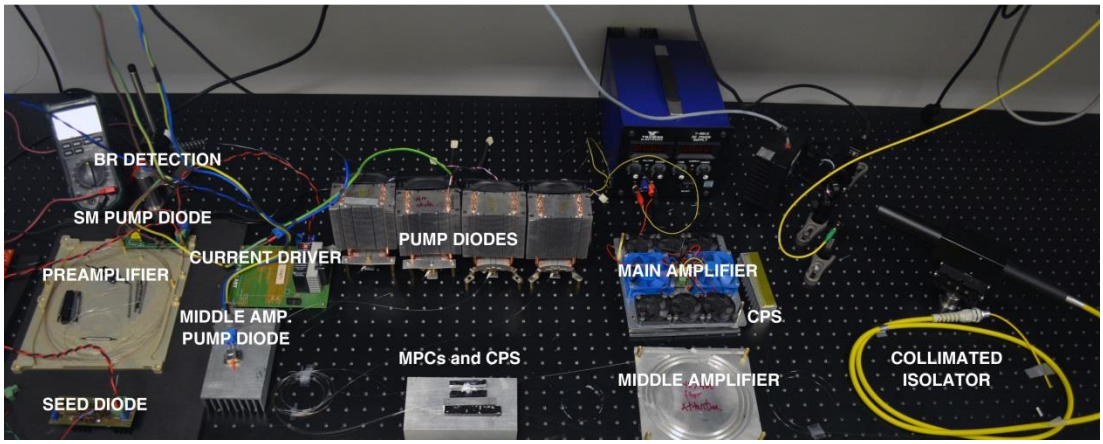

Figure 4.36 Photo of the experimental setup

4.6 Industrialization of the Fiber Laser Amplifier

The developed fiber laser amplifier was industrialized by casing in a compact module for material processing applications. To industrialize an output of a research and development process, several factors should be considered together. First, it is very important to reduce number of components in order to reduce the case of amplifier. Second, choosing high reliable components provides a reliable long term operation to amplifier. Third, managing thermal flow inside the case is important to increase reliability of the amplifier since efficiency of the diodes and laser medium are affected from high temperatures. Fourth, designing the electronic controllers and cards is important for they should be small and reliable for providing pulse and current generation. Therefore, a compact laser amplifier was developed by taking into all of these factors.

To achieve modulated signal from SM pump diode, I had electronic control card that was developed by METRA Electronics. The card has an input for providing signal frequency to the diode and a microcontroller to determine the duration of the pulse. The important specification of the card enable changing pulse duration while the repetition rate is constant The trigger signals generated by a pulse generator are sent to microcontroller and the duration of the generated pulse is determined by the user from 200 ns to 500 ns in 50 ns interval independently from repetition rate. After switch on the electronic card, it starts from 200 ns pulse duration. To control pulse duration, a pulse width controller was used and it sent command to the microcontroller according to

determination of the user. The modulated signal is sent to current controller and a modulated current is provided to the diode. Then, pulse duration is generated by the modulated current. Moreover a current driver for SM pump diode and a current driver for MM pump diodes are integrated on the card. The current of the diodes is set at operating current by a control knob. In addition, circuit of the electronic card include a TEC (thermo electronic cooler) for providing a constant temperature to the signal diode and pump diode. Another electronic card with TEC was developed to cool SM pump diode. A simple schematic of the control card is shown in the following figure.

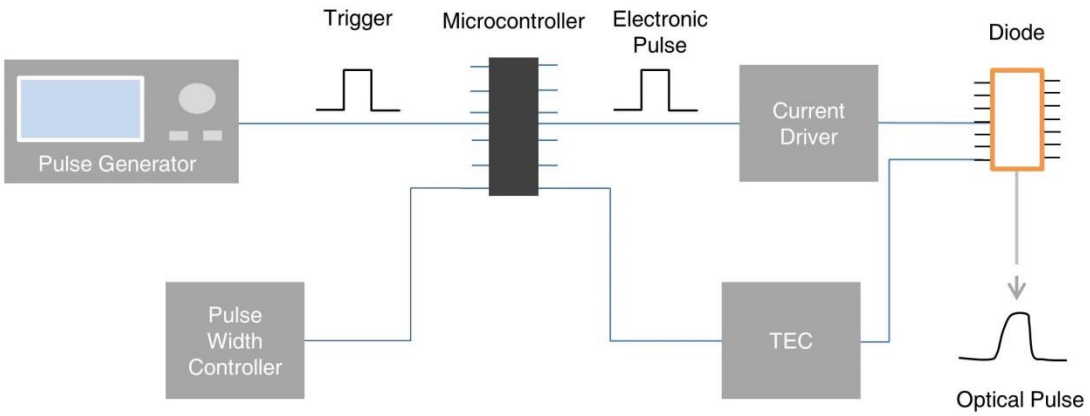

Figure 4.37 Simple schematic of the signal modulation mechanism in electronic card.

The same current as experimental setup was applied to current controller and same output was achieved. In preamplifier design, one pump module with 400 mW output current was used as different from experimental setup. 400 mW pump power was divided to ~300 mW and ~100 mW by using a 25/75 single mode fiber coupled coupler. The configuration of the preamplifier is shown in the following figure.

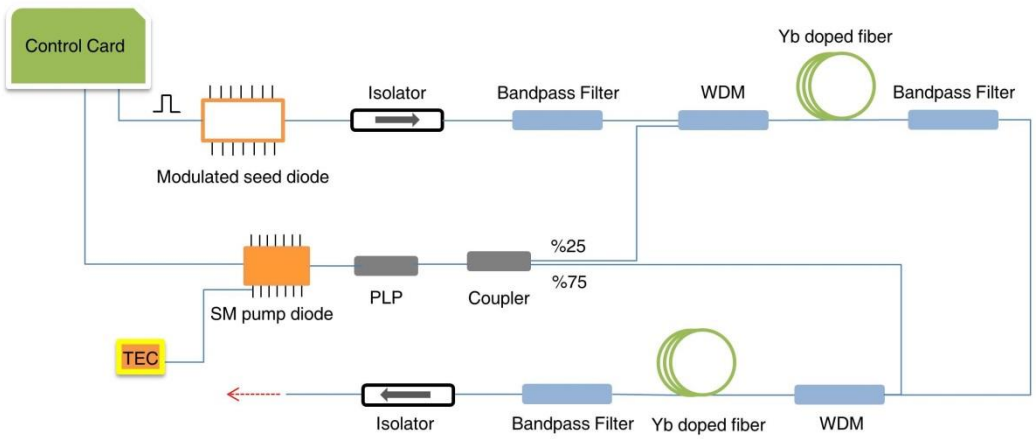

Figure 4.38 Industrialized design of the preamplifier stage.

In preamplifier, while switch on button is used to activate modulated seed diode and SM pump diode, they are operated simultaneously at operating current.

A 630/1064 nm coupler was used between middle and preamplifier stage in order to add a 635 nm SM diode to guide processing area on the material. A control card, which operates at 5V and limits the current of the circuit for 630 nm diode, was developed and the diode was integrated on it. Then system design was re-constructed to straiten the area of components. It is easy to decrease and stabilize the temperature of the cooling zone by five 5200 rpm fan if the temperature is distributed homogenously. Hence a 310 x 255 mm aluminum cooling profile with air blast cooling was used to cool diodes at operating current. The diodes were placed homogenously on the cooling zone. The ytterbium doped fiber of the middle amplifier stage and fiber of the other components were placed into a thermally conductive silicone adhesive. The cooling zone was also used to cool ytterbium doped fiber, PLP and MPC of the middle amplifier stage and ytterbium doped fiber and MPC of the main amplifier stage. A current driver which is integrated with electronic control card was used to drive all five MM pump diodes which were connected serially. While increasing pump level of the middle amplifier stage, pump power of the main amplifier stage also increases. This situation provides a low ASE level in low power levels. A simple schematic of the whole system is seen in Figure 4.39.

The current driver of the pump diodes operates with a signal between 0-5 V and generates maximum 10.5 A. It can work at 30 V operational voltage. The design of the

electronic control card allows to get signal in order to operate pump driver externally. An input was taken on the case of the laser amplifier system for external power control.

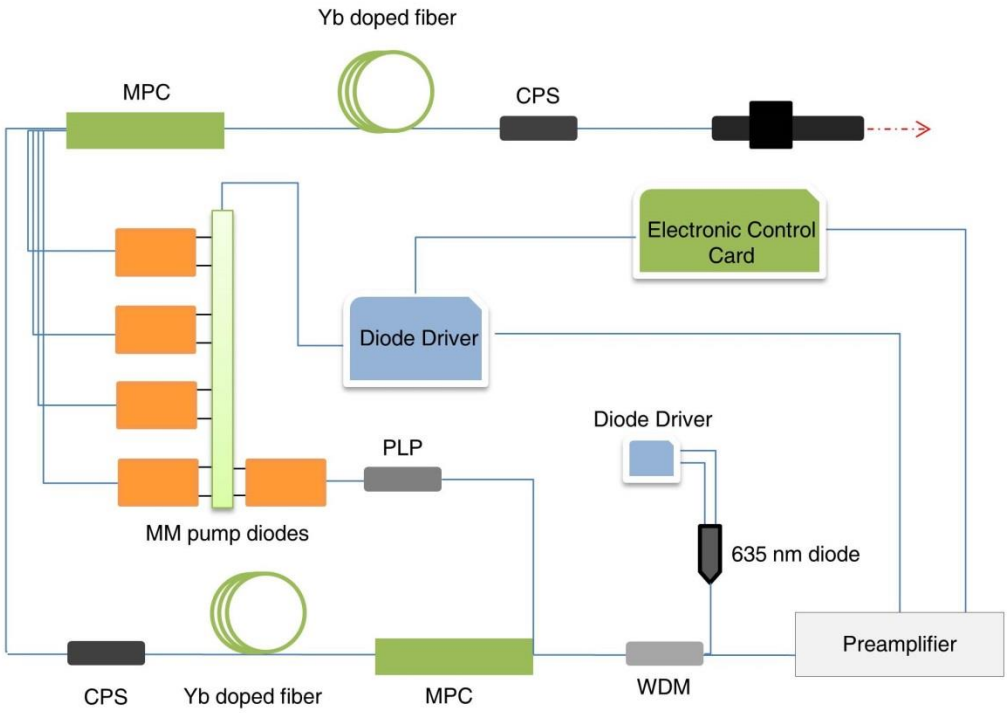

Figure 4.39 A simple schematic of industrial system.

Ytterbium doped fiber of the main amplifier stage was placed into a fiber coiling stage with an thermally conductive adhesive and a fan was used to cool fiber and inside the amplifier case. Total dimension of the laser amplifier case is 310 x 155 mm x 250 mm and this dimension consists of not only amplifier source but also electronic control card of galvanometric scanner. The mechanical case has 4 buttons in front of it. While two of them allow the user to open preamplifier and amplifier respectively, the others allow controlling pulse width of the laser beam. A 7-segment display was used to show pulse duration of the system. When laser amplifier is opened, 7 segment display on with 0 indication which means pulse duration is 200 ns. Each incrimination of 1 means increasing a 50 ns pulse duration. Another two LED display “ready” and “mark” was used on front face of mechanical case. While laser is ready for operation, ready led on. On the one hand, mark display become on if laser amplifier is active. After constructing all electronic

configuration, a wall plug efficiency 28% was achieved. One of the advantage of the system is that if fiber length of the amplifier and signal seed in amplification stage are chosen right, its MOPA design allow us to upgrade its average power by only adding pump diodes to amplifier without changing design of the whole system.

Photograph of the industrialized laser amplifier and whole system with power supply and galvanometric scanner is shown in the following figures.

Figure 4.40 The industrialized laser amplifier.

Figure 4.41 Laser system with galvanometric scanner.

4.7 Comparison with other industrial systems

There are some of fiber laser manufacturers in the world and a few company has an ability to develop all fiber nanosecond pulsed MOPA structure with more than 50 W average power laser amplifier. The most known companies that develop and sell pulsed MOPA configuration fiber laser more than 50 W average power are SPI Lasers [46] and Max Photonics [47]. As shown in the following table, developed fiber laser in this study has several advantages in comparison to others in industry. It is clearly seen that the beam

quality of our laser amplifier is better than others while pulse energy is lower. Despite lower pulse energy, lower pulse duration provides higher peak power than others. On the other hand, pulse duration range, output power stability and weight of mechanical case are preferable to others.

Table 4. 3 The parameters of other industrial MOPA lasers

Specifications	**SPI RM 50**	**SPI RM 70**	**SPI 70HS**	**MP MFPT 50**	**MP MFPT70**
Average power (W)	50	70	70	50	70
Max. pulse energy (mJ)	0.5	>1	>1.25	0.91	0.91
Beam quality	<1.6	<1.6	2.5-3.5	<2	<2
Pulse width range (ns)	40-260	40-260	10-250	10-250	10-250
Peak power	>10	>10	>20	NA	NA

CHAPTER 5

MATERIALS PROCESSING WITH FIBER LASER AMPLIFER

Materials processing with a pulsed fiber laser is a very common technique for many different application areas and several types of the lasers are demonstrated in the literature to show laser-material interaction behaviors on the material by drilling, scribing, marking, cutting, engraving and marking. The most of the pulsed fiber lasers in materials processing area relies on Q-switch configuration. In this configuration, external crystals are used to releasing and storing the energy, however these types of laser are limited by the Q-switch technology. This limitation causes an inflexibility of the pulse energy, pulse duration and repetition rate. In addition, there are lots of studies for material processing applications but it is also limited with regard to the target material. The developed MOPA design fiber laser amplifier in this study have some special properties such as independently adjustable pulse duration and repetition rate, nearly diffraction limited beam quality, high peak and average power, all fiber design, and pulse to pulse stability. In this chapter, by using several materials and applications, there will be discussions on how these properties are related with each other while processing of the materials with laser and performance of the developed laser amplifier.

5.1 Introduction

To process materials, several setup configurations were used, however all of them are mainly parallel to configuration showed in Figure 3.9. While several configurations are used, effects of the main parameters such as average power, pulse energy, pulse duration, repetition rate, focal length of the objective and scan speed are characterized according to materials and applications. Hence, all of these parameters has different effects in processing. If pulse energy, pulse duration and peak power parameters are changed individually, it is very easy to determine effects of them on the materials. While processing the

materials with pulsed lasers, adjusting pulse overlapping with scan speed and repetition rate and spot diameter of the beam are also very important. A demonstration for pulse overlapping is shown in the following figure.

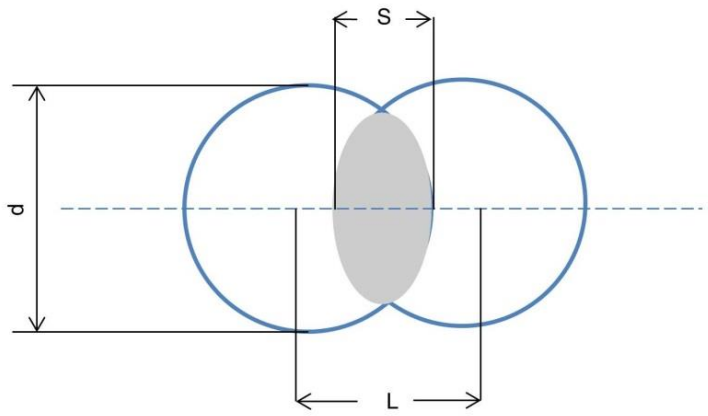

Figure 5.1 The demonstration of the pulse overlapping.

The gray area is pulse overlap area and L is the distance from center to center. The L value can be calculated by $scan\ speed/repetition\ rate\ (pps)$, d is the laser spot diameter and S is the length of overlap. Then the percentage of pulse overlapping can be calculated by

$$O_{\%} = \frac{s}{d} = \left[1 - \frac{L}{d}\right] \times 100 \tag{4.1}$$

The scan speed and repetition rate were changed in different applications, this means it is very important to choose best overlapping result for each process. In this study, 100 mm and 160 mm focal length objectives were used to focus laser beam. For the 160 mm and 100 mm focal length objective, the spot diameter of the developed laser is 38 μm and 25 μm respectively. The percentage of the overlapping of pulses of developed fiber laser amplifier for different repetition rate and scan speed was calculated for each material processing applications. For

instance, the overlapping percentage for 160 mm objective as a function of repetition rate of laser with different scan speed is shown in the following graph.

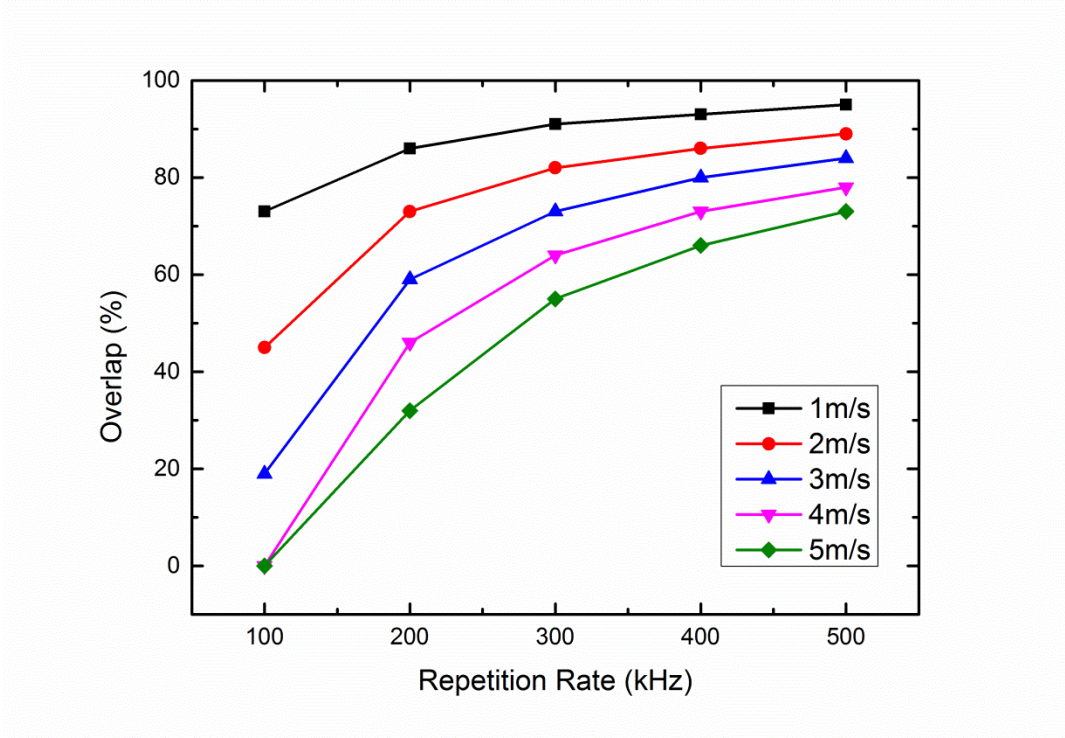

Figure 5.2 Percentage of pulse overlap as a function of repetition rate in different scan speeds.

The pulse to pulse stability on the material is another important factor and it was controlled visually by using a setup as Figure 3.9 and a bulk silicon was scanned by with 160 mm objective by repetition rate of 100 kHz laser beam and two different scan speeds of 3800 and 2200 mm/s. The surface of the bulk silicon was inspected by scanning electron microscope (SEM). The formation of the pulses with different scan speed is shown in Figure 5.3. As shown in the figure, adjusting scan speed of the laser beam is very important in processing the materials. In this section, all of laser parameters were characterized for different material types and capability of the laser is explained by processing different material and characterizing of laser processing parameters for each of them.

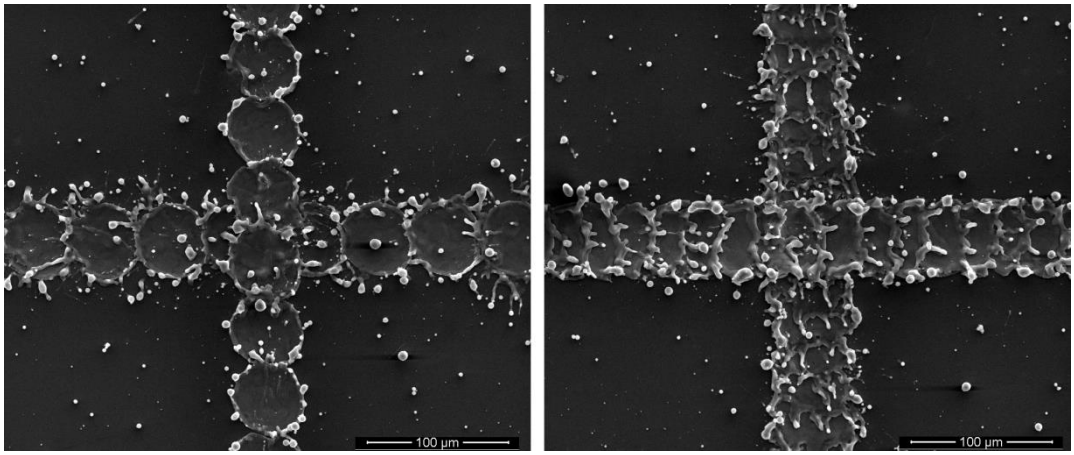

Figure 5.3 Pulse to pulse formation at 100 kHz repetition rate on the material with scanning speed a)3800 mm/s b) 2200 mm/s.

5.1.1 Microdrilling Efficiency

In this section, comparison of different pulse durations of laser beam effect on two different material targets with same thickness such as stainless steel and aluminum was performed. The average power and pulse peak power were kept same by adjusting repetition rate of the laser beam for each microdrilling process. In the experiments maximum 20 W average power and minimum 100 kHz were used to drill since pulse distortion of the laser beam was started (Figure 4.28) after 20 W average power. The galvanometric scan head named as Scancube II from ScanLab company was used. A software and control card which are named as SamLight and USC1 respectively by SCAPS company was used to control galvanometer scanner. In addition, objective with 160 mm focal length was used to keep intensity of the laser same for each process. The experimental setup is shown in the following figure.

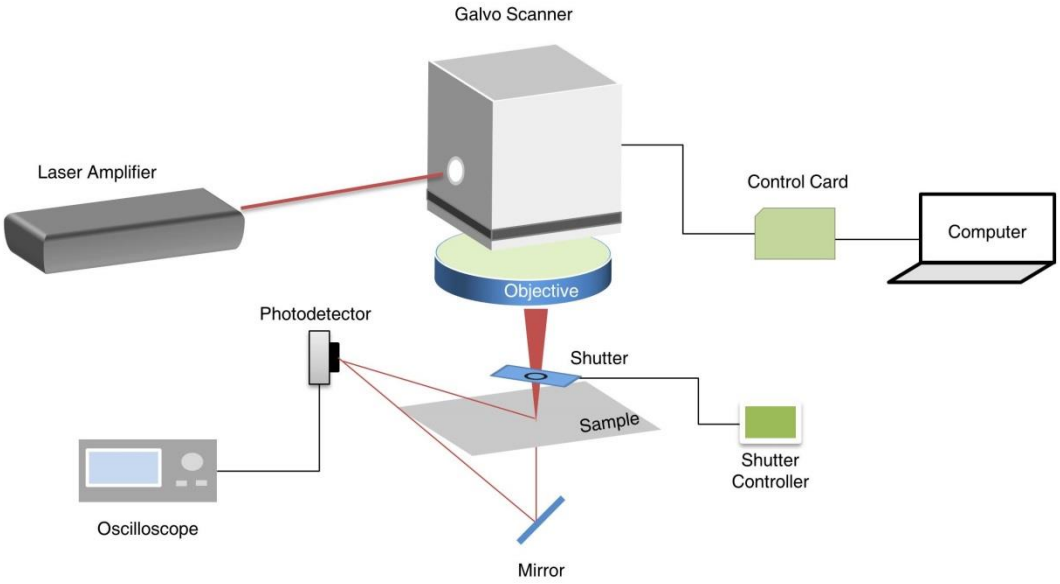

Figure 5. 4 Schematic diagram of microdrilling experimental setup.

A silicon biased photo detector from Thorlabs Inc. with 75 mm^2 active area and a shutter controller were used to determine removal rate of the material. The photodetector was placed on the side of the samples to collect light from the sample directly and bottom of this sample by a 45^0 inclined mirror. A shutter with shutter controller was used to protect material from the laser beam before the experiment. The laser was operated, then shutter was set on. Immediately before starting of the micromachining process, a spike was observed due to high reflectance of the targets, then it was decreased when the material is disrupted by ablation process. The signal of the photodetector remains constant during drilling process. After the laser beam reaches the bottom of the sample namely mirror, the signal suddenly increases and the delay between the two spikes allows an accurate measurement for drilling time. Calculating the time between the two spikes allowed a precise measurement.

The output power of the laser was adjusted from 2 W to 5 W, then 5 W to 20 W by 5 W incrementations and pulse duration of the laser was adjusted from 203 ns to 407 ns by nearly 100 ns incremantations. The peak power of the system was kept same for each experiment by adjusting the frequency of the laser. For instance, the repetition rate was set to 100 kHz for 407 ns, while it was adjusted to 200 kHz for 203 ns pulse duration

at same average power. For the experiments, 100 μm thick stainless steel and Al samples were used. To check quality and morphology of the holes, SEM was used. The microdrilling time of the processing with respect to average power for steel and aluminum is shown in the following graphs.

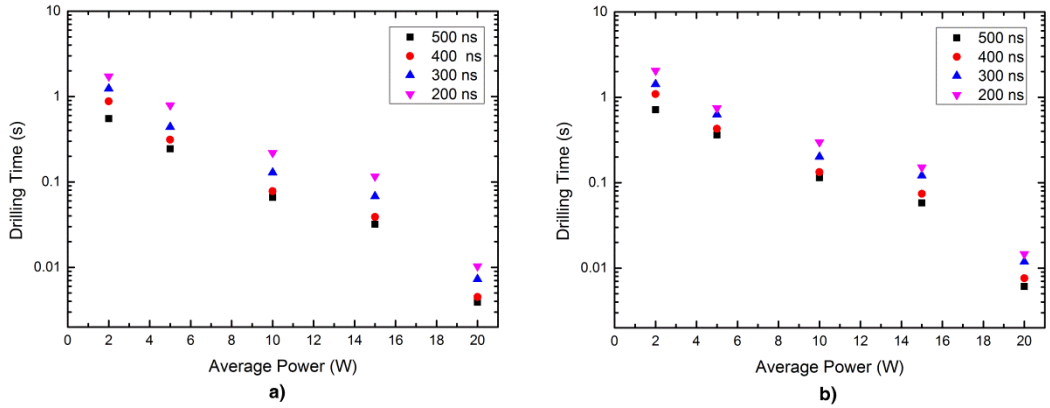

Figure 5.5 Microdrilling time with respect to average power and pulse duration for a) steel b) Al.

There are several results which were induced from the experimental data. First, the aluminum has thermal conductivity that is more than 12 times higher thermal than stainless steel [48; 49] and drilling rates increase with decreasing thermal conductivity and heat diffusivity of targets. Second, the drilling rates are longer for short pulse durations because higher repetition rates were applied for short pulse duration experiments in order to keep peak power constant. In experiments with higher repetition rate and short pulses, energy of the pulses are lower than low repetition rate experiments. The more "on and off process" of laser beam leads to reduced efficiency and at first leading edge of each pulse heat the target material towards critical temperatures. Third, the exposure time to drill material increases sharply while average power is lower than a required threshold power. The threshold power of the laser beam is higher for the material with larger thermal conductivities than the materials with lower thermal conductivities.

In addition the quality and morphology of the holes are analyzed with taking images by SEM. Figure 5.6 shows the images of the stainless steel and Al samples which

were drilled by an average power of 15 W and different pulse durations but same peak power. It is shown that longer pulses are ideal for a good quality microdrilling applications on metallic thin foils since they produce less crater formation around the drilling area than short ones with same peak power. This can be explained in the way that the required exposure time is low for long pulses with respect to short ones. On the one hand, long pulses were sent to material with lower repetition rate which mean higher pulse energy and higher pulse to pulse time duration. Hence, there is enough time between the pulses to cool material and higher pulse energy allows faster drilling and lower oxidation.

On the other hand, to see the amount of ablation at the same peak power was observed visually by applying the laser beam to the material with different pulse duration but equal exposure time. The SEM images of the stainless steel which was processed with four different pulse durations and same peak power laser beam is shown in the Figure 5.7.

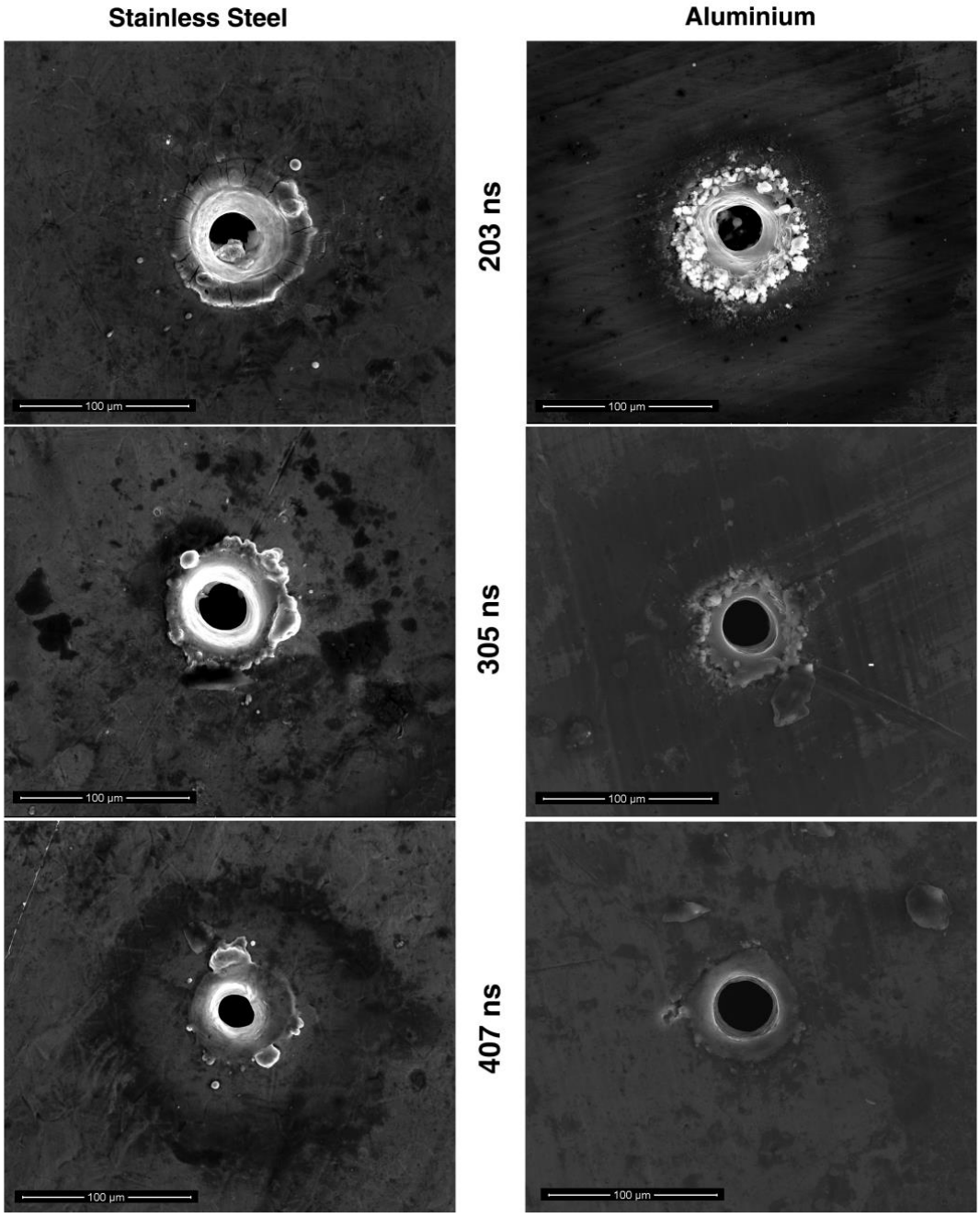

Figure 5.6 SEM images of microdrilling applications on stainless steel and aluminum with 15 W average power and 203, 305 and 407 ns pulse duration

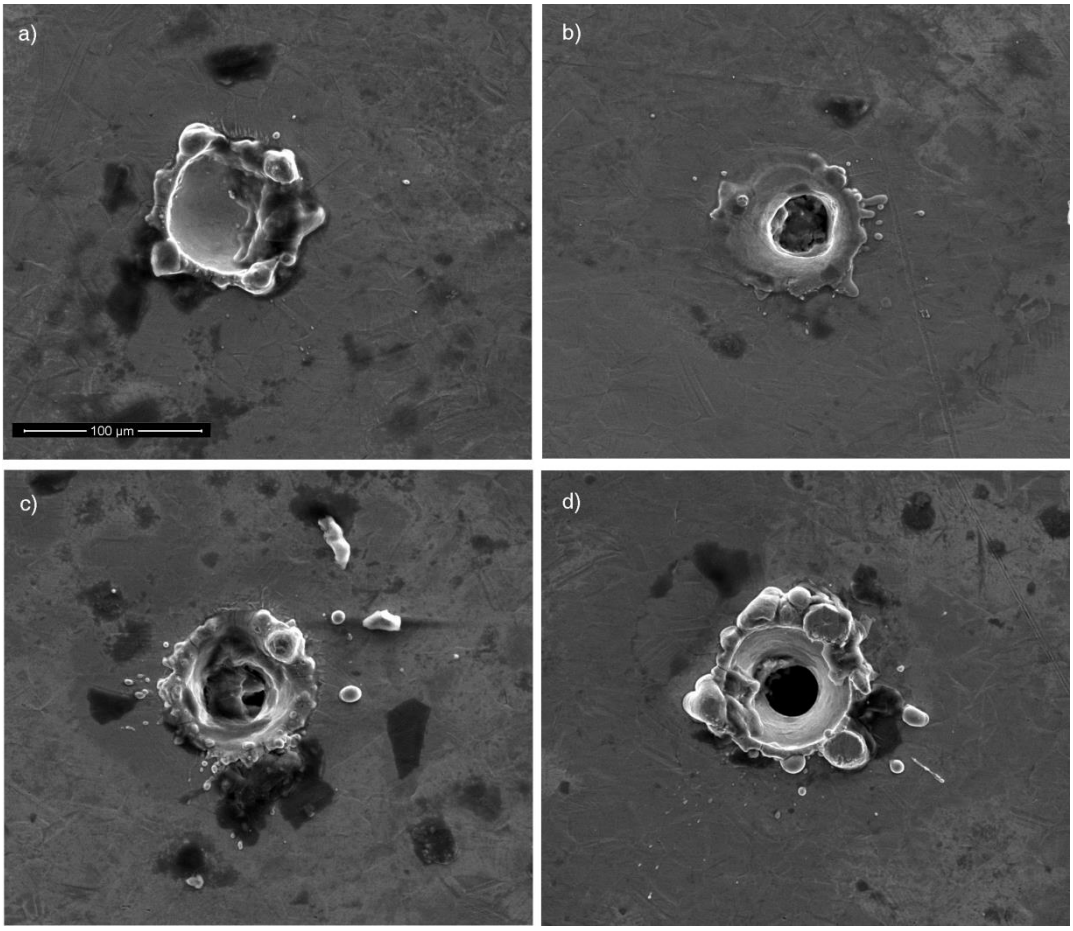

Figure 5.7 SEM images of microdrilling attempts on 0.1 mm stainless steel in same exposure time 8 ms at 20 W average power and different pulse durations a) 100 ns b) 200 ns c) 300 ns d) 400 ns.

5.2 Edge Isolation of Silicon Solar Cell

The solar cell studies offers several important options for renewable energy applications. While solar cell technology evolves day by day, it uses other technologies to achieve higher efficiencies. The laser is one of the key technologies for several c-Si and thin film based solar cell applications such as edge isolation, drilling, cutting and marking wafers, thin film patterning and scribing since it provides precise and high speed results. Besides, it is environment friendly as no hazardous chemicals are used. In this section, edge isolation application was demonstrated by using our fiber laser amplifier and scanning speed was characterized to achieve fast scanning speed.

5.2.1 Introduction to Edge Isolation

There are several important steps of process in manufacturing solar cells and one of them is edge isolation. The edge isolation of the c-Si based solar cell is performed by removing the phosphorous diffusion area around the cell edge. To develop a p-n junction for generating electricity, an n-doped outer layer is used on the p-doped wafer. [50; 51]. After this process the front emitter of the wafer is isolated from the cell rear electrically and efficiency of the cell increases. To isolate edge of the solar cells, several methods such as the plasma dry etching, dispensing of etching paste etc. are used [52]. One of the other techniques for edge isolation is performed by laser source since it is a non-contact, fast and easy method. The edge isolation process with laser that is based on vapor induced melt ejection by nanosecond laser pulse durations. While performing a laser machining of Si based material, optical properties of the Si should be examined. Because of their high absorption coefficients, visible and ultra-violet range wavelengths (532,355,266 nm) are used for processing of the Si based materials over the past three decays. Today, advances in 1064 nm fiber based laser sources redefine processing options with reference its brightness, lower costs and performance [53]. Adjusting laser parameters such as electromagnetic spectrum, pulse duration, pulse energy and scanning speed in processing is very important. Choice of the correct wavelength of laser is essential for an effective processing of Si since amount of the absorption of the light determines heating level of the material. If the rate of heating is enough, material can be removed by melting and vaporization process. The melting and vaporization process depends on the type of the material and duration of the pulses and effect of them was discussed in 3.1.

To achieve a high quality isolated zones with fast scanning speed and to determine the effects of the 1064 nm fiber laser pulses of our laser on the Si based cells, a series of the experiments were conducted by our 60 W fiber laser amplifier.

5.2.2 Experimental Setup and the Results

In the first experiments, A saw damage and a textured 150 μm thick single crystalline silicon wafer was used for experimental studies to understand efficiency of machining for different surfaces. The experimental setup was configured as shown in Figure 3.9 and different sized objectives were used to understand the effect of the spot size. To optimize the laser parameters

for processing, several scribing grooves was created under several pulse durations and pulse energies. The repetition rate of the laser was kept constant at 100 kHz and the scan speed is very important for achieving a continuous grooving on the material for this repetition rate. The maximum scan speed was determined for 100 kHz repetition rate as about 3000 mm/s to avoid from discontinuous grooving. A textured silicon wafer was used for scribing experiments and it was processed with 1000 mm/s scanning speed and 40 W,50 W and 60 W average power with one repetition cycle. It can be seen in Figure 5.8 which indicates SEM image of silicon in different power where the grooves are continuous and the depth of the groove increases by increasing average power of the laser.

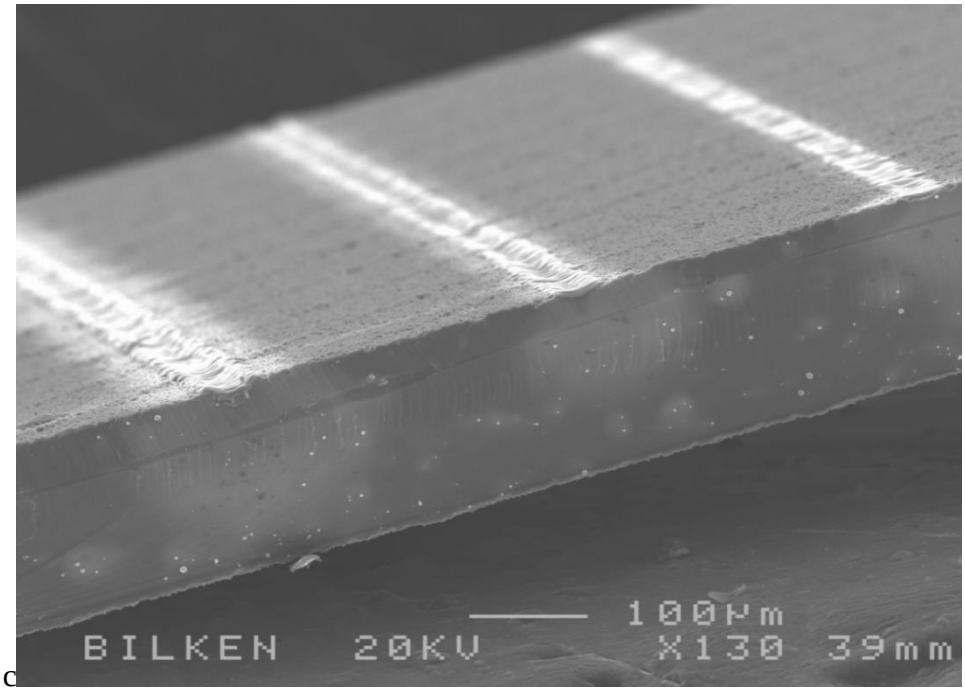

Figure 5.8 SEM image of laser processing on silicon with scan speed 2500 mm/s and different average power. Laser power at 60 W, 50 W and 40 W from left to right.

It is shown that width of groove and width of heat affected zone increase with increasing average power. On the one hand, after understanding behavior of the laser spot size on solar cell, another experimental series was done by different objectives with 100 mm and 160 mm focal length. 40W average power with 500 mm/s scan speed and one repetition cycle were performed with two different spot sizes on textured silicon solar cell. Then, it can be seen in

the following figure that decreasing spot size creates deeper but narrow grooves since decreasing spot size increases fluence of the laser beam and lower the processing area.

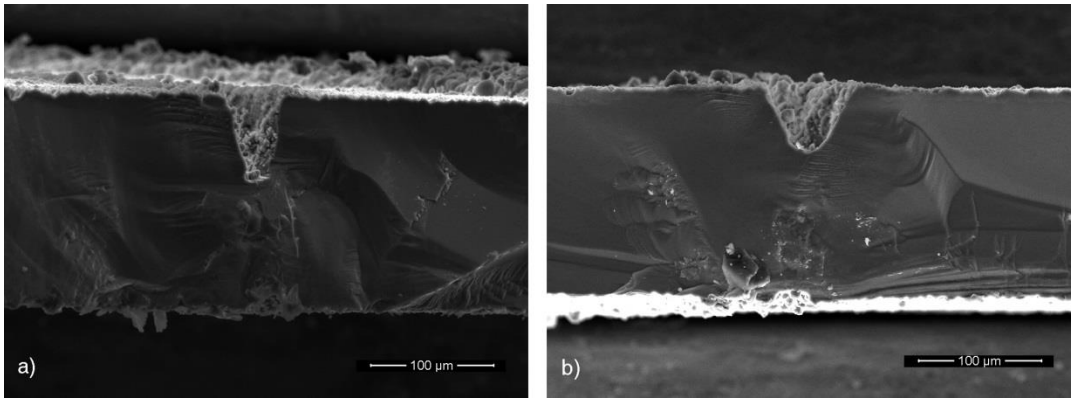

Figure 5.9 Laser edge isolation process on textured Si cell by same average power and scan speed but different laser beam spot sizes by a) 100 mm b) 160 mm focal length objectives.

To understand behavior of the laser pulses on the silicon, several trying with different parameters was realized. It is obvious that the overlapping of the pulses also affects the heating zone and quality of the isolated area. It is easy to achieve ablation of the silicon from surface to end of the material. However, morphology of the surface is affected from increasing exposure time and high overlapping. As shown in the following figure, 60 W power was used to process silicon with different overlapping. The SEM image of solar cell from top of the cell is shown on the bottom of the each figures.

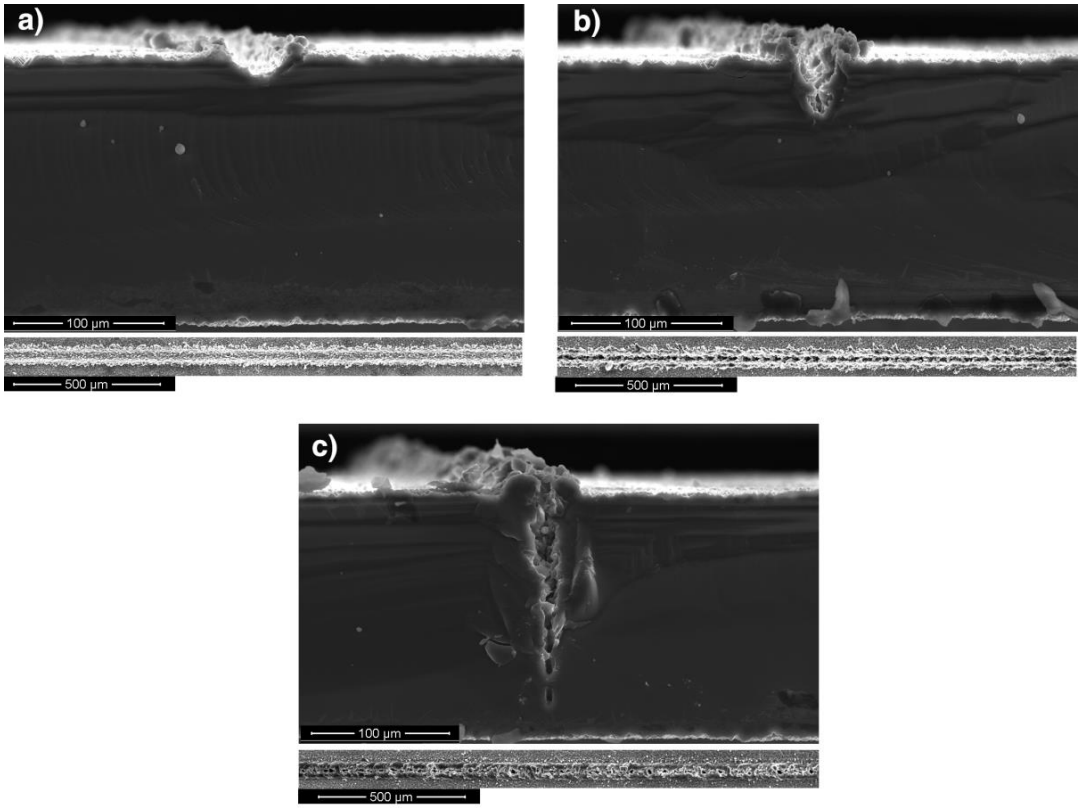

Figure 5.10 Processing of silicon wafer with different pulse overlapping a) 2000 mm/s b) 1500 mm/s c) 500 mm/s scan seeds at 100 kHz repetition rate.

As shown in the Figure 5.10c and Figure 5.10b, heat effected zone of the silicon increases with decreasing overlapping namely increasing total exposure time. While the depth of the processed area increases, the morphology of the silicon is corrupted. In addition crater formations were seen. Hence, the power should be chosen lower to achieve better morphology and lower heat affected zone but scan speed also should be chosen lower. However, our aim is to achieve highest speed so we didn't prefer to decrease average power. These three different parameters were applied three different full scale solar cell wafers which were produced by GÜNAM (The Center for Solar Energy Research and Applications). The efficiency of wafers were measured without isolation as 14 %, 13.7 %, 14.1 %. Each of them was processed with laser about at the 200 µm distance from edge of the wafer. The experimental IV measurements which indicated that increasing depth of the isolated area doesn't increase efficiency too much. The increasing exposure time increases thermal effects on the processing area and the sides of the scribed areas were merged. Hence, the isolation become difficult since electrons can pass from that merged areas. The best result was achieved for the sample which was scanned with

2000 mm/s where the depth of the isolated area is nearly 30 μm and light conversion efficiency increased from 14 % to 16.2%. For the samples which were scanned with 1500 mm/s and 500 mm/s efficiency increased from 13.7 % to 15.4 % and 14.1 % to 14.4 respectively. The SEM images of the wafer from the top view are seen in the following figure.

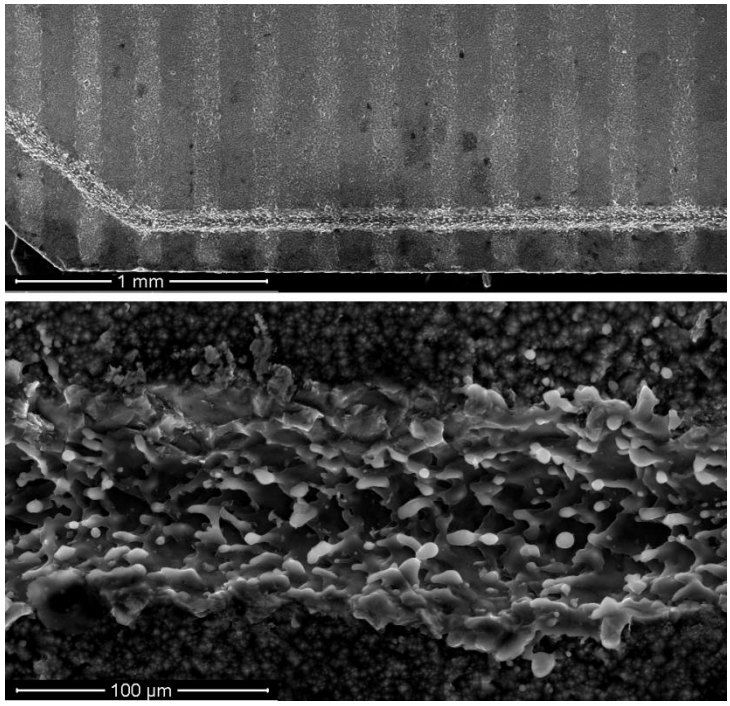

Figure 5.11 Top view of the processed full scale silicon wafer with 2000 mm/s scan speed and 60 W average power

The experimental studies show that developed laser amplifier is a fast and good tool for edge isolation applications and has an ability to scribe cells with several depths.

5.3 Color Marking on Metallic Surfaces

To create a high quality marking area on a metal surface, it is required to have a high quality laser beam. Hence, fiber based laser systems are the best technologies for these type applications. The developed MOPA design fiber laser system also allows creating colored marking applications on metallic surfaces by optimizing laser parameters. Color marking applications by lasers have a high potential for many industrial applications

since it is harmless and cheap procedure and it provides permanent colors on material [54]. The color marking is performed by creating oxide layers on surface by using laser beam and the colors depend on thickness of layer In this section, effect of the laser parameters for creating colored marking area will be discussed by using the advantage of independent adjusting of laser pulse duration and repetition rate and using different laser parameters on a stainless steel surface.

5.3.1 Principle of Color Marking

The principle of color marking by laser depends on surface oxidation of material in oxidizing agent. The thin films on the material can be created by heating of the surface. Several parameters such as average power, fluence, direction of marking, depth of focus, pulse duration, scan speed are the main parameters for laser marking applications. If we provide a constant temperature on the metallic material, a colored surface can be created by growing oxide layer deposited on the surface. Then, the thickness of the thin film, which defines visible color, is defined by laser parameters. The simple schematic of interference effect on thin film is shown in the following figure.

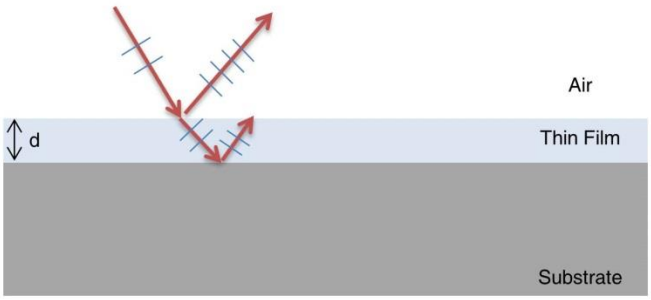

Figure 5.12 Schematics of inference based color marking mechanism .

The roughness of the surface and homogeneity of layer affect the color of the sample. Moreover, the color changes can be seen in different angles according to quality of oxide layers.

5.3.2 Experimental Details of Color Marking

To create colored surfaces, experimental setup which is shown in Figure 3.9 was used. The laser beam was controlled by SamLight software which controls the galvo scanner by a control card. A 1 mm thick stainless steel 304 was used for processing applications. In this experiment, creating very high spot overlaps by low pulse energy was aimed. The sample was cleaned with isopropyl alcohol. First, an ideal average power at minimum repetition rate 100 kHz and 10 W was determined respectively for marking process. After 10 W power level, material was started to ablate especially in low repetition rate due to high peak power. Then, 10x10 mm areas were crated in software and hatched with 10 μm line intervals on the 1 mm thick stainless steel. The spot size of the laser is 39 μm and fluence is 93 mJ/cm² with 160 mm F-tetha objective. There are several number of parameters so experiments were performed by keeping several parameter constant while adjusting others. First, several laser scan speeds were tried on stainless steel at 100 kHz repetition rate, 203 ns pulse duration and 8W average power parameter to reveal the effect of scan speed. The speed of laser beam changed from 20 mm/s to 1000 mm/s in 20 mm/s intervals. As shown in the following figure, marking in faster speeds create bright surface since material doesn't have enough time to create thin film layer due to fast cooling. On the one hand, higher speeds create dark area because of creating thicker thin film layers to absorb visible spectrum.

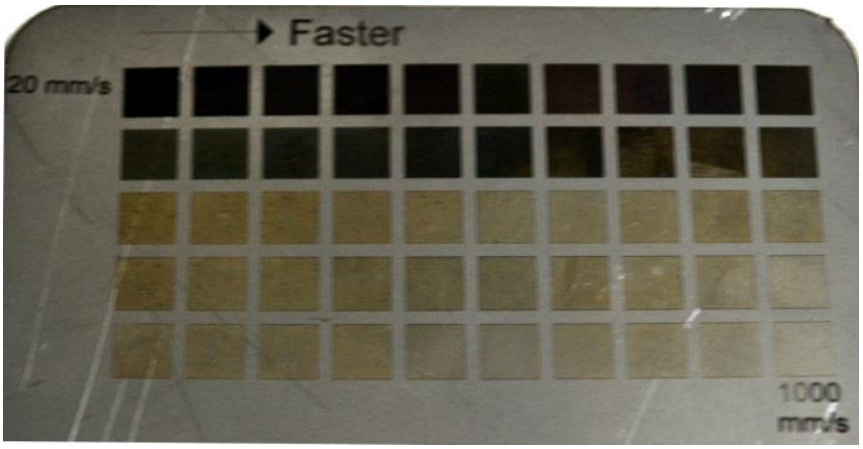

Figure 5.13 Effect of scan speed on color marking of stainless steel.

The first experiment to create color marking areas was performed by keeping peak power constant. The repetition rate was kept 100 kHz while changing the average power from 4-8 W and pulse width from 200-400 ns. The scanning speed was varied from 25 mm to 250 mm/s with 25 mm/s intervals. The highest quality colors were seen at 200 – 300 ns pulse duration interval at 55 - 65 μJ pulse energy level.

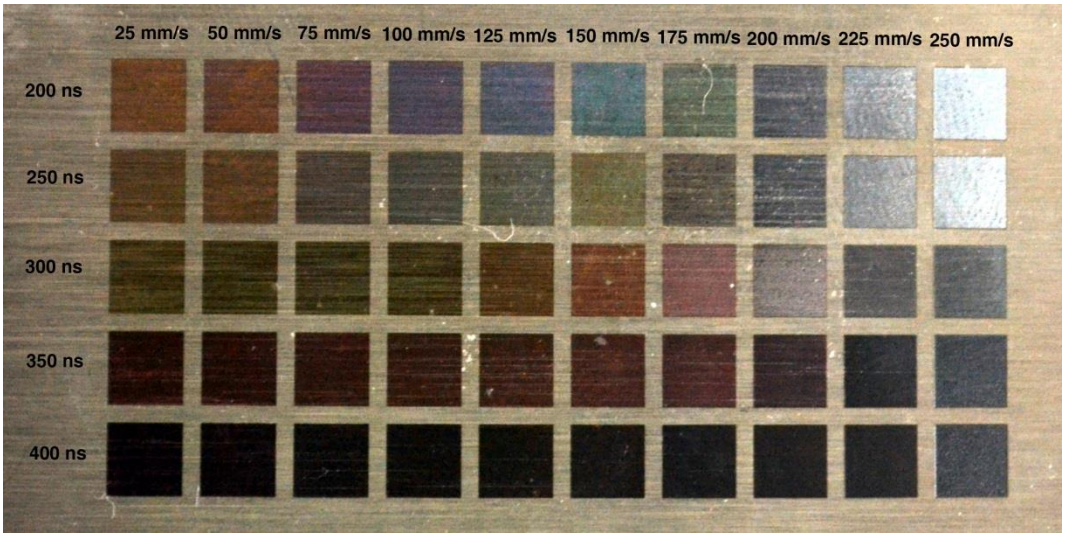

Figure 5.14 Marking stainless steel with constant peak power varied average power and pulse duration.

Then the second experiment was done with varied pulse width and repetition rate to keep peak power constant while average power is constant. 5 W average power was used to process and pulse duration and repetition rate was changed between 200 to 400 ns and 100 kHz to 200 kHz respectively. The best contrast color was seen at 100-130 kHz repetition rate with 40-50 μJ pulse energy. The results of oxidated layers by the experiment is shown in the Figure 5.15.

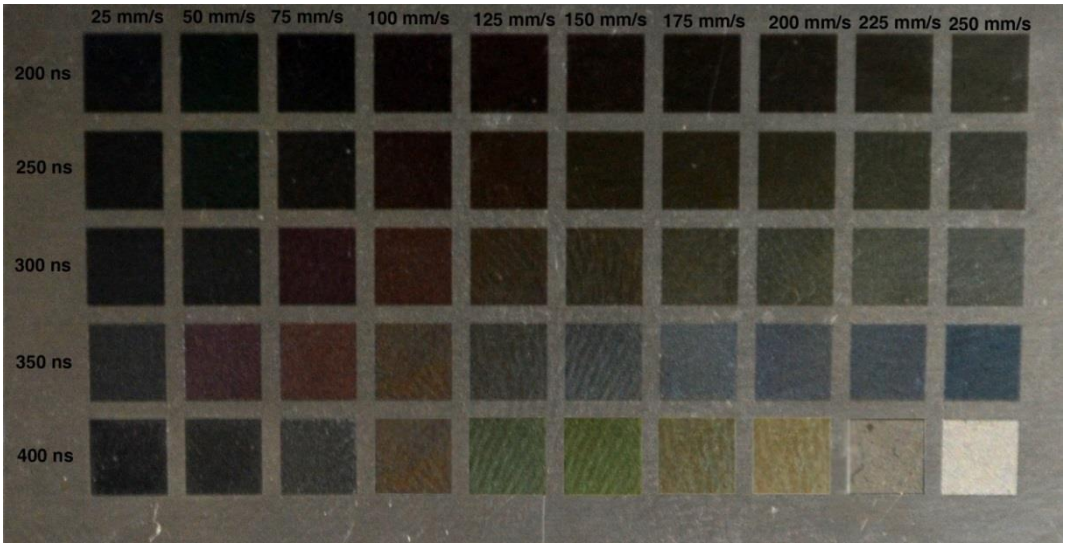

Figure 5.15 Marking stainless steel with constant peak and average power

Alternatively from adjusting constant peak power, to determine the effect of increasing peak power and to achieve better results on the material another experiment was performed. The constant repetition rate was chosen at 130 kHz with constant pulse energy 50 μJ which is an optimal energy determined from first two experiments. The pulse duration was varied between 200 ns to 400 ns and results of the experiment are shown in the following figure.

Figure 5.16 Marking stainless steel with varied peak power and constant pulse energy.

As shown in the Figure 5.16 the colors varied for different peak powers if the pulse energy and average power is constant. The better and more variety of colors were achieved. The capability of the laser amplifier for color marking was investigated and several parameters were used to show how parameters affect the contrast of the color. This capability of laser amplifier can be used for several applications such as, logo marking for industrial goods and jeweler design. Some of the logo samples were done by using parameters which are achieved in the experiments and they all are shown in the following figure.

Figure 5.17 Color marking samples.

5.4 Deep Engraving Applications

The laser engraving applications offer many advantages once compared to traditional engraving processes such as being a non-contact method, cheap and precise [55]. The developed laser in this study has a capability for engraving many types of metal

by the help of its 60 W average power and 20 kW peak power and independently adjustable pulse length and repetition rate. In addition, pulse profile of developed laser amplifier has a fast pulse rise which ensures to overcome the energy absorption thresholds of most of metallic materials. On the other hand, capability of producing a range of pulse duration allows a fine control on the materials. The engraving processing requires the selection of appropriate parameters and materials. In this section, ability and capability of laser amplifier for engraving applications were investigated by using different materials and ablation rates of the materials in atmospheric air were studied and discussed. In addition, to maximize material removal rates with a good surface quality, different parameters were optimized and discussed.

5.4.1 Introduction to Deep Engraving

The engraving process is slower for lower average power but it is more controlled and finer than applications performed with higher average powers. The rate of ablation while processing a material with laser, the parameters such as beam quality, beam diameter, pulse energy, pulse to pulse overlap and spot size have an important effect on ablation of materials [56]. It also depends on absorptivity, thermal conductance mass density, surface reflectivity of the material and environmental conditions [39; 57].

A setup as shown in the Figure 3.9 was used to engrave Al sample and laser beam was controlled similarly as explained in 3.3.1. As differently from this setup, a vacuum with exhaust fan was used to collect ablated particles from material surface. First, an experiment was investigated to show effect of laser scan speed and repetition rate for engraving aluminum material. The engraved surface was determined as 2x2 cm and it is created by 20 μm lines. The laser amplifier was operated at full average power namely 60 W with different repetition rates at 100, 120,140 and 160 kHz. Then the number of scans was varied on different areas on the material and scan speed is constant 1000 mm/s. After engraving process, a cleaning pass with 20W average power and 2000 mm/s scan speed was applied to the engrave area to achieve a shiny appearance. A 160 mm objective was used to focus laser beam. The depth of engraving as a function of scan number is shown in the following figure.

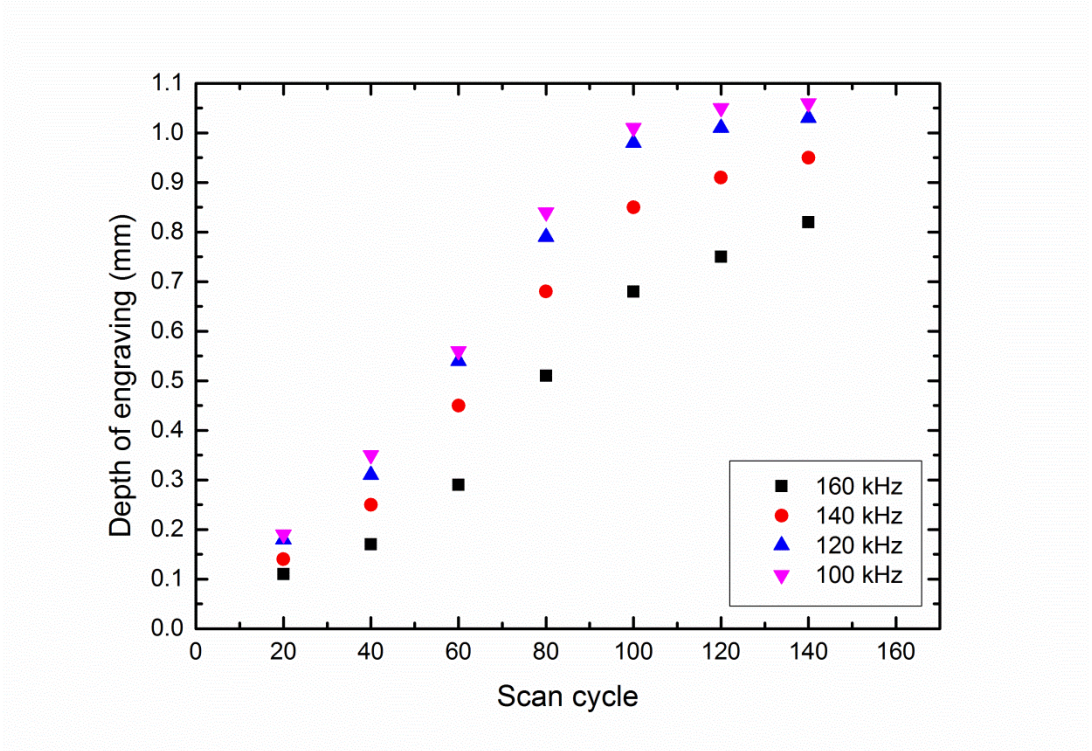

Figure 5.18 The depth of engraving as a function of scan number at different repetition rates (100,120,140,160 kHz) with 1000 mm/s scan speed.

As shown in the graph, while interaction time of laser with the material increases by increasing scan number, the depth increases. The same approach is valid for decreasing line spacing and increasing scan speed, hence increasing line spacing and scan speed does also cause lower engraved depth due to low interaction time of laser beam with material. As shown in the Figure 5.19 below, the material doesn't get deep after for a length of time since it is limited DOF of laser beam. The DOF is determined by focal length of objective, wavelength and beam size of the laser, as shown in the Eq. 3.3 Hence it is very important to choose appropriate focal length of objective for processing applications. The maximum engraved depth which is created by using a 160 mm objective was 1.055 mm and it almost corresponds to theoretical value. After going out of DOF, the process expeditiously slows down .The engraved Al sample is shown in the following figure.

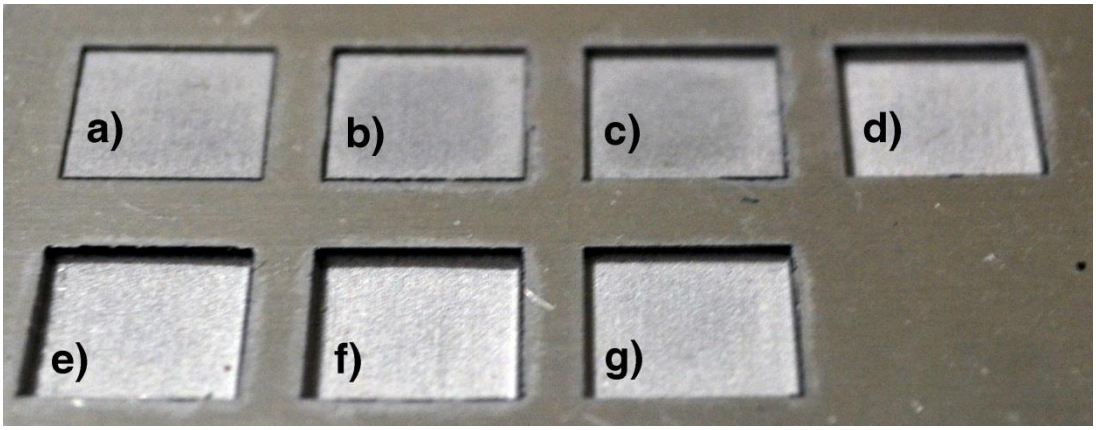

Figure 5.19 The engraved Al sample with different scan cycle a) 20 b) 40 c) 60 d) 80 e)100 f) 120 g) 140 times.

On the other hand, repetition rate of the laser affect the engraved depth. While processing material with lower repetition rate namely higher pulse energy, the material is engraved more deeply. The effect of the decreasing depth with increasing repetition rate is also due to decreasing peak power of the laser.

To achieve higher material removal rates, the surface temperature of the material can be increased [58] since every laser pulse act for increasing the temperature up to vaporization threshold, then vaporize the material. The surface temperature of the material depends on the material as well as repetition rate and overlap of the pulses and irradiance. Hence, another experiment was investigated to increase material removal rate. The overlapping of the pulses was increased from 73% to 86% by decreasing scan speed from 1000 mm/s to 500 mm/s for 100 kHz repetition rate. However, scan cycle was reduced by half to remain interaction time of the first experiment. Achieving maximum depth of engraving is quicker than first experiments since heat of the material increases with increasing overlapping of the pulses. The results in the following figure shows that an increase in removal rate was achieved.

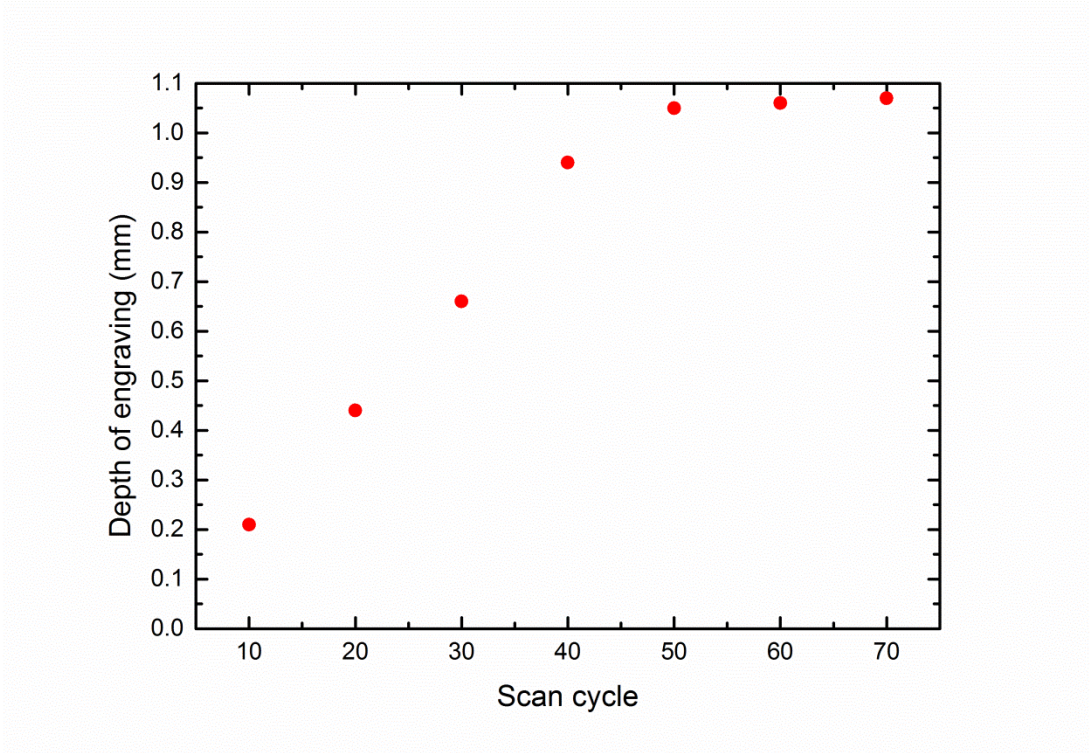

Figure 5.20 The depth of engraving as a function of scan number at 100 kHz repetition rate and 500 mm/s scan speed.

The developed laser amplifier has a capability of engraving several materials such as Al, steel, copper, silver, bronze, brass etc. and it is a convenient source for several industrial engraving applications. The engraving process depends on several parameters and the best results changes from material to material depending upon laser parameters. In addition, choosing appropriate lines allows the laser to provide cutting applications by ablation process. However it is also limited by DOF of the laser beam. Some of the samples which are engraved by developed laser amplifier is shown in the following figure.

Figure 5.21 Some of the engraving and cutting samples prepared by laser amplifier; engraving of a) 14 carat gold, b) stainless steel, d) brass, cutting of c-d) aluminum.

5.5 Some Other Applications

There are several applications which can be done by developed fiber laser amplifier. We tried by using several parameters on several materials to show which other applications can be achieved by laser amplifier. The material processing applications such as, marking and cutting several types of material, barcoding, sintering, cutting, surface micromachining, day&night marking etc. can be done by developed laser amplifier. The application samples is shown in the following figure.

Figure 5.22 Application samples done by developed fiber laser amplifier : marking of a stainless steel a), plastics b) and c), brass d), denim e), stainless steel f), leather g), cart i); day&night marking of aluminium h); precise cutting of a stainless steel k); micromachining of titanium j) ; dye removal of aluminum l); microdrilling of silver m); sintering n); label marking o).

CHAPTER 6

CONCLUSION

The rare earth metal doped fiber lasers are used in many different areas such as material processing, spectroscopy, optical communication, medicine, defense industry etc. In addition, applications of fiber lasers are increasing day by day since its advantage against conventional solid state laser. Fiber lasers provide alignment free operation, high beam quality, high efficiency and power scability. In this study, a nanosecond pulsed MOPA type 1064 nm wavelength all fiber laser amplifier system with 60 W average power, more than 20 kW peak power and 0.6 mJ pulse energy, was developed and industrialized for materials processing applications and its efficiency on the materials processing was studied by using several types of applications. In this amplifier, MOPA design provides a major advantage, which is the independent tunibility of pulse duration and repetition rate. The parameters of laser amplifier were adjusted to achieve optimal, high-speed and high quality processing results.

The experimental studies showed that there are several important points to be regarded while designing a fiber laser amplifier. Careful analysis of the influence of a several parameters is required to optimize the performance of the laser amplifiers. First of all, selection of ideal passive components for each step of amplifier is crucial for reliability of the system. For instance, while determining the MPC, it is not only important to choose correct core and clad size, but also NA of the core and clad of the fiber. Second, determining the fiber lengths and fiber types are important in many aspects such as achieving a ASE, nonlinearity and residual pump free spectrum and a high beam quality. Third, characterization of the fiber splices has significant influence on transmission losses of the laser light especially in splicing different core and clad size fibers. Fourth, it is important to choose high absorptive wavelength of the pump diode to decrease nonlinear effects by decreasing length of the amplification (active) medium. In addition, cooling the laser diodes is critical for long-term stability of amplifier. Fifth, protection of the MOPA stages from back reflection of the laser beam by isolators is a required step in design process.Sixth, elimination of the some components such as diodes

provide a low cost design and lower component area for industrialization of the laser amplifier. In addition, developed splicing techniques in Chapter 4 can be used in many other clad pumping fiber laser amplifiers. Moreover, to protect components from the residual pump, developed CPS in Chapter 4 also can be used in different clad pumping laser amplifiers.

Material processing applications also showed that several significant points affect the application quality. First of all, determining beam size of the collimator and objective size to focus beam are important since they affect the depth of field, beam size on the material, maximum processing area and influence of the laser beam. Hence, they have an impact on the materials. Second, adjusting an ideal repetition rate of the laser beam and scan speed are major parameters for achieving optimal exposure time of the material. Third, deciding average power has critical importance to achieve low heat affected and melted zone on the material.

Almost every commercially developed fiber laser with nanosecond pulse duration, that is used for material processing, is Q-switched systems. The developed laser amplifier, which is different from Q switch and many of the other industrialized systems, has many advantages . First, its pulse shape and repetition rate can be changed independently which provides to use several different pulse energy with different pulse duration on the materials. Second, the beam quality of the system at 60W average power and more peak power at maximum average power and minimum repetition rate is better than many other nanosecond pulse duration MOPA lasers in industry. In addition, wide range of repetition rate and pulse duration allow to use several different pulse energies with different pulse durations. Third, if fiber length of the amplifier and signal seed are chosen right, its MOPA design allow us to upgrade its average power by only adding pump diodes to amplifier without changing design of the whole system. The whole industrialized system is free of misalignment –namely all fiber- and compact, hence it can be transported without any alignment problem. In addition, electricity consumption of the laser amplifier is about 250 W and it is more than 8 times lower than a nearly same average power Nd-YAG laser source [58; 59].

Pulsed laser amplifiers have a lot of potential applications in many areas and specification of our laser amplifier allows to perform several type of materials applications apart from processing examples which were demonstrated in this study. For example, it is

possible to perform removal of thin films for photovoltaic applications by finding exact laser parameters [60]. In addition, marking and cutting of the wafers are possible by our laser amplifier [61]. In industry, most of the laser type for processing organic materials is CO_2. However, the ability of the adjustable pulse duration and repetition rate and nearly diffraction beam quality of our laser amplifier provide marking of some organic materials such as plastics, cartoon and some types of wood. The developed laser amplifier is a suitable tool for many industries such as automotive, consumer products, energy, electronics, jewelry, medical, giftware, semiconductor.

In future works on this system, following areas will be important ;

- The increasing output power of the system will be studied for cutting and fast marking and engraving applications.

- The lower repetition rate is important for increasing pulse energy of the system and decreasing thermal effects on the materials. Hence increasing pulse energy of the system by characterizing pulse shape of the seed diode to eliminate nonlinear effect will be studied.

- The type of the doped fibers effects the nonlinearities and thermal condition of the fiber. Therefore, different doping concentrated fibers on amplifier stage will be appreciated.

REFERENCES

1. *British Patent.* **J., Baird.** 738, 1928, Vol. 285.

2. *A flexible fiberscope using static scanning.* **Hopkins, H. H. and Kapany, N. S. .** 39, s.l. : Nature , 1954, Vol. 173.

3. *A new method of transporting optical images without aberrations.* **Heel, A. C. S. van.** 39, s.l. : Nature, 1954, Vol. 173.

4. *Optical Maser Action in Nd3+ in a Barium crown Glass.* **Snitzer, E.** 444–446, s.l. : Physical Review Letters , 1961, Vol. 12.

5. *Proposed fiber cavities for optical lasers.* **Snitzer, E.,.** 36-39, s.l. : J. Appl. Phys, 1961, Vol. 32.

6. *Amplification in a fiber laser.* **C. J, Koester, . and E, Snitzer.** 1182–1186, s.l. : Appl. Opt, 1964, Vol. 3.

7. **Etzel , H. W, Gandy, H.W. and Ginther, R.J.** 534-536, s.l. : Appl. Opt. 1, 1962, Vol. 4. Stimulated Emission of Infrared Radiation from Ytterbium Activated Silicate Glass.

8. *Dielectric-fibre surface waveguides for optical frequencies.* **Hockham, G. A. and Kao, C. K.** 7, s.l. : Proc. IEE, 1966, Vol. 113.

9. *Neodymiumdoped silica lasers in endpumped fiber geometry.* **Stone, J. and Burrus, C.A.** 7, s.l. : Applied Physics Letters, 1973, Vol. 23. 388-389.

10. **Maurer, Robert and Schultz, Peter.** *Fused Silica Optical Waveguide. 3659915* 1972.

11. *Low noise Erbium Doped Fiber Amplifier Operating at 1.54 um.* **Mears, R. J, et al.** 1026-1028, s.l. : Electronics Letter 23, 1987, Vol. 19.

12. **Snitzer, E et Al.** s.l. : Proc. Of Optical sensors, 1988. 88'PD5.

13. *Ytterbium-doped silica fiber lasers: versatile sources for the 1–1.2 μm region.* **Pask, H.M, et al.** 1, s.l. : Journal of Selected Topics in Quantum Electronics, 1995, Vol. 1.

14. *35-W single-mode ytterbium fiber laser at 1.1 μm.* **Kea, D., et al.** CPD30, s.l. : Proc. Conf Lasers Electro-Optics,CLEO'97, Postdeadline paper, 1997.

15. *110 W fibre laser.* **Dominic, V., et al.** 14, s.l. : Electronic Letters, 1999, Vol. 35.

16. *Ytterbium-doped large-core fibre laser with 1 kW of continuous-wave output power.* **Jeong, Y., et al.** 8, s.l. : Electron. Lett, 2004, Vol. 40.

17. *Ytterbium-doped large-core fiber laser with 1.36 kW continuous-wave output power.* **Jeong, Y., et al.** 25, s.l. : Optics Express, 2004, Vol. 12. 6088-6092.

18. *10 kW single mode fiber laser.* **Fomin, M., et al.** St. Petersburg : Proc. of 5th International Symposium on High-Power Fiber Lasers and Their Applications, 2010, Vols. Session HPFL-1.3.

19. *Femtosecond fibre CPA system emitting 830 W average output power.* **Eidam, T., et al.** 2, s.l. : Opt. Lett., 2010, Vol. 35. 94-96.

20. *131 W 220 fs fiber laser system.* **Röser, F., et al.** 20, s.l. : Optics Letters, 2005, Vol. 30. p 2754.

21. *Fiber chirped-pulse amplification system emitting 3.8 GW peak power.* **Eidam, T., et al.** 1, s.l. : Optics Express, 2011, Vol. 19. 255.

22. *Average power of 1.1 kW from spectrally combined, fiber-amplified, nanosecond-pulsed sources.* **Schmidt, O., et al.** 10, s.l. : Optics Letters, 2009, Vol. 34.

23. *11 mJ all-fiber-based actively Q-switched fiber master oscillator power amplifier.* **Fang, Q., et al.** 11, s.l. : Laser Phys. Lett., 2013, Vol. 10.

24. *High-power fibre lasers.* **Jauregui, C., Limpert , J. and Tünnermann, A.** s.l. : Nature Photonics, 2013.

25. *Generation of 36-femtosecond pulses from a ytterbium fiber laser.* **Ilday, F.Ö., et al.** s.l. : Opt. Exp., 2003, Vol. 11. 3550-3554.

26. **Steen, W.M. and Mazumder, J.** *Laser Material Processing, 4th Ed.* s.l. : Springer, 2010.

27. **Ion, J.C.** *Laser Processing of Engineering Materials.* s.l. : Elsevier Ltd., 2005.

28. **O'Neill, G.J.** The Rotarian. *Laser : The space age tool.* June 1983. pp.18.

29. *Ytterbium-doped fiber amplifiers.* **Paschotta, R., et al.** 7, s.l. : Quantum Electronics, IEEE Journal of , 1997, Vol. 33.

30. *Analytical Model for Rare-Earth-Doped Fiber Amplifiers and Lasers.* **Barnard, C., et al.** 8, s.l. : Quantum Electronics, IEEE Journal of, 1994, Vol. 30.

31. *Nonlinear Fiber Optics, 3rd ed.* **Agrawa, G. P.** s.l. : Academic Press, San Diego,, 2001. Chapter 9.

32. *Rare-Earth-Doped Fiber Lasers and Amplifiers,2nd ed.* **Agrawal, G. P.** s.l. : Marcel Dekker, Inc. Chap. 7.

33. *Erbium-Doped Fiber Amplifiers: Principles and Applications. 1 ed.* **Desurvire, E.** s.l. : Wiley-Interscience, 1994.

34. **M.Von Allmen.** *Laser Beam Interactions with Materials , Vol 2* . Berlin : Springer, 1987.

35. **Duley, W.W.** *Laser Processing and Analysis of Materials. Plenum Press, New York.* New York : Plenum Press, 1983.

36. **Carslaw , H.S. and Jaeger, J.C.** *Conduction of Heat in Solids.* Oxford : Oxford University Press, 1959.

37. **Bäuerle, D.** *Laser Processing and Chemistry.* Berlin : Springer, 2000.

38. **Dahotre, N.B. and Harimkar, S.** *Laser Fabrication and Machining of Materials.* Berlin : Springer , 2008.

39. *Therapeutic and diagnostic application of lasers in ophthalmology.* **Thompson, K.P., Ren, Q.S. and Parel, J.M.** 6, s.l. : Proc. of the IEEE, 1992, Vol. 80.

40. *Laser-scattering-based method for investigation of ultra-low-loss arc fusion-spliced single-mode optical fibers.* **El-Diasty, F.** 6, s.l. : J.Lightw. Technol, 2004, Vol. 22. 1539-1542.

41. *High power cladding light strippers.* **Wetter , A., Fauche, M. and Sévig, B.** s.l. : Proc. of SPIE, 2008, Vols. 6873 687327-3.

42. *Dynamic Characteristics of Double-Clad Fiber Amplifiers for High-Power Pulse Amplification.* **Wang , Y. and Po , H.** 10, s.l. : Journal of Lightwave Technology, 2003, Vol. 21.

43. *Cladding-pumped ytterbium-doped large-core fiber laser with 610 W of output power.* **Jeong, Y., et al.** 1-6, s.l. : Opt. Comm., 2004, Vol. 234. pp. 315-319.

44. Standards catalogue. *ISO.* [Online] [Cited: 07 05, 2014.] http://www.iso.org/iso/catalogue_detail.htm?csnumber=33626.

45. Red Energy G4. *SPI Lasers.* [Online] [Cited: 05 07, 2014.] http://www.spilasers.com/Products/redENERGY_G4.aspx?.

46. MFPT. [Online] Max Photonics. [Cited: 05 07, 2014.] http://www.maxphotonics.com/en/maxContent.asp?ID=510.

47. **Young, H.D.** *University Physics, 7th ed.* s.l. : Addison Wesley, 1992. Table 15-5.

48. **Incropera, F.P., et al.** *Fundamentals of Heat and Mass Transfer, 6th ed.* s.l. : Wiley & Sons, 2007.

49. *Shunt types in crystalline silicon solar cells.* **Breitenstein, O., et al.** 7, s.l. : Progress in Photovoltaics: Research and Applications, 2004, Vol. 12.

50. **Schulze, M. and Venkat, S.** 38, s.l. : Laser Technik J., 2008, Vol. 5.
51. *Laser Edge Isolation for High-efficiency Crystalline Silicon Solar Cells.* **Dohyeon, et al.** 1, s.l. : Journal of the Korean Physical Soc., 2009, Vol. 55. p. 124-128.

52. *High-Quality Micromachining of Silicon at 1064 nm Using a High-Brightness MOPA-Based 20-W Yb Fiber Laser.* **O'Neill, W. and Li, K.** 2, s.l. : Selected Topics in Quantum Elec., Vol. 15.

53. *Modeling of laser-colored stainless steel surfaces by color pixels.* **Lehmuskero, A., et al.** 2-3, s.l. : Applied Physics B, 2010, Vol. 98.

54. *Laser Machining - Theory and Practice.* **Chryssolouris, G.** New York : Springer - Verlag, New York Inc, 1991.

55. *Laser-Beam Interaction with Materials, Springer-Verlag (1995).* **Allemen, M.von and Bllatter, A.** s.l. : Springer-Verlag, 1995.

56. *Rate dependence of short-pulse laser ablation of metals in air and vacuum.* **Wynne, A. E and Stuart, B. C.** 3, s.l. : Appl. Phys. , Vol. 76. pp 373-378.

57. *Deep Engraving of Metals for the Automotive Sector Using High Average Power Diode Pumped Solid State Lasers.* **Wendland, J. et al.** s.l. : Presented at ICALEO 2005, 2005.

58. *fobalaser.com.* [Online] Foba Laser. [Cited: 5 21, 2014.] http://www.fobalaser.com/products/basic-laser-marking-systems/with-ndyag-laser/.

59. *DGP-50 Diode Pump Laser Marking Machine.* [Online] Glory Laser. [Cited: 5 20, 2014.] http://www.glorylaser.com/productshow.asp?id=364&catid=89.

60. *Thin film removal mechanisms in ns-laser processing of photovoltaic materials.* **Bovatsek, J. , et al.** 10, s.l. : Thin Solid Films, 2010, Vol. 518.

61. *Laser Material Processing in Crystalline Silicon Photovoltaics.* **W, Bernard, et al.** s.l. : Proceedings of the 2012Mechanical Engineering Conference on Sustainable Research and Innovation, 2012. Vol. 4. 2079-6226.